

**ON THE K -MER FREQUENCY SPECTRA OF
ORGANISM GENOME AND PROTEOME SEQUENCES
WITH A PRELIMINARY MACHINE LEARNING
ASSESSMENT OF PRIME PREDICTABILITY**

by

Nathan O. Schmidt

A thesis

submitted in partial fulfillment

of the requirements for the degree of

Master of Science in Computer Science

Boise State University

August 2012

BOISE STATE UNIVERSITY GRADUATE COLLEGE

DEFENSE COMMITTEE AND FINAL READING APPROVALS

of the thesis submitted by

Nathan O. Schmidt

Thesis Title: On the k -mer frequency spectra of organism genome and proteome sequences with a preliminary machine learning assessment of prime predictability

Date of Final Oral Examination: 12 August 2012

The following individuals read and discussed the thesis submitted by student Nathan O. Schmidt, and they evaluated his presentation and response to questions during the final oral examination. They found that the student passed the final oral examination.

Tim Andersen, Ph.D.

Chair, Supervisory Committee

Amit Jain, Ph.D.

Member, Supervisory Committee

Greg Hampikian, Ph.D.

Member, Supervisory Committee

The final reading approval of the thesis was granted by Tim Andersen, Ph.D., Chair, Supervisory Committee. The thesis was approved for the Graduate College by John R. Pelton, Ph.D., Dean of the Graduate College.

ACKNOWLEDGMENTS

This thesis was supported by Dr. Tim Andersen and the United States Department of Defense through the DNA Safeguard Project.

ABSTRACT

A regular expression and region-specific filtering system for biological records at the National Center for Biotechnology database is integrated into an object-oriented sequence counting application, and a statistical software suite is designed and deployed to interpret the resulting k -mer frequencies—with a priority focus on nullomers. The proteome k -mer frequency spectra of ten model organisms and the genome k -mer frequency spectra of two bacteria and virus strains for the coding and non-coding regions are comparatively scrutinized. We observe that the *naturally-evolved* (NCBI/organism) and the *artificially-biased* (randomly-generated) sequences exhibit a clear deviation from the *artificially-unbiased* (randomly-generated) histogram distributions. Furthermore, a preliminary assessment of prime predictability is conducted on chronologically ordered NCBI genome snapshots over an 18-month period using an artificial neural network; three distinct supervised machine learning algorithms are used to train and test the system on customized NCBI data sets to forecast future prime states—revealing that, to a modest degree, it is feasible to make such predictions.

TABLE OF CONTENTS

ABSTRACT	iv
LIST OF TABLES	x
LIST OF FIGURES	xiii
LIST OF ABBREVIATIONS	xv
1 Introduction	1
1.1 Overview	1
1.2 Statement and Hypothesis	3
1.3 Significance	4
2 Background	5
2.1 Overview	5
2.2 Literature Review	5
3 Implementation Phase	16
3.1 Overview	16
3.2 CSeq Application Enhancement	16
3.2.1 Object-Oriented Sequence Iterator	17
3.2.2 NCBI Data Stream Filtering	19
3.2.3 GeneSIS Cluster Optimizations	20

3.3	Statistical Analysis Applications	24
3.3.1	Rankseq: k -mer Arrangement and Classification	24
3.3.2	NcbiStat: Genome Sequence Summarization	25
3.3.3	Genseq: Artificial Sequence Generation	27
3.3.4	Freqseq: Identifying the k -mer Frequency Spectra	27
3.3.5	Nullcountseq: Nullomer Set Cardinality and Intersection Ratio	28
3.3.6	Predictseq: Prime Prediction	29
3.3.7	Tdataformat: Predictseq Data Set Formatting	31
3.3.8	Tdatamerge: Predictseq Data Set Consolidation	32
3.3.9	34Seq: Nucleotide 3-mers, 4-mers, and GC Statistics	33
3.3.10	SetStat: Default Accuracy and Prime Error Superset Reporting	34
3.4	Format and Display Applications	34
3.4.1	Rangestat: The Global Rankseq Range	35
3.4.2	Histoseq: Histogram Compilation	36
3.4.3	Histoavg: Histogram Consolidation	36
3.4.4	Scriptgen: Cluster Execution Script Generation	37
4	Result and Analysis Phase	38
4.1	Overview	38
4.2	A Preliminary k -mer Language	38
4.2.1	Genetic Strings, Substrings, and k -mers	38
4.2.2	Superregions, Regions, and Subregions	40
4.2.3	k -mers: Frequency, Boolean Observed State, and Probability	42
4.3	Experiment 1: Organism k -mer Frequency Spectra and Nullomer Sequence Investigation	46

4.3.1	Objective Summary	46
4.3.2	Ten Model Organism Results and Analysis	47
4.3.3	Bacteria Strain Results: <i>Escherichia coli</i>	57
4.3.4	Virus Strain Results: <i>Human immunodeficiency virus</i>	65
4.4	Experiment 2: NCBI Genome Database Evolution and Time Series Analysis: Prime Prediction Assessment	71
4.4.1	Objective Summary	71
4.4.2	Training, Testing, and Prediction Results: The Artificial Neural Network.	71
5	Conclusion	80
5.1	Results Discussion	80
5.1.1	Experiment 1	80
5.1.2	Experiment 2	82
5.2	Implication	83
5.2.1	Experiment 1	83
5.2.2	Experiment 2	84
5.3	Future Exploration	84
5.3.1	Experiment 1	84
5.3.2	Experiment 2	86
5.4	Recapitulation	87
	REFERENCES	89
A	User Manual	93
A.1	Overview	93

A.2	CSeq	93
A.2.1	Processor	93
A.2.2	Reprocessor	94
A.2.3	FASTA Filtering	94
A.2.4	Genbank Filtering	94
A.3	Analysis Applications	96
A.3.1	Rankseq	96
A.3.2	NcbiStat	96
A.3.3	Genseq	96
A.3.4	Freqseq	97
A.3.5	Nullcountseq	98
A.3.6	Predictseq	98
A.3.7	Tdataformat	98
A.3.8	Tdatamerge	99
A.3.9	34Seq	99
A.3.10	Setstat	99
A.4	Format and Display Applications	99
A.4.1	Rangestat	99
A.4.2	Histoseq	99
A.4.3	Histoavg	100
A.4.4	Scriptgen	100
B	Source Code Snippets	102
B.1	Overview	102
B.2	Analysis Applications	102

C Detailed Experimentation Procedures	104
C.1 Overview	104
C.2 Experiment 1	104
C.2.1 Preparation	104
C.2.2 Procedure	105
C.3 Experiment 2	107
C.3.1 Preparation	107
C.3.2 Procedure	108
D Graphical Results	111
D.1 Overview	111
D.2 AA k -FS Results: <i>Apis mellifera</i> Example	111

LIST OF TABLES

4.1	The ten model organism’s AA k -FS analysis configuration	50
4.2	The ten model organism’s AA k -FS data sets. The total sequence length $ S $ is used for the Genseq’s “generation_size”	50
4.3	The ten model organism’s AA 4-nullomer set cardinality and intersection ratio comparisons for statistics with length-3 subsequence partitioning	51
4.4	The ten model organism’s AA 5-nullomer set cardinality and intersection ratio comparisons for statistics with length-3 subsequence partitioning	51
4.5	The ten model organism’s AA 5-nullomer ranking histogram chi-square comparisons for statistics with length-3 subsequence partitioning	52
4.6	The ten model organism’s 3-FS, 4-FS, and 5-FS histogram chi-square comparisons for the $[0, 10000]$ frequency spectral-range	53
4.7	The analysis summary of the ten model organism 3-FS distributions in Figures 4.1, 4.2, 4.3, 4.4, and 4.5	54
4.8	The EC bacteria’s DNA k -FS analysis configuration	59
4.9	The EC bacteria’s DNA sequence data sets. Here, the superregion length $ R^7 $ is used as Genseq’s “generation_size”	60
4.10	The EC bacteria’s DNA 8-nullomer set cardinality comparisons for statistics with length-7 subsequence partitioning	60

4.11	The EC bacteria’s DNA 8-nullomer set intersection ratio comparisons for statistics with length-7 subsequence partitioning	60
4.12	The EC bacteria’s DNA 9-nullomer set cardinality comparisons for statistics with length-7 subsequence partitioning	60
4.13	The EC bacteria’s DNA 9-nullomer set intersection ratio comparisons for statistics with length-7 subsequence partitioning	61
4.14	The EC bacteria’s DNA 10-nullomer set cardinality comparisons for statistics with length-7 subsequence partitioning	61
4.15	The EC bacteria’s DNA 10-nullomer set intersection ratio comparisons for statistics with length-7 subsequence partitioning	61
4.16	The EC bacteria’s DNA 10-nullomer ranking histogram chi-square comparisons for statistics with length-7 subsequence partitioning	62
4.17	The analysis summary of the EC bacteria 5-FS distributions in Figures 4.6 and 4.7	63
4.18	The HIV’s DNA/RNA k -FS analysis configuration	67
4.19	The HIV’s DNA/RNA sequence data sets. Here, the superregion length $ R^\tau $ is used as Genseq’s “generation_size”	68
4.20	The HIV’s DNA/RNA 5-nullomer set cardinality and intersection ratio statistical comparisons with length-3 subsequence partitioning	68
4.21	The HIV’s DNA/RNA 6-nullomer set cardinality and intersection ratio statistical comparisons	68
4.22	The HIV’s DNA/RNA 7-nullomer set cardinality and intersection ratio statistical comparisons	68
4.23	Rankseq’s HIV DNA/RNA 7-nullomer probability histogram chi-square comparisons with length-3 subsequence partitioning	69

4.24	The analysis summary of the HIV 3-FS distributions in Figures 4.8 and 4.9	69
4.25	The size statistics for the <i>balanced</i> NCBI data set snapshots	73
4.26	The size statistics for the <i>unbalanced</i> NCBI data set snapshots	74
4.27	The ANN training configuration for the observed prime state predictions on the monthly NCBI database snapshots	78
4.28	The ANN training accuracies for 16-prime state prediction on the <i>balanced</i> monthly DNA data sets ranging from January 2010 to July 2011	78
4.29	Predictseq’s ANN prediction accuracies for the 16-prime state <i>unbalanced</i> monthly DNA data sets ranging from February 2010 to July 2011. We see that Predictseq’s accuracy Λ_{total} outperformed the random biased guessing Λ_{BRG} in $\frac{14}{16}$ cases.	79

LIST OF FIGURES

4.1	Apis mellifera vs. Bos taurus: The $\Gamma_3^{S_{Honeybee}}$ and $\Gamma_3^{S_{Cattle}}$ comparison with a frequency spectral-range $[0, 10000]$ for \mathbb{N} data sets (only $[0, 200]$ is shown)	54
4.2	Canis familiaris vs. Gallus gallus: The $\Gamma_3^{S_{Dog}}$ and $\Gamma_3^{S_{Chicken}}$ comparison with a frequency spectral-range $[0, 10000]$ for the \mathbb{N} data sets (only $[0, 200]$ is shown)	55
4.3	Danio rerio vs. Stronglyocentrus purpuratus: The $\Gamma_3^{S_{Zebrafish}}$ and $\Gamma_3^{S_{SeaUrchin}}$ comparison with a frequency spectral-range $[0, 10000]$ for the \mathbb{N} data sets (only $[0, 200]$ is shown)	55
4.4	Homo sapien vs. Pan troglodytes: The $\Gamma_3^{S_{Human}}$ and $\Gamma_3^{S_{Chimp}}$ comparison with a frequency spectral-range $[0, 10000]$ for the \mathbb{N} data sets (only $[0, 200]$ is shown)	56
4.5	Mus musculus vs. Rattus norvegicus: The $\Gamma_3^{S_{Mouse}}$ and $\Gamma_3^{S_{Rat}}$ comparison with a frequency spectral-range $[0, 10000]$ for the \mathbb{N} data sets (only $[0, 200]$ is shown)	56
4.6	EC-536: The DNA $\Gamma_5^{S_{EC-536}}$ region comparison with a frequency spectral-range $[0, 10000]$ for the \mathbb{N} data sets (only $[0, 200]$ is shown)	63
4.7	EC-55989: The DNA $\Gamma_5^{S_{EC-55989}}$ region comparison with a frequency spectral-range $[0, 10000]$ for the \mathbb{N} data sets (only $[0, 200]$ is shown) . . .	64

4.8	HIV-1: The DNA/RNA $\Gamma_3^{S_{HIV-1}}$ region comparison with a frequency spectral-range $[0, 300]$ for the N data set (only $[0, 20]$ is shown)	70
4.9	HIV-2: The DNA/RNA $\Gamma_3^{S_{HIV-2}}$ region comparison with a frequency spectral-range $[0, 300]$ for the N data set (only $[0, 20]$ is shown)	70
4.10	The FASTA DNA monthly NCBI database sizes ranging from January 2010 to July 2011	75
4.11	The DNA 16-prime set cardinalities for the NCBI database snapshots ranging from January 2010 to July 2011	76
4.12	The DNA 16-prime set sizes (in megabytes) for the NCBI ANN training and testing data sets ranging from January 2010 to July 2011	77
4.13	A depiction of the ANN 16-prime state prediction accuracies for the (unbalanced) monthly DNA data sets ranging from February 2010 to July 2011	79
B.1	Rankseq’s sequence probability ranking algorithm	103
D.1	The honey bee’s length-5 AA nullomer ranking histogram for the <i>NCBI</i> data set	111
D.2	The honey bee’s length-5 AA nullomer ranking histogram for the <i>length-1 statistically generated</i> data set	112
D.3	The honey bee’s length-5 AA nullomer ranking histogram for the <i>length-2 statistically generated</i> data set	113
D.4	The honey bee’s length-5 AA nullomer ranking histogram for the <i>length-3 statistically generated</i> data set	113
D.5	The honey bee’s length-5 AA nullomer ranking histogram for the <i>randomly generated</i> data set	114

LIST OF ABBREVIATIONS

DNA – Deoxyribonucleic acid

AA – Amino acid

NCBI – National Center for Biotechnology Information

***k*-FS** – *k*-mer frequency spectra

HIV – Human immunodeficiency virus

EC – Escherichia coli

ANN – Artificial neural network

RAM – Random access memory

PVFS – Parallel Virtual File-System

CHAPTER 1

INTRODUCTION

1.1 Overview

The *k-mer frequency spectra* (*k*-FS) is the set of all short-length words resident to a genome or proteome, where each *k*-mer is mapped to an occurrence frequency. Upon sequencing, organism sequences are digitized and stored at the National Center for Biotechnology Information (NCBI) as FASTA and Genbank records to promote computational examination. The sequence studies of [26, 7, 8] reveal a non-linear variation in the genome distribution of these frequencies on a multitude of model organism species; while some *k*-mers enjoy an occurrence plethora, others remain absent. The minimum-length sequences that are absent from an organism are termed *nullomers* and those that are absent from nature are termed primes. Are there interesting proteome *k*-FS and nullomer properties? Can statistical distinctions be made between the genome *k*-FS and nullomers of complete, coding, and non-coding regions? In terms of the *k*-FS and nullomers, are the natural data sets of specific organisms distinct from the artificial generated? If so, to what degree? As the advances in bio-technology continue to yield a faster genome and proteome sequencing rate, the total size of the NCBI database accelerates. So how might this rapid technological expansion influence the prime phenomena? Is it possible to train an intelligent system to analyze the NCBI database and forecast future prime states?

We investigate the k -FS properties for various subject organisms, with a priority-focus on the nullomer/prime phenomena in terms of ranking and predictability.

In Chapter 2, we highlight the literature that influences this thesis and discuss how these fundamental concepts direct our investigation.

In Chapter 3, we introduce the statistical software application suite that is designed to instrument the k -mer-based sequence analysis. First, we present structural and algorithmic enhancements to our core sequence processing utility, in terms of (1) the GeneSIS cluster space and run-time optimizations, (2) the new object-oriented iterator implementation, and (3) the logic-oriented sequence filtering sub-system. Second, we discuss the purpose and key components to each individual application. Third, we explain how the NCBI genomes and proteome data sets are processed, interpreted, and evaluated by our software to statistically analyze the subject k -FS and nullomers/primes.

In Chapter 4, we discuss the two distinct categories of experiments. In Experiment 1, the k -FS analysis, the natural data set frequency statistics are systematically compared against those of the artificially-generated data sets (including randomly-*biased* and randomly-*unbiased*) to determine the degree (if any) of similarity. First, we examine the proteome of ten distinct model organisms to determine the amino acid (AA) k -FS statistics. Second, we examine the genome of two *Escherichia coli* (EC) strains and two Human immunodeficiency virus (HIV) strains, where we use our sequence filtering sub-system to determine the deoxyribonucleic acid (DNA) k -FS statistics for the complete, coding, and non-coding regions. In Experiment 2, the prime prediction assessment, the month-by-month time-series evolution of the NCBI database is chronologically analyzed by an artificial neural network (ANN); the ANN is trained using three distinct machine learning techniques and used to forecast future

prime states.

In Chapter 5, we summarize this research, discuss implications, and suggest future projections along this mode of bio-informatics exploration.

1.2 Statement and Hypothesis

In [26], Hampikian and Andersen introduce a publicly available algorithm for identifying absent sequences and demonstrate its use by reporting the smallest k -mers *not* found in NCBI's organism genome database. These nullomers define the maximum set of potentially lethal k -mers. Additional k -mer studies of complete organism genome sequences have identified a non-linear variation in the frequency distribution using statistical analysis software [7, 8]. The modalities of the k -FS distributions range from uni-modal to multi-modal, generally depending on whether the organism is a eukaryote or prokaryote. This series of experiments suggests evidence of deterministic k -mer structure in complete organism genome sequences. This thesis seeks knowledge of the k -FS and nullomer/prime phenomena by answering the following inquiries:

1. Experiment 1: Do the DNA and AA k -FS of the subject organisms exhibit evidence of (1) structural bias or (2) are they completely random? How do the nullomer set cardinalities and overlap (intersection) ratios comparatively differ between the natural and artificial data sets?
2. Experiment 2: Does the time-dependent evolution of the NCBI database enable us to predict future prime states? If so, to what degree of accuracy?

Our research tests a distinct hypothesis for both experiments. Our hypothesis for

1. Experiment 1 is: *the k -FS for the selected subject organisms is non-random and will therefore exhibit structural bias*; and

2. Experiment 2 is: *the future prime states are inherently unpredictable* (due to, for example, an insufficient amount of genome information housed at NCBI, and the unattainable degree of influential factors to consider, such as the environment, the organisms, and the order of NCBI submission content).

1.3 Significance

The knowledge obtained from the results of this thesis may help establish a rational basis for species identification, environmental characterization, genetic engineering, and could someday prove useful to fields such as medicine. If science can develop a fundamental understanding of the k -FS and nullomer/prime phenomena, then perhaps someday it may be possible to identify the physical, chemical, and biological mechanisms, or natural “algorithms” responsible for genetic mutations.

CHAPTER 2

BACKGROUND

2.1 Overview

In this chapter, we summarize the background literature that forms the foundation of this thesis and explain how these concepts influenced this k -mer research deployment.

2.2 Literature Review

In [7], evolutionary features based on k -FS distributions of various organisms are analyzed. There are three distinct groups based on their evolutionary periods, where each category exhibits a distinct modality:

1. **E. coli and T. pallidum**: unimodal;
2. **yeast, zebrafish, A. thaliana, and fruit fly**: unimodal with peaks generally shifted to smaller frequencies of occurrence; and
3. **mouse, chicken, and human**: bimodal.

Furthermore, a model based on the DNA cytosine-guanine “CG” content is introduced and shown to provide reasonable agreements with the data.

In [8], the empirical frequencies of DNA k -mers in complete genome sequences provide a distinct and interesting perspective on genome structure. More than 100

species from Archea, Bacteria, and Eukaryota are investigated, with a focus on the k -FS modalities. They found that a few species, including all mammals, have multimodal spectra (these species coincide with the tetrapods) and discovered that low-order Markov models capture this property fairly well. The multimodal spectra are characterized by specific ranges of values of C+G content and of CpG dinucleotide suppression, a range that encompasses all tetrapods analyzed. Other genomes, like that of the protozoa *Entamoeba histolytica*, which also exhibits CpG suppression, do not have multimodal k -FS. Groupings of functional elements of the human genome also have a clear modality, and exhibit either a unimodal or multimodal behaviour, depending on the two above mentioned values.

In [26], a novel algorithm for identifying nullomers is introduced, where the authors use it on NCBI Genbank records to report nullomer statistics for various model organisms. They demonstrate that nullomers and primes provide a rational basis for selecting artificial DNA sequences for molecular barcodes and may provide insight into environmental characterization, antibiotic development, species identification, comparative genomics, and potential target identification for therapeutic intervention. It is shown that nullomers and primes can be used to delineate between the set of natural and potentially unused sequences, where the boundary nullomers surround various branches of the phylogenetic tree of life.

In [1], the authors demonstrate that the hypermutability of CpG dinucleotides, rather than natural selection against nullomers, is likely the reason for the nullomer phenomena. They investigate various human, chimpanzee, cow, dog, and mouse genome instances. They observe that for these species, nullomers differ by only one nucleotide, which suggests that mutation, rather than natural selection, is responsible for the nullomer evolution and nullomer generation in species populations.

In [20], the authors present correlation analysis results of k -mer presence/absence distributions ranging from 5 to 20 in more than 1500 microbial and virus genomes, along with five multicellular organisms (including human). For organisms that are not close relatives, the genome k -mer distributions are not correlated, but for close biological relatives, some correlation is observed, but is not as strong as expected. The results suggest that suppressed correlations of various genome n -mers leads to the possibility of using random n -mer sets to discriminate genomes of different organisms and possibly individual genomes of the same species, including human, with a low error probability.

In [27], the authors demonstrate how a number of sequence comparison tasks can be accomplished efficiently without an alignment step. This procedure is based on the shortest unique substrings. These are k -mers that only occur once within the sequence or set of sequences analyzed and that cannot be further reduced in length without losing the uniqueness property. They report that the shortest unique substrings in *C. Elegans*, human, and mouse are no longer than 11 base pairs in the autosomes of these organisms. In mouse and human, these unique substrings are significantly clustered in upstream regions of known genes. They derive an analytical expression for the nullomer distribution of the shortest unique substrings, based on the GC-content of the query sequences and apply this method to the rapid detection of unique genomic regions in various bacteria strains.

In [23], the authors examine the relative abundances of dinucleotides and their biases in various eukaryotic genomes and chromosomes, including human chromosomes 21 and 22, *Saccharomyces cerevisiae*, *Arabidopsis thaliana*, and *Drosophila melanogaster*. They report that the dinucleotide relative abundances are remarkably constant across human chromosomes and within the DNA of a particular species.

Moreover, the dinucleotide biases differ between species, and provide a genome signature that is characteristic of an organism's DNA.

In [39], the authors report that the CpG dinucleotide is present at approximately 20% of its expected frequency in vertebrate genomes. They examine the hypothesis that the 20% frequency represents an equilibrium between the rate of creation of new CpGs and the accelerated rate of CpG loss from methylation. From this, they calculate the expected reduction in the CpG equilibrium frequency and find that the observed CpG deficiency can be explained by mutation from methylated CpG to TpG/CpA at approximately 12 times the normal transition rate, the exact rate depending on the ratio of transitions to transversions. This indicates that it would take 25 million years or less, a small fraction of the time for vertebrate evolution, for CpG frequency to be reduced from undepleted levels to the current depleted levels.

In [36], the authors compare various studies on the exact distribution of word counts in random sequences in terms of approximation accuracy and computational cost. They propose rules for choosing between the Gaussian approximations, compound Poisson approximation, and exact distribution. They apply these concepts to the detection of exceptional words in the phage Lambda genome.

In [35], the authors provide an overview based on the statistical and probabilistic properties of words, as occurring in the analysis of biological genomes, where they distinguish between various word frequencies and exact distributions as well as the derivation of various approximation methods. They model a sequence as a stationary ergodic Markov chain. A test is proposed for determining the appropriate order of the representative Markov chain.

In [31], the authors aim to characterize protein databases, where they engage in a systematic attempt to reveal protein database characters that could contribute to

revealing how protein chains are constructed. For this, they focus on using the set of all the possible 3-mer, 4-mer, and 5-mer frequency distribution combinations. The results suggest that these 3D information structures are protein functions that exist in the context of short constituent sequence connections, which are reflected on their availability differences in the database. These results may have biological implications for protein structural studies.

In [40], the authors demonstrate that there are thousands of penta-peptides that are absent from all known proteomes, but many of them are coded for multiple times in the non-coding genomic regions. This suggests a strong selection process that prevents these peptides from being expressed. They show that the characteristics of these forbidden penta-peptides vary among various phylogenetic groups, where they claim to provide the first steps toward understanding the grammar of the forbidden penta-peptides.

In [19], the authors identify and investigate a large population of pseudogenes in four sequenced eukaryotic genomes: the worm, yeast, fly, and human (chromosomes 21 and 22 only). Each of the 2500 pseudogenes is characterized by one or more disablements, such as premature stops and frameshifts. They conduct a comprehensive frequency survey of the amino acid and nucleotide composition in these non-functional genes and compare them to functional genes and intergenic DNA. They correlate the pseudogene amino acid composition to the intermediate composition between genes and translated intergenic DNA. They establish that the pseudogene intermediate composition applies even though the gene composition in the four organisms is markedly different, showing a strong correlation with the overall A/T content of the genomic sequence. They classify pseudogenes into ancient and modern subsets, where modern pseudogenes typically exhibit a much closer sequence

composition to genes than ancient pseudogenes. Altogether, their results indicate that the composition of pseudogenes that are not under selective constraints progressively drift from that of coding DNA towards non-coding DNA. Therefore, they propose that the degree to which pseudogenes approach a random sequence composition may be useful in dating different sets of pseudogenes, as well as to assess the rate at which intergenic DNA accumulates mutations.

In [22], the authors analyze the amino acid frequency distribution in seven nuclearly-encoded and five mitochondrial-encoded inner membrane proteins. They establish that the mitochondrially encoded proteins have many more positively charged residues in their non-translocated, as compared to their translocated, domains. However, most of the nuclearly-encoded proteins do not show such a bias, but instead have a surprisingly skewed distribution of Glu residues. These results suggest that some, but possibly not all, nuclearly-encoded proteins may insert into the membrane by a mechanism that does not depend on the frequency distribution of positively charged amino acids.

In [30], the authors investigate the frequency and binding of short linear motifs (peptides of lengths three to eight) in terms of protein interaction networks. Their objective is to explain how one protein is able to bind to very different partners. The fact that they often reside in disordered regions in proteins makes them difficult to detect through sequence comparison or experiment. So they demonstrate that binding motifs can be detected using data from genome-scale interaction studies, which avoids the normally slow discovery process in proteome-scale interactions. They focus on motif over-representation in non-homologous sequences, rediscovering known motifs, and predicting dozens of others. Of the predicted, direct-binding experiments reveal that two motifs are indeed protein-binding modules. They estimate that there may be

dozens or even hundreds of linear motifs yet to be discovered that will give molecular insight into protein networks and greatly illuminate cellular processes.

In [34], the authors propose an amino acid k -string frequency analysis as a systematic way of inferring evolutionary relatedness of microbial organisms from the oligopeptide content. Their method contains only one parameter, the length k of the oligopeptides, and therefore avoids the ambiguity of choosing the genes for phylogenetic reconstruction and variable length sequence alignment. This method is applied to a total of 109 organisms, including 16 Archaea, 87 Bacteria, and 6 Eukarya, and yields an unrooted tree that agrees with the biologists phylogenetic “tree of life,” based on basic branching majorities on SUU rRNA. The tree-based topology converges with k increasing.

In [41], the authors provide a novel method for efficient reconstruction of phylogenetic trees, based on complete genome and proteome sequences, whose lengths may vary greatly. The technique measures the pairwise distances between sequences, which is based on computing the average lengths of the maximum common substrings. They propose an algorithm on suffix arrays for efficiently computing these distances in $O(k)$ time, where k is sequence length. An initial analysis of the results exhibits a remarkable agreement with accepted phylogenetic and taxonomic truth. They discuss five distinct applications of the method, which suggests a number of novel phylogenetic insights.

In [6], the authors describe a hidden markov model used for detecting local correlations in protein sequence structures based on the I-sites library. The model is unlike the linear hidden Markov models because it employs a highly branched topology and captures recurrent local features of protein sequences and structures to predict protein secondary structure. The model achieves an accuracy of 74.3% and

recognizes a considerably higher probability to coding sequence regions. They suggest that these methods will be useful for tertiary structure prediction.

In [16], the authors propose a chaos game representation to display short oligonucleotide sequences in genomes in the form of fractal images. These images are considered as a genomic signature. They demonstrate that short fragments of genomic sequences retain most of the characteristics of the species they come from, and suggest that it is possible to perform a global species comparison by using genome fragments found in databases. They evaluate the efficiency of this approach as a function of the fragment size and the oligonucleotide length.

In [5], the authors investigate the relative abundance functional for lengths 2, 3, and 4 nucleotides in a broad phylogenetic range to discern tendencies and anomalies in the frequency occurrences of these oligonucleotides. They find that for dinucleotides, TA is almost universally under-represented, with the exception of vertebrate mitochondrial genomes, and CG is strongly under-represented in vertebrates and in mitochondrial genomes. Moreover, for trinucleotides, GCATGC tends to be under-represented in phage, human viral, and eukaryotic sequences, and CTATAG is strongly under-represented in many prokaryotic, eukaryotic, and viral sequences. They consider various explanations for the over- and under- representations in terms of DNA/RNA structures and regulatory mechanisms are considered.

In [4], the authors seek to understand how amino acid composition of proteins has changed over the course of evolution. In doing so, they introduce a method and simulation for estimating the composition of proteins in an ancestral genome. The estimates are based upon the composition of conserved residues in descendant sequences, and the relative probability of conservation in various amino acids. Relative to the modern protein set, the ancestral protein set was found to be generally

richer in those amino acids that are believed to have been most abundant in the prebiotic environment and poorer in those amino acids that are believed to have been unavailable or scarce. They propose that the inferred amino acid composition of ancestral proteins reflects historical events in the establishment of the genetic code.

In [24], the author compares representative genomes from each of the three kingdoms of life in terms of protein structure, with a focus on a bacteria, an archaeon, and yeast. This comparison is a frequency analysis of secondary and tertiary structures in the genomes. The author discusses the similarities and differences between the data sets in terms of degree of duplication, degree of overlap, the number of protein folds, and the most common short-length strands. From these results, the author suggests that the last common ancestor correlations to the three kingdoms are the most basic molecular parts, including the TIM-barrel, Rossmann avodoxin, thiamin-binding, and P-loop hydrolase folds.

In [17], the authors explored genome DNA structures by means of a new tool derived from chaotic dynamical systems theory, which allows them to depict oligonucleotide frequencies as images. They observe that the subsequences of a genome exhibit the main characteristics of the complete genome, reinforcing the validity of the genome signature concept. The main factors explaining the observed sequence variability are due to base concentrations, stretches (of complementary bases), and patches (of over- or under-represented words of varying lengths). They demonstrate that the distance between images may be considered a measure of phylogenetic proximity, where eukaryotes and prokaryotes can be identified merely on the basis of their DNA structures.

In [37], the authors establish that the rates and patterns of evolution at silent sites in codons reveal much about the basic features of molecular evolution. They found

that for recent increases in the amount of sequence data available for various species and more precise knowledge of the chromosomal locations of those sequences, coming in particular from genome projects, reveal that some features of molecular evolution vary around the genome.

In [18], the authors report two Chaos Game Representation (CGR) algorithms that can predict the presence or absence of a stretch of nucleotides in any gene family. They explain how the CRG can recognize patterns in nucleotide sequences of a class of genes using the techniques of fractal structures and by considering DNA sequences. These algorithms can provide a mathematical basis of the CGR patterns obtained using nucleotide sequences from genome databases.

In [21], the author compares the trinucleotide frequencies in long sequences and their shuffled counterparts. A frequency hierarchy is observed among the 32 complementary trinucleotide pairs, which is influenced both by base composition (not affected by shuffling the order of the bases) and by base order (affected by shuffling). The author observes that the influence of base order is greatest in DNA with a GC-content of 50 percent and appears to reflect a more fundamental hierarchy of dinucleotide frequencies. Therefore, if TpA is at low frequency, all eight TpA-containing trinucleotides are at low frequency. Moreover, the author reports that mammals and their viruses share similar hierarchies, with genomic differences being generally associated with differences in base composition (percentage of GC content). *E. coli* and, to a lesser extent, *Drosophila melanogaster* hierarchies differ from mammalian hierarchies; this is associated with differences both in base composition and in base order. Therefore, the author proposes that Chargaff's rule applies to single-stranded DNA because there has been an evolutionary selection pressure favoring mutations that generate complementary oligonucleotides in close proximity, thus creating a

potential to form stem-loops. These are dispersed throughout genomes and are rate-limiting in recombination. These results suggest that GC-content delineations between species would impair interspecies recombination by interfering with stem-loop interactions.

In [10, 9, 14, 12, 11, 13, 32, 25], the authors investigate low-frequency vibrations in biomacromolecules. They explain that these structures possess significant biological functions. They demonstrate that biomolecule helices generate low frequency collective vibrations in the form of phonons.

In [3], the authors reveal a parametric resonance in DNA dynamics, generated by pumping hypersound. From this, they observe that the DNA double helix naturally generates localized phonon modes, which propagate along base pair sequences, and suggest that these results provide valuable methods of bio-diagnostics.

In [38], the authors investigate the normal mode harmonic dynamics of double-stranded DNA in a viscous fluid. They find that the sugar phosphate backbone dynamics are over-damped and shield the DNA bases from direct bombardment by the solvent, whereas the DNA bases exhibit under-damped low frequency vibrational modes. These results indicate that the backbone plays a significant role in modulating the double-stranded DNA dynamics in an over-damping environment. They briefly discuss the connection with protein and drug interactions, as well as gene regulation.

CHAPTER 3

IMPLEMENTATION PHASE

3.1 Overview

In this chapter, we introduce the statistical software application suite that is designed to instrument the k -mer sequence analysis. First, we present structural and algorithmic enhancements to our core sequence processing utility, including the (1) new object-oriented iterator implementation, (2) GeneSIS cluster space and run-time optimizations, and (3) logic-oriented sequence filtering sub-system. Second, we discuss the purpose and key features of each individual application. Third, we explain how the NCBI genome and proteome data sets are processed, interpreted, and evaluated by our software to statistically analyze the subject k -FS and nullomers/primes.

Note: The usage for each utility (including examples of sequence filter definitions) can be found in the User's Manual (Appendix A).

3.2 CSeq Application Enhancement

Here, we discuss structural and algorithmic enhancements to CSeq: the modular version of the k -mer sequence processing and reprocessing application originally developed by Greg Hampikian and Tim Andersen [26]. This utility is central to our k -mer frequency investigation. The newly incorporated object-oriented sequence iterator

design, the Genesis cluster optimizations, and the integrated filtering sub-system were crucial prerequisites to deploying the remaining set of statistical software applications used in our analysis.

3.2.1 Object-Oriented Sequence Iterator

We extracted the core CSeq k -mer sequence processing algorithm from original source code (provided by Hampikian and Tim Andersen [26]) and translated it into a modular, object-oriented framework. Here, we summarize the key classes to this upgrade.

Class: Sequence

The *Sequence* class stores sequence data (and if applicable, the associated meta data).

Class: Sequence Iterator

The *Sequence Iterator* class manages a dynamic set of Sequence objects, allowing the calling procedure to iterate over and access the contents of each individual Sequence one-by-one. The class implements the abstract iterator interface and supports operations such as increment and decrement. Depending on the NCBI input type, the Sequence Iterator will manage an underlying *Genbank Sequence Iterator* or *FASTA Sequence Iterator*. These iterator classes load, parse, and store NCBI sequence data and meta data by iteratively populating Sequence objects.

If the user defines filters, the class will additionally manage an *Filtering Sequence Iterator* (which is further embedded in the iterator). During the screening process, only the Sequence objects that satisfy the Filter Set constraints are accessible to the calling procedure (the rest are simply discarded).

Class: Filter

The *Filter* class stores NCBI filter parameters for both regular expression (both FASTA and Genbank) and region (Genbank only) filtering. Each object corresponds to a single (user-defined) filter. The class is capable of housing screening information pertinent to both FASTA-specific and Genbank-specific filters. Each filter is used to determine whether the supplied input parameter “passes” the screening constraints associated with itself by returning a Boolean value as output.

Class: Filter Set

The *Filter Set* class manages static set of Filter objects. The class accepts a user-defined filter configuration file for either Genbank-specific (Appendix A.2.3) and FASTA-specific (Appendix A.2.4) filtering as input. If the user defines multiple filters, the Filter Set manages the conjunctive and disjunctive relationships expressed between the objects of the set. The filter set is used by the Sequence Iterator to determine whether the current Sequence object being considered “satisfies” the screening constraints by returning a Boolean value as output.

Classes: Factory, Genbank Factory, FASTA Factory, and Filter Factory

The *Factory* class constructs a Sequence iterator and returns it to the calling procedure. In doing so, the class first determines whether the NCBI record input is Genbank or FASTA and subsequently returns a constructed *Genbank Factory* or *FASTA factory*, respectively. Underlying this process, the class determines whether the input is genome or proteome, and if GZip compression is used. Also if filters

are being used, it additionally constructs a *Filter Factory*, which it embeds into the identified factory type.

3.2.2 NCBI Data Stream Filtering

The NCBI Data Stream Filtering sub-system we integrated into CSeq enables the analysis of specific NCBI database subsets by applying user-defined filter definitions. The user supplies CSeq with a filter file to “look at” specific types of sequences in greater depth. For example, these additional capabilities allow us to analyze the k -FS of coding regions for specific organisms.

Classification

CSeq interprets two distinct types of logic-based filters, namely *regular expression* and *region*. Both types can optionally be combined into a filter set, depending on the user preference—a user may define as many filters as they wish and associate them with conjunction, disjunction, and negation statements. Regular expression filters provide a concise and flexible means for matching strings of text, such as particular characters, words, or patterns of characters in the genome data—these filters are written in a formal language that is interpreted by CSeq’s filtering modules. Region filters provide a means to screen for specific genome subsequences, such as coding and/or promoter sites, etc.

Note: For specific examples of FASTA and Genbank filter definitions, grammar, and syntax consult Sections A.2.3 and A.2.4, respectively.

File Format

NCBI partitions the genome data into records, where each record contains two general components that are treated as pairs. The first component is the *meta data* descriptor, which identifies properties inherent to the second component, namely the *sequence data*. The amount of meta data associated with each sequence record depends on the file format; NCBI provides all amino acid and nucleotide sequence data in both FASTA and Genbank file formats.

In brief, the FASTA file format (consult A.2.3) contains a single-line meta data descriptor for each sequence record. FASTA does not contain region-specific meta data, and therefore, only regular expression filters can be applied to FASTA sequence records.

The Genbank file format (consult A.2.4) contains multi-line meta-data descriptors for each sequence record. In addition to supporting regular expression filtering, Genbank files also contain region-specific meta-data tags that identify specific subsequence sites within the described genome sequence. Therefore, Genbank files are used in the experimental phase (Sections 4.3.2, 4.3.3, and 4.3.4) to screen for coding regions.

3.2.3 GeneSIS Cluster Optimizations

The initial CSeq implementation did not scale properly on the GeneSIS cluster, in particular, it actually ran slower on GeneSIS than the conventional workstation. So clearly, the application required cluster optimizations in order to sufficiently harness the computational power provided by the system hardware. In this section, we document this task of adding space and run-time enhancements to CSeq.

General Methodology

To attack this problem, we divided CSeq into three distinct function categories: (1) disk reading, (2) data processing, and (3) disk writing. Next, we started a development branch of CSeq, namely CSeqSpeed. From here, we manually extracted code from CSeq and moved it to the development branch (via copy-and-pasting) to independently test the performance of each function category.

In all test cases, we used uniform data sets (approximately 1 Gigabyte). We created four distinct genome data sets: (1) an uncompressed FASTA, (2) a Gzip compressed FASTA, (3) an uncompressed Genbank, and (4) a Gzip compressed Genbank. For each data set, we observed the performance of the compiled CSeqSpeed executable and compared it with the expected (theoretical) target performance of the Parallel Virtual File-System (PVFS) disk subsystem I/O. The 7.0TB PVFS partition of the 24.8TB total usable space on the GeneSIS Cluster housed the NCBI database snapshots used for in the sequence processing tests.

Tuning: Disk Reading

First, we constructed the initial base version of CSeqSpeed: a skeleton program that simply opened an NCBI database file, sequentially read each block in the file using a circular buffer, and terminated. Using the Linux “time” command, we established the expected PVFS read performance in MB/sec by testing CSeqSpeed on the uncompressed FASTA data set—we found that the optimal CSeqSpeed read-buffer size for GeneSIS was 1MB - 2MB. Next, we tested CSeq on the compressed FASTA data set—we found that use of the Gzip compression library degraded performance slightly but was consistent with our expectations. Once we found the optimal read

block size, we used Cachegrind to verify that CSeqSpeed contained zero memory leaks. At this point, we had completed our base version of CSeqSpeed, which represented the expected target performance.

So we copy-and-pasted the data structures and algorithms from CSeq to CSeqSpeed one-by-one to iteratively test the disk read performance on the uncompressed FASTA data set. For each case, we compared the observed performance with the expected performance. If the observed performance was less than the expected performance, then we used Cachegrind and GProf to identify software bottlenecks and eliminate them. Based on our analysis, we found that the following enhancements to CSeq significantly improved space and run-time performance in the disk reading domain:

1. **Character Iterator Class Removal:** We found that invoking the Character Iterator's increment operator for each character significantly degraded disk read run-time performance, so we completely removed this class and replaced it with a circular buffer in the File Iterator class.
2. **String/C-String Concatenation Minimization:** We reduced the total number of string buffer concatenations in the disk reading process by setting the File Iterator's circular buffer to a static size of 2MB.
3. **Pointers and References:** We used pointers and references to efficiently pass the read buffer between various objects to eliminate unnecessary and redundant memory allocation and copying.
4. **Function In-Lining:** We in-lined the most frequently used disk read functions (based on GProf statistics) in the Sequence, Sequence Iterator, FASTA Sequence Iterator, and Genbank Iterator classes.

Tuning: Data Processing and Filtering

Once the disk reading enhancements were complete, we turned to the data processing and filtering enhancements; here, the CSeqSpeed copy-and-paste, Cachegrind, GProf, and code adjustment methodology for tuning the data processing algorithms was similar to that of the disk reading. Based on our analysis, we found that the following enhancements to CSeq significantly improved space and run-time performance in the data processing and filtering domain:

1. **Disk Swapping and Memory Usage Reduction:** We reduced the RAM requirements for the Sequence, Sequence Iterator, Genbank Sequence Iterator, FASTA Sequence Iterator, Genbank Feature, Filter Set, and Filter classes used by the core processing and filtering algorithms to reduce the disk swap potential.
2. **Data Globalization:** We globalized the Genbank Lookup Table and certain Filtering enumerations to provide faster access to the processing and filtering algorithms.
3. **Pointers and References:** We used pointers and references to efficiently pass the Sequence objects to the various processing and filtering algorithms.
4. **Function In-Lining:** We in-lined the most frequently used data processing and filtering functions (based on GProf statistics) in the Filter Factory, Filtering Sequence Iterator, Filter Set, Filter, Sequence, Sequence Iterator, FASTA Sequence Iterator, and Genbank Iterator classes.

Tuning: Disk Writing

Once the data processing enhancements were complete, we turned to the disk writing enhancements; here, the CSeqSpeed copy-and-paste, Cachegrind, GProf, and code adjustment methodology for tuning the data processing algorithms was similar to that of the data processing. Based on our analysis, we found that the following enhancements to CSeq significantly improved space and run-time performance in the disk writing domain:

1. **Output Buffering:** We adjusted the disk writing algorithms to export 2MB blocks to the PVFS file system (during data processing), so the total number of output file access requests were reduced.

3.3 Statistical Analysis Applications

In this section, we discuss the applications used to conduct k -mer-based experiments on NCBI genome and proteome sequences.

3.3.1 Rankseq: k -mer Arrangement and Classification

Summary

The Rankseq application calculates the Bayesian probability and composition statistics for a list of k -mers. The utility outputs ranked k -mer results in comma-separated columns, enabling the user to sort the arrangements in a spreadsheet program. Typically, the supplied list of k -mers are nullomers/primes.

- **Input:** A file containing a list of CSeq binary k -mer frequency files and a file containing a list of k -mers.

- **Configuration:** Operates on both DNA and AA sequences using a supplied integer subsequence partitioning length, p_{max} , where $1 \leq p_{max} < k$.
- **Output:** Rankable k -mer statistics.

Detail

Rankseq directly utilizes the CSeq output as input. The user supplies a set of k -mer sequences and the binary k -mer frequency count files to produce sequence ranking statistics for each k -mer in the list. For each k -mer, $\forall p$ where $1 \leq p \leq p_{max}$ subsequence partition lengths, Rankseq calculates the observed probability using Bayes theorem. For a description of this process, see the algorithm in Section B.2.

The column-valued output format presents one k -mer per row, with columns describing the statistical properties corresponding to each sequence. This utility is particularly useful for ranking the nullomer set pertaining to a particular set of organism genome sequences. Note that the output is used as input (both directly and indirectly) for the additional applications such as Histoseq (see Section 3.4.2) and Rangestat (see Section 3.4.1). For Rankseq usage, see the corresponding operation manual in A.3.1.

3.3.2 NcbiStat: Genome Sequence Summarization

Summary

NcbiStat calculates length statistics pertaining to a list of genome files by iterating over sequence records without actually processing the sequence data. The resulting output is used to setup and configure experiment tasks such as those listed in Chapter

4, which require these attributes to generate the appropriate Genesis cluster scripts and to optimize the object-oriented CSeq iterator as mentioned in Section 3.2.

- **Input:** A list of NCBI genome input files (either Genbank or FASTA records).
- **Configuration:** Operates on both DNA and AA sequences. Supports stream filtering.
- **Output:** Record statistics, such as the maximum, total, and average number of bytes associated with relevant record entries (i.e., meta data and data lengths, attribute lengths, etc.).

Detail

NcbiStat calculates and interprets various statistics regarding the sequence data and meta data associated with the observed Genbank and/or FASTA records. Upon completion, NcbiStat outputs the maximum, total, and average number of bytes associated with each type of entry in the supplied record format. This information is used not only to optimize various aspects of the CSeq iterator (see Section 3.2), but to determine the sequence size/length (in bytes) of the NCBI data subset itself—as these attributes are requisite to performing experiments (see Chapter 4). The size of the practical data set must be recorded and supplied as an argument to the Genseq utility to produce a sufficiently comparable artificial data set of precisely equivalent length.

For NcbiStat usage, see the corresponding operation manual in A.3.2.

3.3.3 Genseq: Artificial Sequence Generation

Summary

Genseq randomly generates an alphabet-specific (artificial genome) sequence of a specified particular length.

- **Input:** A list of CSeq binary k -mer frequency count files (optional).
- **Configuration:** Generates both DNA and AA sequences; capable of generating sequences with or without frequency bias.
- **Output:** CSeq-style binary k -mer frequency count files.

Detail

Genseq is capable of randomly generating artificial protein and nucleotide sequences with or without frequency bias. If the optional CSeq output is supplied as input, Genseq uses the relevant k -mer frequencies to induce bias in the generation process. To determine which k -mer length Genseq will use for the transitional probabilities, the user specifies the word length k . Genseq randomly populates sequence objects, where it subsequently processes each by using CSeq's modular Sequence Iterator and Factory framework. Therefore, Genseq's output is identical to that of CSeq.

For Genseq usage, see the corresponding operation manual in A.3.3.

3.3.4 Freqseq: Identifying the k -mer Frequency Spectra

Summary

Freqseq uses k -mer frequency statistics to generate a k -FS histogram and reports the results.

- **Input:** A file containing a list of CSeq binary k -mer frequency files.
- **Configuration:** Number of histogram bins n ; the maximum sequence motif length s ; the maximum frequency count m ; the alphabet type a .
- **Output:** A comma-separated value k -FS histogram.

Detail

Freqseq accepts as input a list of binary CSeq frequency files to produce the corresponding k -FS histogram by keeping track of the number of length- N sequences yielding a specific frequency count. These frequencies are then converted to transitional probabilities, normalized, and output in a (comma-separated value) histogram format.

For Freqseq usage, see the corresponding operation manual in A.3.4.

3.3.5 Nullcountseq: Nullomer Set Cardinality and Intersection Ratio

Summary

Nullcountseq calculates the size and overlap/intersection ratio of multiple nullomer/prime sets and reports the results.

- **Input:** A file containing a list of path names to nullomer files.
- **Configuration:** n/a
- **Output:** The nullomer count and overlap ratio results in a comma-separated value format.

Detail

Nullcountseq accepts a list of nullomer set files to determine the size and overlap ratio between each set. The input list has a specific ordering and can be automatically generated by the Scriptgen utility (see Section 3.4.4); the first file contains the real NCBI data nullomers, the subsequent files contain the statistically-generated (artificial data set) nullomers, and the final file contains the randomly-generated (artificial data set) nullomers. Furthermore, Nullcountseq calculates the average size and overlap between the nullomer sets. The objective is to compare and contrast the three types of nullomer sets.

The results are displayed in an $s \times n$ matrix comma-delimited format, where s is the maximum length of the nullomer sequence set and n is the number of data sets being compared/contrasted. For Nullcountseq usage, see the corresponding operation manual in A.3.5.

3.3.6 Predictseq: Prime Prediction

Summary

Predictseq attempts to predict which nullomer/prime sequences for a given month A are most likely to remain absent for the subsequent month B.

- **Input:** Rankseq output for the initial/first month; the nullomer/prime set for the final/next month.
- **Configuration:** Operation modes for training, testing, and prediction; machine learning parameters; ANN architecture.

- **Output:** Either a trained ANN configuration, a tested precision and accuracy, or the predicted nullomer set.

Detail

Predictseq comprises a highly customizable and flexible ANN, which may be trained to predict which nullomer/prime sequences are most likely to remain absent based on Rankseq's Bayesian probability and composition statistics for those sequences. A trained Predictseq network accepts chronologically ordered Rankseq output for months A and B, respectively, and uses the statistical properties associated with each nullomer/prime sequence listed in month B to deduce a hypothesis for month C. Predictseq supports three distinct supervised learning training algorithms. The fitness of a given network instance may be expressed in terms of nullomer/prime state prediction accuracy and therefore evaluated as such. During the training phase, the evolutionary state of the ANN at each generation is reported to the console.

Predictseq is intended for post-processing, which first compiles usable data sets for a specific NCBI snapshot from CSeq and Rankseq output. The utility is capable of compiling normalized, balanced data sets not only from a single month, but multiple months at once. The program determines which of the nullomers in the set for a particular month remain as such in the subsequent month(s), and which are finally observed.

Predictseq incorporates various supervised machine learning techniques in order to generalize and discriminate between each element in the nullomer set, based on previously observed statistical attributes. The prediction process effectively maps each subject motif to a binary classification based on these properties. Predictseq

measures its own accuracy and precision by tabulating the total number of correct and incorrect predictions.

The fitness of any given network instance is expressed as prediction accuracy. During training, the evolutionary state of the network and the prediction accuracy for each generation is calculated and exported to the state buffer as standard output. These attributes are appended to the state file (which utilizes disk I/O buffering and optimization routines), including the network's parameters, architecture, interconnected weight values, and overall fitness.

For testing and prediction, the ANN attempts to guess which nullomer/prime sequences in month A will remain in the absent state for month B. Here, Predictseq imports a trained network state file. By default, the final (and generally best fit) network state is loaded, however the user may pass an additional index parameter that indicates to the application the exact implicit network state they wish to load. For Predictseq usage, see the corresponding operation manual in A.3.6.

3.3.7 Tdataformat: Predictseq Data Set Formatting

Summary

The Tdataformat utility compiles a Predictseq-compatible data set from Rankseq and CSeq output for assessing the predictability of nullomer sequences.

- **Input:** A Rankseq output file (pertaining to month A nullomers) and a CSeq output file (pertaining to month B nullomers).
- **Configuration:** ANN data set formatting; minority oversampling.
- **Output:** A Predictseq-compatible data set.

Detail

All (training, testing, and prediction) data sets used by Predictseq are compiled using Tdataformat. In general, the Rankseq output corresponds to the set of ranked nullomer sequences for the initial month, namely A, whereas the CSeq output corresponds to the set of nullomer sequences for the subsequent month, namely B. Tdataformat determines which nullomers in A remain as such in month B and uses this information to construct a data set consisting of Boolean-state examples; nullomers in both months are assigned a 0, whereas the nullomers that transition to oligomers are assigned a 1. The Tdataformat data sets are intended for an ANN supervised learning methodology.

For Tdataformat usage, see the corresponding operation manual in A.3.7.

3.3.8 Tdatamerge: Predictseq Data Set Consolidation

Summary

The Tdatamerge utility consolidates a list of Tdataformat data sets to a single file.

- **Input:** A list of Tdataformat data sets.
- **Configuration:** n/a
- **Output:** A finalized (consolidated) Predictseq-compatible data set.

Detail

In order to train and/or test Predictseq on a specific time interval consisting of multiple months, the Tdataformat data sets corresponding to each month must be consolidated to a single file via Tdatamerge. Tdatamerge is a simple utility that

accepts a filename containing a list of Tdataformat data set path names as input to produce a single consolidated Predictseq-compatible data set as output. The utility automatically identifies the file format to update the header meta data and subsequently merges all training examples into the single file.

For Tdatamerge usage, see the corresponding operation manual in A.3.8.

3.3.9 34Seq: Nucleotide 3-mers, 4-mers, and GC Statistics

Summary

34Seq determines the number of triplets, quadruplets, and GC percentage for a supplied set of nucleotide k -mers.

- **Input:** A list of nucleotide k -mer sequences.
- **Configuration:** n/a
- **Output:** Number of k -mers analyzed; the triplet k -mers; the quadruplet k -mers; and GC-content statistics.

Detail

In the process of determining k -mer nucleotide statistics, 34Seq incorporates an efficient circular buffering system, which allows it to quickly analyze properties inherent to contiguous k -mer subsequences.

For 34Seq usage, see the corresponding operation manual in A.3.9.

3.3.10 SetStat: Default Accuracy and Prime Error Superset Reporting

Summary

Calculates the default accuracies and NCBI absent-sequence resubmission errors, given a filename list of nullomer/prime sets.

- **Input:** A filename list of nullomer/prime sequences.
- **Configuration:** n/a
- **Output:** Default accuracies; # negative examples; # positive examples; # nullomer/prime resubmission errors

Detail

SetStat accepts a filename list of nullomer/prime sequences and systematically calculates the default accuracies, the # of positive and negative examples, and the # of nullomer/prime resubmission errors. The # of nullomer/prime errors are the number of sequences absent in the latter month that are non-absent in the former month—a superset calculation. These errors arise due to NCBI database resubmissions. For SetStat usage, see the corresponding operation manual in A.3.10.

3.4 Format and Display Applications

In this section, we discuss the applications used to calculate output of the statistical analysis utilities in a normalized, comparable, spreadsheet-compatible format.

3.4.1 Rangestat: The Global Rankseq Range

Summary

Rangestat determines the global minimum/lower and maximum/upper probabilistic bounds given a list of Rankseq output ranges.

- **Input:** A file containing list of Rankseq output files.
- **Configuration:** Capable of operating on both oligomers and nullomers.
- **Output:** The global bounds.

Detail

For each Rankseq output file supplied in the input list, Rangestat iterates over each k -mer entry to calculate global lower and upper probabilistic bounds.

This utility is a prerequisite to the final (Histoseq output) result merging process carried out by Histoavg. Rangestat is a relatively simple application that loads in a list of Rankseq range values and determines the absolute upper and lower bounds on the value ranges. The resulting output is supplied as parametrized input to Histoseq to construct normalized, comparable histograms in the experimental phase (consider Section 4.3) to unify and/or average the histogram bin values requisite to the consolidation/merging process. For Rangestat usage, see the corresponding operation manual in A.4.1.

3.4.2 Histoseq: Histogram Compilation

Summary

Histoseq generates a histogram or set of histograms (in comma-separated value format) using the user-supplied Rankseq output file as a basis.

- **Input:** A Rankseq output file.
- **Configuration:** Global Rankseq range from p_{min} to p_{max} ; number of histogram bins b ; histogram title; auto-merge flag; normalize flag.
- **Output:** A histogram.

Detail

Histoseq transforms Rankseq statistical output to normalized histogram distributions that describe probabilistic trends pertaining to various k -mer attributes.

For Histoseq usage, see the corresponding operation manual in A.4.2.

3.4.3 Histoavg: Histogram Consolidation

Summary

Histoavg merges/consolidates a set of (uniform-sized) Histoseq-generated histograms.

- **Input:** A list of Histoseq histogram output files.
- **Configuration:** Histogram title; normalize flag.
- **Output:** A consolidated (Histoseq-formatted) histogram.

Detail

Histoavg merges a set of (uniformly-sized) histograms to produce a single, consolidated histogram, where the observed bin values are averaged in the final result with respect to the supplied global Rankseq ranges. For Histoavg usage, see the corresponding operation manual in A.4.3.

3.4.4 Scriptgen: Cluster Execution Script Generation

Summary

Scriptgen generates the Genesis cluster execution scripts for the k -FS analysis experiment (see Section 4.3).

- **Input:** An experiment-specific configuration file.
- **Configuration:** n/a
- **Output:** The set of cluster execution scripts.

Detail

Scriptgen uses the parameters in the supplied configuration file as a basis to generate the execution scripts. The complete configuration for such experiments is specified in a single file that is supplied as input to the program. Scriptgen generates a set of 13 command scripts each of a specific category (i.e., CSeq processing, CSeq reprocessing, Rankseq, Histoseq, Freqseq, etc.), which must be sequentially executed on the Genesis cluster in order to produce the desired results. The number of unique commands residing in each generated script is a function of the configuration parameters.

For Scriptgen usage, see the corresponding operation manual in A.4.4.

CHAPTER 4

RESULT AND ANALYSIS PHASE

4.1 Overview

In this chapter, we discuss and report the results for the *two* distinct k -mer-based computational experiments that are conducted on various subsets of the NCBI database (recall the software applications used to instrument this analysis in Chapter 3). The *first* experiment investigates the k -FS for a set of organism subjects, whereas the *second* experiment assesses prime predictability by chronologically analyzing complete monthly DNA snapshots of the NCBI database. Prior to discussing these results, we introduce a preliminary k -mer language that enables us to formally analyze and summarize our findings.

4.2 A Preliminary k -mer Language

4.2.1 Genetic Strings, Substrings, and k -mers

First, let us define the *genetic alphabets*

$$\Sigma_D = a, t, g, c \tag{4.1}$$

and

$$\Sigma_A = F, M, P, Y, N, E, R, L, V, T, H, K, C, G, I, S, A, Q, D, W \quad (4.2)$$

for base-4 DNA and base-20 AA symbols, respectively. We define a *genetic string* as a *contiguous discrete ordered sequence-set* of Σ_D or Σ_A symbols stored as an *array data structure*. Hence, we define ${}^D S$ and ${}^A S$ as the complete genome and proteome genetic strings for an arbitrary subject organism, respectively; ${}^D S$ and ${}^A S$ are expressed in the form

$${}^D S = (S_0, S_1, \dots, S_{|{}^D S|-1}) = \{S_0, S_1, \dots, S_{|{}^D S|-1}\} = {}^D S_{0,|{}^D S|-1}, \quad (4.3)$$

$${}^A S = (S_0, S_1, \dots, S_{|{}^A S|-1}) = \{S_0, S_1, \dots, S_{|{}^A S|-1}\} = {}^A S_{0,|{}^A S|-1}, \quad (4.4)$$

$\forall S_i \in {}^D S | {}^A S$, such that $S_i \in \Sigma_D | \Sigma_A$, where $|{}^D S|$ and $|{}^A S|$ denote the string length, set cardinality, and array size. From this, specifically for genomes, we define ${}^D S[i] = {}^D S_i$ as the DNA base at the i th index position of the genome ${}^D S$, such that ${}^D S_i \in \Sigma_D$, and define ${}^D S^{-1}[i] = {}^D S_i^{-1}$ as the complementary (nucleotide) base of ${}^D S_i$. Additionally, we define ${}^A S[i] = {}^A S_i$ as the AA base at the i th index position of the proteome ${}^A S$, such that ${}^A S_i \in \Sigma_A$. For convenience of definition, let S generalize ${}^D S$ and ${}^A S$. So we define

$$S[i, k] = (S_i, \dots, S_{i+k-1}) = \{S_i, \dots, S_{i+k-1}\} = S_{i,k} \quad (4.5)$$

as the length- k (or equivalently length- $|S_{i,k}|$) *genetic substring* starting at the i th index position of S , such that $S_{i,k} \subset S$, where $0 \leq i < (i+k) < |S|$. Specifically for genomes, we define

$${}^D S^{-1}[i, i, k] = (S_{i+k-1}^{-1}, \dots, S_i^{-1}) = \{S_{i+k-1}^{-1}, \dots, S_i^{-1}\} = S_{i,k}^{-1} \quad (4.6)$$

as the length- k *reverse complement genetic substring* at the i th index position of the genome ${}^D S$ corresponding to $S_{i,k}$. We may imagine ${}^D S$ and ${}^D S^{-1}$ as being arranged in the DNA double helix of two distinct and complementary one-dimensional lattices. The lattice concept is generalized to arbitrary genetic substrings ${}^D S_{i,k}$ and ${}^D S_{i,k}^{-1}$, which clearly arrange to sub-lattices. Next, we define Σ_{D_k} as the k -mer genome vocabulary for $1 \leq k < |{}^D S|$, such that

$$\Sigma_{D_1} = \{a, t, g, c\}, |\Sigma_{D_1}| = |\Sigma_D|^1 = 4^1, \quad (4.7)$$

$$\Sigma_{D_2} = \{aa, \dots, cc\}, |\Sigma_{D_2}| = |\Sigma_D|^2 = 4^2, \quad (4.8)$$

$$\dots = \dots, \quad (4.9)$$

$$\Sigma_{D_k} = \{\dots\}, |\Sigma_{D_k}| = |\Sigma_D|^k = 4^k, \quad (4.10)$$

and we define Σ_{A_k} as the k -mer proteome vocabulary for $1 \leq k < |{}^A S|$, such that

$$\Sigma_{A_1} = \{F, \dots, W\}, |\Sigma_{A_1}| = |\Sigma_A|^1 = 20^1, \quad (4.11)$$

$$\Sigma_{A_2} = \{FF, \dots, WW\}, |\Sigma_{A_2}| = |\Sigma_A|^2 = 20^2, \quad (4.12)$$

$$\dots = \dots, \quad (4.13)$$

$$\Sigma_{A_k} = \{\dots\}, |\Sigma_{A_k}| = |\Sigma_A|^k = 20^k. \quad (4.14)$$

Therefore, we label $S_{i,k} \in \Sigma_{D_k} | \Sigma_{A_k}$ as the k -mer (substring) at the i th position index of S .

4.2.2 Superregions, Regions, and Subregions

Here, we formally define specific regions within an arbitrary organism genome ${}^D S$. For notational simplicity, let ${}^D S = S$. In the Genbank version of the NCBI genome

database, a distinct *region* of S is defined as a discrete ordered sequence-set of *subregions*, where a subregion (element) is a contiguous substring of S . We define the *superregion* of S as a discrete ordered sequence-set of all regions for a specific type. There are different *region types*, which we label as τ , with distinct structure and function, which interconnect and interrelate across S in various ways. For example, Genbank records identify coding regions, non-coding regions, gene regions, promoter regions, and many others—the CSeq filtering system is designed to screen for and process such τ . Regions and subregions may or may not intersect/overlap. For this thesis, our genome analysis specifically investigates the complete regions (unfiltered), coding regions (filtered), and non-coding regions (filtered), which we label as $\tau = ALL$, $\tau = CDS$, and $\tau = -CDS$, respectively.

First, we define a the n th subregion of the m th region of S of region type τ as $R_S^\tau[m][n]$ in the form

$$R_S^\tau[m][n] = S_{i_n, j_n}, \quad (4.15)$$

such that $0 \leq i_n < (i_n + j_n) < |S|$, where $R_S^\tau[m][n] \subset S$ is simply a length- j (or equivalently a length- $|R_S^\tau[m][n]|$) genetic substring of S , but is identified by NCBI as having a specific genetic structure and/or performing a specific genetic function for the organism such as gene expression or gene regulation. Second, we define the m th region of S of region type τ as $R_S^\tau[m]$, which is a discrete ordered sequence-set of subregions in the form

$$R_S^\tau[m] = \bigcup_n R_S^\tau[m][n], \quad (4.16)$$

such that the *region length*

$$|R_S^\tau[m]| = \sum_n |R_S^\tau[m][n]| \quad (4.17)$$

is the concatenated sum of all subregion lengths, and the *region cardinality* $||R_S^\tau[m]||$ is the number of subregions in the set. Third, we define the superregion of S of region type τ as R_S^τ , which is a discrete ordered sequence-set of regions in the form

$$R_S^\tau = \bigcup_m R_S^\tau[m], \quad (4.18)$$

where the *superregion length*

$$|R_S^\tau| = \sum_m |R_S^\tau[m]| \quad (4.19)$$

is the concatenated sum of all region lengths, and the *superregion cardinality* $||R_S^\tau||$ is the number of regions in the set. From this, we can define a range of (ordered) subregions within $R_S^\tau[m]$ as

$$R_S^\tau[m][n_0, n_l] = \bigcup_{i=n_0}^{n_l} R_S^\tau[m][i], \quad (4.20)$$

where $[n_0, n_l]$ is the *subregion range*, and similarly a range of (ordered) regions within R_S^τ as

$$R_S^\tau[m_0, m_l] = \bigcup_{j=m_0}^{m_l} R_S^\tau[j], \quad (4.21)$$

where $[m_0, m_l]$ is the *region range*.

4.2.3 k -mers: Frequency, Boolean Observed State, and Probability

We let the string λ as an arbitrary superregion, region, subregion, substring of the genome or proteome string S such that $0 < |\lambda| \leq |S|$. We define the abstract function $F(s_k, \lambda)$ as the (CSeq calculated) frequency of the k -mer $s \in \Sigma_{D_k} | \Sigma_{A_k}$ such that $s \subset \lambda$,

where $F(s_i, \lambda)$ is a non-negative integer. Next, we define the function $B(s, \lambda)$ as the observed state of the k -mer s_i in λ , where $B(s_i, \lambda)$ is a Boolean value, such that

$$B(s_i, \lambda) = \begin{cases} 1 & \text{if } F(s_i, \lambda) > 0, \\ 0 & \text{if } F(s_i, \lambda) = 0, \end{cases} \quad \forall s_i \in \Sigma_{D_k} | \Sigma_{A_k}. \quad (4.22)$$

So we define an observed (non-absent) k -mer as a k -oligomer and a non-observed (absent) k -mer as a k -nullomer/ k -prime. Next, we define ${}^1B_k^\lambda$ as the alphabetically-ordered set of all k -oligomers observed in λ by CSeq in the form

$${}^1B_k^\lambda = \bigcup_{s_i \in \Sigma_{D_k} | \Sigma_{A_k}} s_i | (B(s_i, \lambda) = 1), \quad (4.23)$$

where $(B(s_i, \lambda) = 1)$ is the Boolean oligomer constraint for the *observed state*. Subsequently, we define ${}^0B_k^\lambda$ as the alphabetically-ordered set of all k -nullomers not-observed in λ by CSeq in the form

$${}^0B_k^\lambda = \bigcup_{s_i \in \Sigma_{D_k} | \Sigma_{A_k}} s_i | (B(s, \lambda) = 0), \quad (4.24)$$

where $(B(s_i, \lambda) = 0)$ is the Boolean prime/nullomer constraint for the *absent state*.

So clearly

$${}^1B_k^\lambda \cap {}^0B_k^\lambda = \emptyset, \quad (4.25)$$

$${}^1B_k^\lambda \cup {}^0B_k^\lambda = \Sigma_{D_k} | \Sigma_{A_k}, \quad (4.26)$$

and therefore

$$|{}^1B_k^\lambda| + |{}^0B_k^\lambda| = |\Sigma|, \quad (4.27)$$

such that Σ is either Σ_{D_k} or Σ_{A_k} , where $|{}^1B_k^\lambda|$ and $|{}^0B_k^\lambda|$ are the k -oligomer and k -nullomer set cardinalities, respectively. So $|{}^1B_k^\lambda[j]|$ and $|{}^0B_k^\lambda[j]|$ are the j th k -oligomer and j th k -nullomer, where $0 \leq j < |{}^1B_k^\lambda|$ and $0 \leq j < |{}^0B_k^\lambda|$, respectively.

Next, we define the function $F_{total}(D_k|A_k, \lambda)$ as the (CSeq calculated) total frequency of all k -mers $s_j \in \Sigma_{D_k}|\Sigma_{A_k}$ observed in λ as

$$F_{total}(D_k|A_k, \lambda) = \sum_{s_j \in \Sigma_{D_k}|\Sigma_{A_k}} F(s_j, \lambda) \quad (4.28)$$

Subsequently, we define the function $P(s_i, \lambda)$ as the (CSeq calculated) probability of the k -mer s_i in λ , with respect to the total frequency of all k -mers $s_j \in \Sigma_{D_k}|\Sigma_{A_k}$ observed in λ as is the total frequency of all k -mers of $\Sigma_{D_k}|\Sigma_{A_k}$, such that $|\Sigma_k|$ is either $|D_k|$ or $|A_k|$, where

$$P(s_i, \lambda) = \frac{F(s_i, \lambda)}{F_{total}(D_k|A_k, \lambda)}, \quad \forall \Sigma_{D_k}|\Sigma_{A_k}, \quad (4.29)$$

so $P(s_i, \lambda)$ is a rational number and thus a fractional statistic. Thus, we define P_k^λ as the probability-ordered set of all k -mer probabilities in λ as

$$P_k^\lambda = \bigcup_{s_i \in \Sigma_{D_k}|\Sigma_{A_k}} P(s_i, \lambda), \quad (4.30)$$

so $P_k^\lambda[i]$ is the probability of the i th k -mer, where $0 \leq i < |P_k^\lambda|$.

Furthermore, we define the function $Q(s_i, \rho, \lambda)$ as the (Rankseq calculated) probability of the k -nullomer s_i in ${}^0B_k^\lambda$, where ρ is the partition length. Hence, we define ${}^0Q_{k,\rho}^\lambda$ as the probability ordered set of all k -nullomer (Rankseq) probabilities for λ , as

$${}^0Q_{k,\rho}^\lambda = \bigcup_{s_i \in {}^0B_k^\lambda} Q(s_i, \rho, \lambda), \quad (4.31)$$

so ${}^0Q_{k,\rho}^\lambda[i]$ is the i th Rankseq probability, such that $0 \leq i < |{}^0Q_{k,\rho}^\lambda|$.

Additionally, we define the function $\Gamma({}^1B_k^\lambda, i)$ as the (Freqseq calculated) number of k -oligomers in the set B_k^λ with a (non-negative integer) frequency of f . Thus, we have the entire k -FS of $0 \leq f \leq f_{Max}$, where f_{Max} is the maximum frequency. Therefore, we define Γ_k^λ as the frequency-ordered set of all k -oligomer frequencies in the spectral-range $[0, f_{Max}]$, such that

$$\Gamma_k^\lambda = \bigcup_{f=0}^{f_{Max}} \Gamma(B_k^\lambda, f), \quad (4.32)$$

so $\Gamma_k^\lambda[f]$ is the number of k -oligomers with a frequency of f .

Moreover, we define the function $H(\varrho, h_{Min}, h_{Max}, h_{Bins})$ as the (Histoseq calculated) histogram, an ordered set of bin-values for the numerical ordered set ϱ of Rankseq probabilities, where h_{Min} is the minimum histogram value, h_{Max} is the maximum histogram value, and h_{Bins} is the number of bins in the histogram. In this case, we define $\varrho = {}^0Q_{k,\rho}^\lambda$, so $H({}^0Q_{k,\rho}^\lambda, \min({}^0Q_{k,\rho}^\lambda), \max({}^0Q_{k,\rho}^\lambda), h_{Bins})$ is the histogram for the k -nullomer Rankseq probabilities of λ , where h_{Bins} is selected by the user. Thus, we have

$$H[{}^0Q_{k,\rho}^\lambda] = H({}^0Q_{k,\rho}^\lambda, \min({}^0Q_{k,\rho}^\lambda), \max({}^0Q_{k,\rho}^\lambda), h_{Bins}), \quad (4.33)$$

so $H[{}^0Q_{k,\rho}^\lambda][i]$ is the value of the i th histogram bin, such that $0 \leq i < |H[{}^0Q_{k,\rho}^\lambda]|$, where $h_{Bins} = |H[{}^0Q_{k,\rho}^\lambda]|$ is the cardinality.

4.3 Experiment 1: Organism k -mer Frequency Spectra and Nullomer Sequence Investigation

4.3.1 Objective Summary

Here we seek answers to the following inquiries:

1. Do the k -FS for complete organism AA sequences exhibit evidence of (1) structural bias or (2) randomness?
2. Is there a quantifiable distinction between (1) the *naturally-evolved* sequences housed at NCBI and (2) the *randomly-biased* and *randomly-unbiased artificially-generated* sequences compiled by our software? Can we draw a quantifiable distinction between the nullomer set cardinalities and overlap ratios for these data sets?

Thus, this procedure identifies the following respective objectives:

1. To calculate the k -FS for the naturally-evolved subject sequence(s); to determine the naturally-evolved nullomer set(s); to rank the naturally-evolved nullomers and store the associated statistics for comparison.
2. To calculate the k -FS for the randomly-biased artificially-generated subject sequences; to determine the randomly-biased artificially-generated nullomer set(s); to rank the randomly-biased artificially-generated nullomers and store the associated statistics for comparison.
3. To calculate the k -FS for the randomly-unbiased artificially-generated subject sequences; to determine the randomly-unbiased artificially-generated nullomer

set(s); to rank the randomly-unbiased artificially-generated nullomers and store the associated statistics for comparison.

4. To compare and contrast the k -FS histogram distributions for the three distinct sequence categories, namely the naturally-evolved, randomly-biased artificially-generated, and randomly-unbiased artificially-generated sequences.
5. To compare and contrast the nullomer ranking histogram distributions and the nullomer set cardinalities and intersection statistics for the three sequence categories.
6. To calculate the chi-square for the three sequence categories to determine the degree to which the *final* histogram results for the k -FS and nullomer statistics deviate from a truly random histogram distribution.

The naturally-evolved data sets are denoted as \mathbb{N} . The randomly-biased artificially-generated data sets for length- k statistics are denoted as \mathbb{A}_B^k . The randomly-biased artificially-generated data sets are denoted as \mathbb{A}_U .

4.3.2 Ten Model Organism Results and Analysis

This section reports the AA k -FS analysis results obtained from conducting this experiment on ten model organism subjects. For the data set statistics comparisons, there are two result categories: (1) the nullomers and (2) the oligomers. There are three types of nullomer results: (1) the chi-squares for the ranking histograms, (2) the nullomer set cardinalities, and (3) the nullomer set intersection ratios. The single type of oligomer results form a bounded k -FS distribution and are displayed as such. Note: Consult D.2 for a graphical depiction of (1) the nullomer ranking histograms and (2) the k -FS oligomer histograms.

Tables 4.1 and 4.2 display the experimental parameters for the Scriptgen utility used to generate scripts for the ten model organism subjects (note: the listed variables do not include the system-specific path names for the Linux file system).

Table 4.3 displays the 4-nullomer set cardinality and intersection ratio statistics for comparison between the three data set categories. There are three lengths for the \mathbb{N} data sets. For all organisms, except for *Apis mellifera*, the \mathbb{N} 4-nullomer set cardinalities are greater than those of the \mathbb{A}_B and \mathbb{A}_U sequences. Moreover, for all organisms, the \mathbb{A}_U 4-nullomer set cardinalities and intersection ratios are zero, and are therefore less than those of the \mathbb{N} and \mathbb{A}_B . Furthermore, for all organisms, except for *Apis mellifera* and *Bos taurus*, the \mathbb{A}_B^1 and \mathbb{A}_B^3 nullomer sets and intersection ratios are greater than those of the \mathbb{A}_B^2 . Additionally, for all organisms except *Homo sapien* and *Stronglyocentrotus purpuratus*, the \mathbb{A}_B^1 intersection ratios are greater than those of the \mathbb{A}_B^3 . To summarize, the \mathbb{N} sequences exhibit the most nullomers and the \mathbb{A}_U exhibit the least nullomers, which implies that the \mathbb{N} sequences are non-random.

Table 4.4 displays the 5-nullomer set cardinality and intersection ratio statistics for comparison between the three sequence categories. There are three lengths for the \mathbb{A}_B data sets. For all organisms, the \mathbb{N} 5-nullomer set cardinalities are greater than those of the \mathbb{A}_B and \mathbb{A}_U . Moreover, for all organisms, the \mathbb{A}_U 5-nullomer set cardinalities and intersection ratios are less than those of the \mathbb{A}_B . Finally, for all organisms, the \mathbb{A}_B 5-nullomer set cardinalities and intersection ratios increase as the partitioning length increases. To summarize, the \mathbb{N} sequences exhibit the most nullomers and the \mathbb{A}_U exhibit the least nullomers, which implies that the \mathbb{N} sequences are non-random.

Table 4.5 displays the chi-squares for Rankseq's 5-nullomer probability histograms. For all organisms and histograms, the \mathbb{A}_U chi-squares are the greatest. Moreover, for all organisms and histograms, the \mathbb{N} chi-squares are the smallest. This suggests that

the \mathbb{N} sequences are non-random. Furthermore, for all organisms and $P(1)$ histograms, the \mathbb{A}_B chi-squares decrease as the partition length increases. Additionally, for all organisms, the chi-squares monotonically increase with the histogram partition length. Moreover, for all organisms and histograms, except for *Pan troglodytes* and *Stronglyocentrotus purpuratus*, the \mathbb{A}_B^1 chi-squares monotonically increase with the histogram partition length. Furthermore, for all organisms and histograms, the \mathbb{A}_B^2 and \mathbb{A}_B^3 chi-squares monotonically increase with the histogram partition length. Finally, for all organisms and histograms, the \mathbb{A}_U chi-squares monotonically decrease with the histogram partition length.

Table 4.6 displays the chi-squares for the 3-FS, 4-FS, and 5-FS, with the frequency spectral-range $[0, 10000]$. For all organisms and 3-FS histograms, the \mathbb{N} chi-squares are greater than the \mathbb{A}_B and less than the randomly-unbiased. Moreover, for all organisms and 4-FS histograms, the \mathbb{N} chi-squares are greater than or equal to the \mathbb{A}_B and less than the \mathbb{A}_U . Furthermore, for all organisms and 5-FS histograms, except for *Danio rerio* and *Gallus gallus*, the \mathbb{N} chi-squares are less than the \mathbb{A}_B and \mathbb{A}_U . Additionally, for all organisms, the \mathbb{N} , \mathbb{A}_B , and \mathbb{A}_U chi-squares increase with the histogram k -mer length (and all of these increases follow the magnitude orders 10^{-3} , 10^{-2} , and 10^{-1} , respectively, except for the \mathbb{N} and \mathbb{A}_B of *Apis mellifera*, the \mathbb{N} of *Gallus gallus*, and the \mathbb{A}_U of all organisms).

Figures 4.1, 4.2, 4.3, 4.4, and 4.5 are depictions of the 3-FS \mathbb{N} results of Table 4.6, which compare pairs of model organisms. In Table 4.7, we see an analysis summary of these distributions. Interestingly, *Apis mellifera* has a significantly higher standard deviation, skew, and kurtosis than the rest of the organisms: the standard deviation (0.0136) and kurtosis (9.856) are distinct by at least one magnitude order. So the honey bee's 3-FS distribution is concentrated to a much broader range than the rest

of the organisms, by one or more magnitude orders. Furthermore, all of the organisms exhibit a positive skew, where *Pan troglodytes* and *Canis familiaris* are the closest to a symmetric distribution. Moreover, *Mus musculus* and *Rattus norvegicus* exhibit remarkably similar values, and have more in common than *Homo sapiens* and *Pan troglodytes*.

Table 4.1: The ten model organism’s AA k -FS analysis configuration

Variable	Value	Affected Program
ncbi_filter	NULL	Cseq
sequence_type	PROTEIN	Cseq
sequence_length	5	Cseq
subsequence_partition_length	3	Rankseq
num_histogram_bins	50	Histoseq
num_dataset_instances	30	Genseq
maximum_count	10000	Freqseq
maximum_sequence_length	5	Freqseq
freqseq_num_histogram_bins	200	Freqseq
normalize	yes	Freqseq

Table 4.2: The ten model organism’s AA k -FS data sets. The total sequence length $|S|$ is used for the Genseq’s “generation_size”

Organism	S	$ S $
<i>Apis mellifera</i>	$S_{Honeybee}$	4,729,600
<i>Bos taurus</i>	S_{Cattle}	18,079,281
<i>Canis familiaris</i>	S_{Dog}	18,079,281
<i>Danio rerio</i>	$S_{Zebrafish}$	14,550,756
<i>Gallus gallus</i>	$S_{Chicken}$	18,079,281
<i>Homo sapien</i>	S_{Human}	18,177,144
<i>Mus musculus</i>	S_{Mouse}	15,318,155
<i>Pan troglodytes</i>	S_{Chimp}	25,293,637
<i>Rattus norvegicus</i>	S_{Rat}	15,335,472
<i>Strongylocentrotus purpuratus</i>	$S_{SeaUrchin}$	18,126,260

The conclusions of this experiment are discussed in Section 5.1.

Table 4.3: The ten model organism's AA 4-nullomer set cardinality and intersection ratio comparisons for statistics with length-3 subsequence partitioning

S	N	\mathbb{A}_B^1	\mathbb{A}_B^2	\mathbb{A}_B^3	\mathbb{A}_U
$S_{Honeybee}$	1,561	1,743 (0.243)	1,593 (0.22)	1,564 (0.236)	0 (0)
S_{Cattle}	323	90 (0.056)	72 (0.055)	69 (0.045)	0 (0)
S_{Dog}	295	111 (0.069)	72 (0.055)	80 (0.061)	0 (0)
$S_{Zebrafish}$	265	149 (0.094)	105 (0.08)	111 (0.085)	0 (0)
$S_{Chicken}$	500	81 (0.037)	51 (0.027)	52 (0.029)	0 (0)
S_{Human}	307	82 (0.059)	63 (0.05)	72 (0.06)	0 (0)
S_{Mouse}	267	127 (0.084)	112 (0.078)	113 (0.074)	0 (0)
S_{Chimp}	333	38 (0.028)	25 (0.021)	25 (0.021)	0 (0)
S_{Rat}	317	136 (0.092)	107 (0.079)	112 (0.082)	0 (0)
$S_{SeaUrchin}$	660	104 (0.052)	82 (0.04)	92 (0.053)	0 (0)

Table 4.4: The ten model organism's AA 5-nullomer set cardinality and intersection ratio comparisons for statistics with length-3 subsequence partitioning

S	N	\mathbb{A}_B^1	\mathbb{A}_B^2	\mathbb{A}_B^3	\mathbb{A}_U
$S_{Honeybee}$	1,406,806	1,308,004 (0.592)	1,337,026 (0.604)	1,351,266 (0.610)	729,948 (0.227)
S_{Cattle}	889,311	483,492 (0.339)	499,870 (0.351)	508,388 (0.367)	11,259 (0.0035)
S_{Dog}	871,822	489,280 (0.346)	499,949 (0.355)	505,585 (0.358)	11,259 (0.003)
$S_{Zebrafish}$	773,570	547,739 (0.398)	565,385 (0.408)	577,894 (0.416)	33,892 (0.01)
$S_{Chicken}$	1,032,173	460,523 (0.3)	475,562 (0.312)	477,204 (0.313)	11,259 (0.003)
S_{Human}	844,289	470,045 (0.339)	486,045 (0.35)	494,015 (0.357)	10,917 (0.003)
S_{Mouse}	833,695	543,160 (0.381)	563,667 (0.395)	575,338 (0.402)	26,669 (0.008)
S_{Chimp}	904,114	338,880 (0.253)	348,609 (0.261)	351,717 (0.264)	1,192 (0.0003)
S_{Rat}	859,661	554,064 (0.381)	573,354 (0.394)	581,061 (0.4)	26,525 (0.008)
$S_{SeaUrchin}$	1,042,842	445,165 (0.298)	463,811 (0.308)	474,058 (0.315)	11,093 (0.003)

Table 4.5: The ten model organism's AA 5-nullomer ranking histogram chi-square comparisons for statistics with length-3 subsequence partitioning

S	Histogram	N	\mathbb{A}_B^1	\mathbb{A}_B^2	\mathbb{A}_B^3	\mathbb{A}_U
$S_{Honeybee}$	$H[{}^0Q_{5,1}^{S_{Honeybee}}]$	0.1894	0.2127	0.2083	0.2032	0.98
$S_{Honeybee}$	$H[{}^0Q_{5,2}^{S_{Honeybee}}]$	0.1997	0.2128	0.2183	0.2113	0.9317
$S_{Honeybee}$	$H[{}^0Q_{5,3}^{S_{Honeybee}}]$	0.2055	0.2143	0.2199	0.2205	0.5082
S_{Cattle}	$H[{}^0Q_{5,1}^{S_{Cattle}}]$	0.2861	0.4876	0.4566	0.4344	0.98
S_{Cattle}	$H[{}^0Q_{5,2}^{S_{Cattle}}]$	0.3062	0.4878	0.4872	0.4580	0.98
S_{Cattle}	$H[{}^0Q_{5,3}^{S_{Cattle}}]$	0.3147	0.4898	0.4892	0.4904	0.7570
S_{Dog}	$H[{}^0Q_{5,1}^{S_{Dog}}]$	0.1613	0.2837	0.2674	0.2543	0.9796
S_{Dog}	$H[{}^0Q_{5,2}^{S_{Dog}}]$	0.1720	0.2838	0.2789	0.2627	0.6842
S_{Dog}	$H[{}^0Q_{5,3}^{S_{Dog}}]$	0.1755	0.2851	0.2802	0.2801	0.4781
$S_{Zebrafish}$	$H[{}^0Q_{5,1}^{S_{Zebrafish}}]$	0.2089	0.2928	0.2765	0.2629	0.98
$S_{Zebrafish}$	$H[{}^0Q_{5,2}^{S_{Zebrafish}}]$	0.2226	0.2928	0.2935	0.2758	0.9443
$S_{Zebrafish}$	$H[{}^0Q_{5,3}^{S_{Zebrafish}}]$	0.2290	0.2944	0.2949	0.2967	0.5161
$S_{Chicken}$	$H[{}^0Q_{5,1}^{S_{Chicken}}]$	0.1561	0.3112	0.2931	0.2812	0.9799
$S_{Chicken}$	$H[{}^0Q_{5,2}^{S_{Chicken}}]$	0.1678	0.3113	0.3093	0.2939	0.7662
$S_{Chicken}$	$H[{}^0Q_{5,3}^{S_{Chicken}}]$	0.1712	0.3129	0.3108	0.3081	0.5528
S_{Human}	$H[{}^0Q_{5,1}^{S_{Human}}]$	0.2646	0.4431	0.4180	0.3972	0.98
S_{Human}	$H[{}^0Q_{5,2}^{S_{Human}}]$	0.2829	0.4436	0.4433	0.4159	0.98
S_{Human}	$H[{}^0Q_{5,3}^{S_{Human}}]$	0.2911	0.4456	0.4453	0.4452	0.8722
S_{Mouse}	$H[{}^0Q_{5,1}^{S_{Mouse}}]$	0.2605	0.3887	0.3686	0.3502	0.98
S_{Mouse}	$H[{}^0Q_{5,2}^{S_{Mouse}}]$	0.2788	0.3890	0.3913	0.3680	0.9799
S_{Mouse}	$H[{}^0Q_{5,3}^{S_{Mouse}}]$	0.2872	0.3909	0.3932	0.3955	0.8131
S_{Chimp}	$H[{}^0Q_{5,1}^{S_{Chimp}}]$	0.1874	0.4256	0.4013	0.3819	0.98
S_{Chimp}	$H[{}^0Q_{5,2}^{S_{Chimp}}]$	0.2010	0.4255	0.4210	0.3970	0.98
S_{Chimp}	$H[{}^0Q_{5,3}^{S_{Chimp}}]$	0.2055	0.4274	0.4229	0.4219	0.9249
S_{Rat}	$H[{}^0Q_{5,1}^{S_{Rat}}]$	0.1673	0.2574	0.2426	0.2316	0.98
S_{Rat}	$H[{}^0Q_{5,2}^{S_{Rat}}]$	0.1799	0.2575	0.2575	0.2432	0.9799
S_{Rat}	$H[{}^0Q_{5,3}^{S_{Rat}}]$	0.1843	0.2588	0.2588	0.2586	0.7196
$S_{SeaUrchin}$	$H[{}^0Q_{5,1}^{S_{SeaUrchin}}]$	0.1624	0.3378	0.3199	0.3020	0.98
$S_{SeaUrchin}$	$H[{}^0Q_{5,2}^{S_{SeaUrchin}}]$	0.1727	0.3376	0.3411	0.3171	0.98
$S_{SeaUrchin}$	$H[{}^0Q_{5,3}^{S_{SeaUrchin}}]$	0.1789	0.3393	0.3428	0.3434	0.8002

Table 4.6: The ten model organism's 3-FS, 4-FS, and 5-FS histogram chi-square comparisons for the $[0, 10000]$ frequency spectral-range

S	Histogram	N	\mathbb{A}_B^1	\mathbb{A}_B^2	\mathbb{A}_B^3	\mathbb{A}_U
$S_{Honeybee}$	$\Gamma_3^{S_{Honeybee}}$	0.0038	0.0026	0.0035	0.0036	0.2058
$S_{Honeybee}$	$\Gamma_4^{S_{Honeybee}}$	0.3084	0.2905	0.2988	0.3041	0.8571
$S_{Honeybee}$	$\Gamma_5^{S_{Honeybee}}$	0.9761	0.9797	0.9792	0.9780	0.98
S_{Cattle}	$\Gamma_3^{S_{Cattle}}$	0.0036	0.0030	0.0032	0.0032	0.0200
S_{Cattle}	$\Gamma_4^{S_{Cattle}}$	0.0770	0.0702	0.0739	0.0757	0.4579
S_{Cattle}	$\Gamma_5^{S_{Cattle}}$	0.8321	0.8693	0.8628	0.8624	0.9800
S_{Dog}	$\Gamma_3^{S_{Dog}}$	0.0078	0.0028	0.0030	0.003	0.02
S_{Dog}	$\Gamma_4^{S_{Dog}}$	0.0274	0.0691	0.0727	0.0744	0.4579
S_{Dog}	$\Gamma_5^{S_{Dog}}$	0.5643	0.8690	0.8633	0.864	0.98
$S_{Zebrafish}$	$\Gamma_3^{S_{Zebrafish}}$	0.0031	0.0030	0.0026	0.0026	0.02
$S_{Zebrafish}$	$\Gamma_4^{S_{Zebrafish}}$	0.0941	0.0871	0.0905	0.0925	0.5201
$S_{Zebrafish}$	$\Gamma_5^{S_{Zebrafish}}$	0.8927	0.9231	0.9145	0.9099	0.98
$S_{Chicken}$	$\Gamma_3^{S_{Chicken}}$	0.0021	0.0032	0.0034	0.0035	0.02
$S_{Chicken}$	$\Gamma_4^{S_{Chicken}}$	0.1702	0.0685	0.0720	0.0736	0.4579
$S_{Chicken}$	$\Gamma_5^{S_{Chicken}}$	0.9490	0.8754	0.8686	0.8686	0.98
S_{Human}	$\Gamma_3^{S_{Human}}$	0.0038	0.0032	0.0033	0.0033	0.02
S_{Human}	$\Gamma_4^{S_{Human}}$	0.0753	0.0690	0.0725	0.0744	0.4533
S_{Human}	$\Gamma_5^{S_{Human}}$	0.8307	0.8704	0.8642	0.8635	0.98
S_{Mouse}	$\Gamma_3^{S_{Mouse}}$	0.0029	0.0027	0.0027	0.0027	0.02
S_{Mouse}	$\Gamma_4^{S_{Mouse}}$	0.0916	0.0842	0.0878	0.0898	0.4667
S_{Mouse}	$\Gamma_5^{S_{Mouse}}$	0.8728	0.9072	0.8986	0.8953	0.98
S_{Chimp}	$\Gamma_3^{S_{Chimp}}$	0.0050	0.0045	0.0046	0.0044	0.02
S_{Chimp}	$\Gamma_4^{S_{Chimp}}$	0.0489	0.0448	0.0476	0.0489	0.3822
S_{Chimp}	$\Gamma_5^{S_{Chimp}}$	0.7071	0.7815	0.7820	0.7863	0.9796
S_{Rat}	$\Gamma_3^{S_{Rat}}$	0.0031	0.0026	0.0027	0.0027	0.02
S_{Rat}	$\Gamma_4^{S_{Rat}}$	0.0921	0.0847	0.0886	0.0905	0.4654
S_{Rat}	$\Gamma_5^{S_{Rat}}$	0.8715	0.9046	0.8960	0.8938	0.98
$S_{SeaUrchin}$	$\Gamma_3^{S_{SeaUrchin}}$	0.0032	0.0035	0.0029	0.0029	0.02
$S_{SeaUrchin}$	$\Gamma_4^{S_{SeaUrchin}}$	0.0704	0.0649	0.0673	0.069	0.4557
$S_{SeaUrchin}$	$\Gamma_5^{S_{SeaUrchin}}$	0.8226	0.8837	0.8752	0.8718	0.98

Table 4.7: The analysis summary of the ten model organism 3-FS distributions in Figures 4.1, 4.2, 4.3, 4.4, and 4.5

S/R^τ	Standard Deviation	Skewness	Kurtosis
$S_{Honeybee}$	0.0136	3.223	9.856
S_{Cattle}	0.006	1.302	0.410
S_{Dog}	0.003	0.407	-1.119
$S_{Zebrafish}$	0.007	0.792	0.792
$S_{Chicken}$	0.009	2.278	0.041
S_{Human}	0.006	1.293	0.421
S_{Mouse}	0.007	1.469	0.920
S_{Chimp}	0.005	0.859	-0.623
S_{Rat}	0.007	1.507	1.072
$S_{SeaUrchin}$	0.006	1.093	-0.073

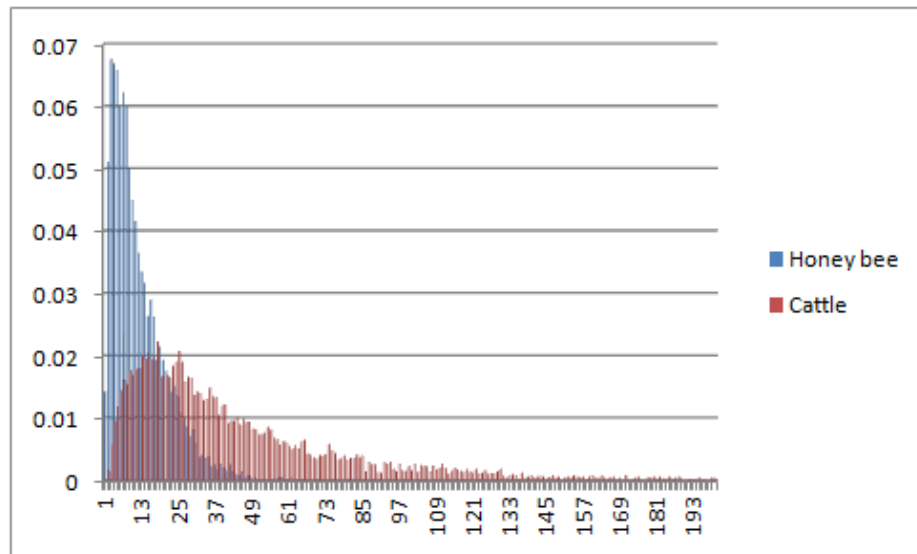


Figure 4.1: Apis mellifera vs. Bos taurus: The $\Gamma_3^{S_{Honeybee}}$ and $\Gamma_3^{S_{Cattle}}$ comparison with a frequency spectral-range $[0, 10000]$ for \mathbb{N} data sets (only $[0, 200]$ is shown)

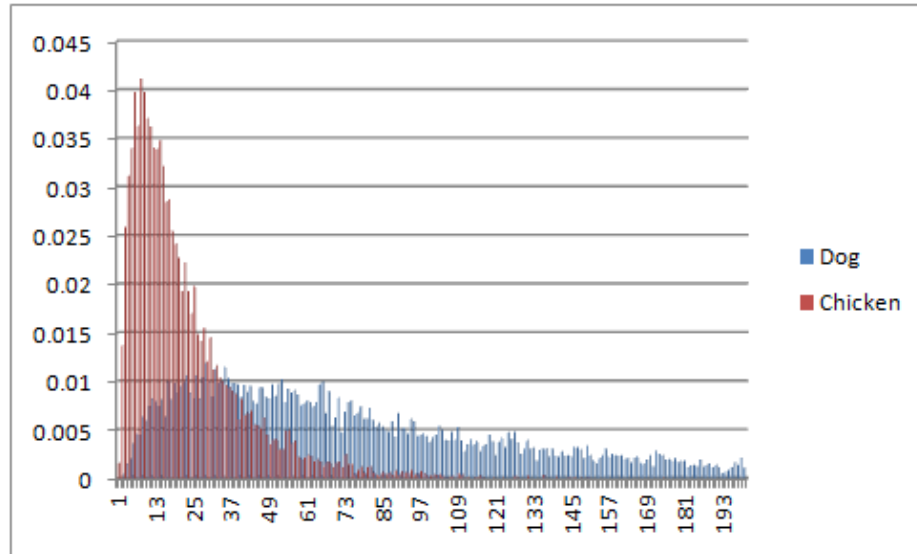


Figure 4.2: *Canis familiaris* vs. *Gallus gallus*: The $\Gamma_3^{S_{Dog}}$ and $\Gamma_3^{S_{Chicken}}$ comparison with a frequency spectral-range $[0, 10000]$ for the \mathbb{N} data sets (only $[0, 200]$ is shown)

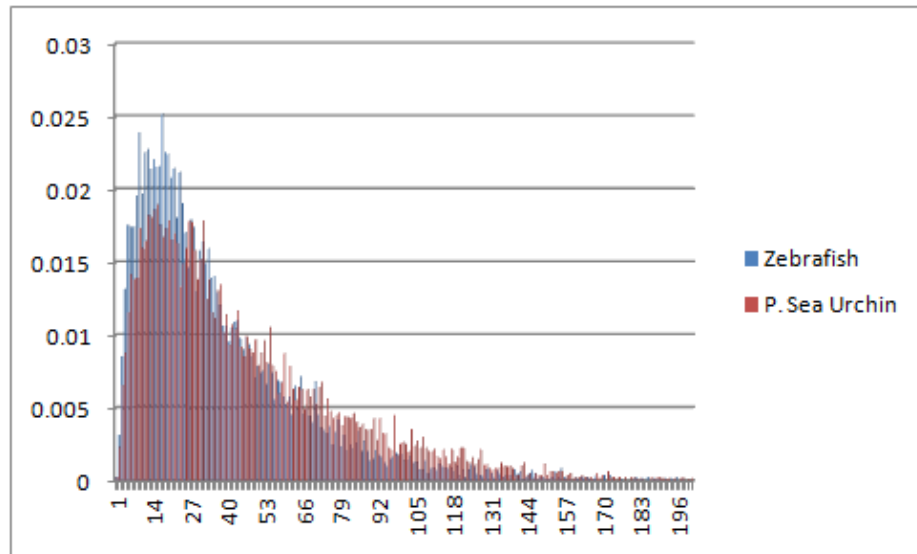


Figure 4.3: *Danio rerio* vs. *Strongylocentrus purpuratus*: The $\Gamma_3^{S_{Zebrafish}}$ and $\Gamma_3^{S_{SeaUrchin}}$ comparison with a frequency spectral-range $[0, 10000]$ for the \mathbb{N} data sets (only $[0, 200]$ is shown)

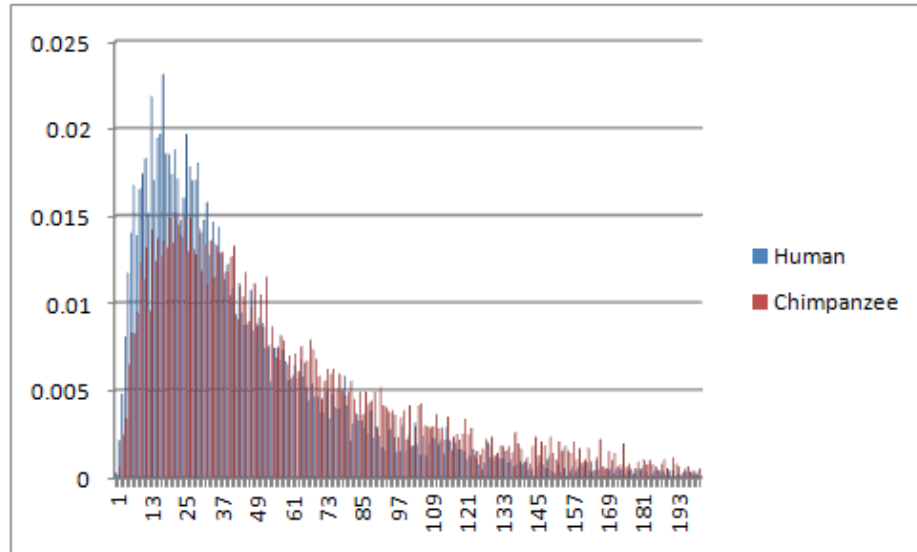


Figure 4.4: Homo sapien vs. Pan troglodytes: The $\Gamma_3^{S_{Human}}$ and $\Gamma_3^{S_{Chimp}}$ comparison with a frequency spectral-range $[0, 10000]$ for the \mathbb{N} data sets (only $[0, 200]$ is shown)

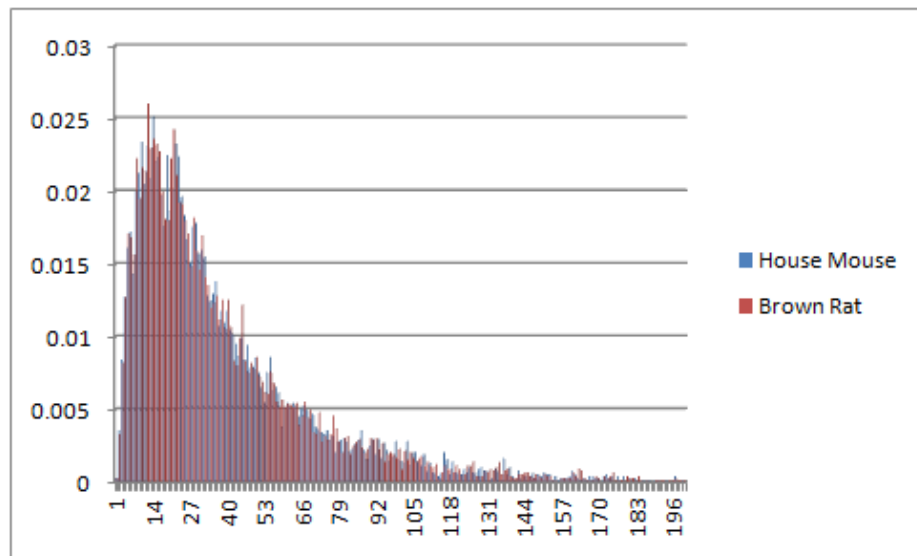


Figure 4.5: Mus musculus vs. Rattus norvegicus: The $\Gamma_3^{S_{Mouse}}$ and $\Gamma_3^{S_{Rat}}$ comparison with a frequency spectral-range $[0, 10000]$ for the \mathbb{N} data sets (only $[0, 200]$ is shown)

4.3.3 Bacteria Strain Results: *Escherichia coli*

This sections reports the *DNA* nullomer and 5-FS histogram results obtained from conducting this experiment on two distinct strains and three distinct regions of the EC bacteria.

Tables 4.8 and 4.9 display the experimental parameters. In Table 4.9, we see that the EC-55989 genome is the longest, and that in both strains, the non-coding region is longer than the coding region.

Tables 4.10 and 4.11, respectively, display the 8-nullomer set cardinality and intersection ratio statistics for comparison between the three data set categories. There are seven lengths for the \mathbb{A}_B data sets. For both strains and for all three regions, the \mathbb{N} 8-nullomer set cardinalities are greater than those of all the \mathbb{A}_B and \mathbb{A}_U , except for the \mathbb{A}_B^7 . Moreover, both strains and all three regions, the \mathbb{A}_U 8-nullomer set cardinalities and intersection ratios are zero. Furthermore, for both strains, the \mathbb{N} 8-nullomer set cardinalities are the smallest for the complete region and the largest for the non-coding region. So for both strains and all three regions, the \mathbb{A}_B 8-nullomer set cardinalities and intersection ratios monotonically increase with the partition length. To summarize, this suggests that in general, the \mathbb{N} sequences are non-random because their 8-nullomer set statistics strongly deviate from the \mathbb{A}_U sequences. Furthermore, the \mathbb{A}_B sequences appear less random as the partition length increases.

Tables 4.12 and 4.13, respectively, display the 9-nullomer set cardinality and intersection ratio statistics for comparison between the three data set categories. There are seven lengths for the \mathbb{A}_B data sets. For both strains and for all three regions, the \mathbb{N} 9-nullomer set cardinalities are greater than those of all the \mathbb{A}_B and \mathbb{A}_U , except for the \mathbb{A}_B^7 of the coding and non-coding regions for both strains.

Moreover, for both strains, with the complete and coding regions, the \mathbb{A}_U 9-nullomer set cardinalities and intersection ratios are zero. Furthermore, for both strains, the \mathbb{N} 9-nullomer set cardinalities are the smallest for the complete region and the largest for the non-coding region. So for both strains and all three regions, the \mathbb{A}_B 9-nullomer set cardinalities and intersection ratios monotonically increase with the partition length. To summarize, this suggests that in general, the \mathbb{N} sequences are non-random because their 9-nullomer set statistics strongly deviate from the \mathbb{A}_U sequences. Furthermore, the \mathbb{A}_B sequences appear less random as the partition length increases.

Tables 4.14 and 4.15, respectively, display the 10-nullomer set cardinality and intersection ratio statistics for comparison between the three data set categories. There are seven lengths for the \mathbb{A}_B data sets. For both strains and for all three regions, the \mathbb{N} 10-nullomer set cardinalities are greater than those of all the artificially-generated. Moreover, both strains and for all three regions, the randomly-unbiased 10-nullomer set cardinalities are less than those of the \mathbb{N} and \mathbb{A}_B . Furthermore, for both strains, with the complete and coding regions, the \mathbb{A}_U 10-nullomer set intersection ratios are zero. Additionally, for both strains, the \mathbb{N} 10-nullomer set cardinalities are the smallest for the complete region and the largest for the non-coding region. Finally, for both strains and all three regions, the \mathbb{A}_B 10-nullomer set cardinalities and intersection ratios monotonically increase with the partition length. To summarize, this suggests that in general, the \mathbb{N} sequences are non-random because they strongly deviate from the \mathbb{A}_U sequences. Furthermore, the \mathbb{A}_B sequences appear less random as the partition length increases.

Table 4.16 displays the chi-square's for Rankseq's 10-nullomer probability histograms. For both strains, for all three regions, and for all histogram lengths, the randomly-unbiased chi-squares are the greatest. Moreover, based on these results, it

is possible to use the chi-square values for the \mathbb{N} and \mathbb{A}_B data sets, for both strains, for all histogram lengths, to delineate the coding region from the non-coding region: the coding region chi-square range is $[0.277, 0.8931]$ and the non-coding region chi-square range is $[0.926, 0.9899]$. To summarize, the non-coding region chi-squares for the \mathbb{N} and \mathbb{A}_B data set 10-nullomer statistics are similar to the \mathbb{A}_U chi-squares, which indicate that the non-coding regions are more random than the coding regions.

Figures 4.6 and 4.7 are depictions of the 5-FS histogram results, which compare the complete (unfiltered), coding-region (filtered), and non-coding region (filtered) \mathbb{N} data sets. In Table 4.17, we see an analysis summary of these distributions. Interestingly, the complete and coding regions of both strains are remarkably similar in terms of standard deviation and skew, but the kurtosis of the complete regions is clearly distinct (5.167 versus -0.894). Moreover, all regions for both strains exhibit a positive skew, with the non-coding regions exhibiting the largest skew by one magnitude order. In general, the coding and non-coding regions for both strains are clearly distinct from each other.

Table 4.8: The EC bacteria’s DNA k -FS analysis configuration

Variable	Value	Affected Program
ncbi_filter	NULL/CDS/Non-CDS	Cseq
sequence_type	DNA	Cseq
sequence_length	10	Cseq
subsequence_partition_length	7	Rankseq
num_histogram_bins	50	Histoseq
num_dataset_instances	30	Genseq
maximum_count	10000	Freqseq
maximum_sequence_length	10	Freqseq
freqseq_num_histogram_bins	100	Freqseq
normalize	yes	Freqseq

The conclusions of this experiment are recapitulated in Section 5.1.

Table 4.9: The EC bacteria’s DNA sequence data sets. Here, the superregion length $|R^\tau|$ is used as Genseq’s “generation_size”

S/R^τ	Region Type	$ R^\tau $
S_{EC-536}/R^{ALL}	Complete	4,938,920
S_{EC-536}/R^{CDS}	Coding	4,324,150
S_{EC-536}/R^{-CDS}	Non-Coding	614,770
$S_{EC-5598}/R^{ALL}$	Complete	5,158,462
$S_{EC-5598}/R^{CDS}$	Coding	4,466,129
$S_{EC-5598}/R^{-CDS}$	Non-Coding	688,733

Table 4.10: The EC bacteria’s DNA 8-nullomer set cardinality comparisons for statistics with length-7 subsequence partitioning

S/R^τ	N	\mathbb{A}_B^1	\mathbb{A}_B^2	\mathbb{A}_B^3	\mathbb{A}_B^4	\mathbb{A}_B^5	\mathbb{A}_B^6	\mathbb{A}_B^7	\mathbb{A}_U
S_{EC-536}/R^{ALL}	32	0	0	0	17	21	25	45	0
S_{EC-536}/R^{CDS}	75	0	0	0	50	64	79	133	0
S_{EC-536}/R^{-CDS}	488	4	3	29	211	278	374	660	0
$S_{EC-5598}/R^{ALL}$	31	0	0	0	17	24	22	35	0
$S_{EC-5598}/R^{CDS}$	95	0	0	0	51	58	74	121	0
$S_{EC-5598}/R^{-CDS}$	425	2	1	19	179	271	347	611	0

Table 4.11: The EC bacteria’s DNA 8-nullomer set intersection ratio comparisons for statistics with length-7 subsequence partitioning

S/R^τ	\mathbb{A}_B^1	\mathbb{A}_B^2	\mathbb{A}_B^3	\mathbb{A}_B^4	\mathbb{A}_B^5	\mathbb{A}_B^6	\mathbb{A}_B^7	\mathbb{A}_U
S_{EC-536}/R^{ALL}	0.0	0.0	0.0	0.089	0.120	0.130	0.329	0.0
S_{EC-536}/R^{CDS}	0.0	0.0	0.0	0.134	0.177	0.261	0.543	0.0
S_{EC-536}/R^{-CDS}	0.0	0.0	0.012	0.140	0.179	0.223	0.468	0.0
$S_{EC-5598}/R^{ALL}$	0.0	0.0	0.0	0.030	0.079	0.085	0.154	0.0
$S_{EC-5598}/R^{CDS}$	0.0	0.0	0.0	0.123	0.147	0.157	0.335	0.0
$S_{EC-5598}/R^{-CDS}$	0.0	0.0	0.010	0.131	0.213	0.256	0.485	0.0

Table 4.12: The EC bacteria’s DNA 9-nullomer set cardinality comparisons for statistics with length-7 subsequence partitioning

S/R^τ	N	\mathbb{A}_B^1	\mathbb{A}_B^2	\mathbb{A}_B^3	\mathbb{A}_B^4	\mathbb{A}_B^5	\mathbb{A}_B^6	\mathbb{A}_B^7	\mathbb{A}_U
S_{EC-536}/R^{ALL}	1,894	0	0	115	1,477	1,619	1,736	1,965	0
S_{EC-536}/R^{CDS}	3,054	0	1	293	2,303	2,596	2,899	3,324	0
S_{EC-536}/R^{-CDS}	28,346	7,450	9,602	13,512	17,978	19,842	22,267	26,597	2,422
$S_{EC-5598}/R^{ALL}$	1,920	0	0	103	1,408	1,576	1,692	1,927	0
$S_{EC-5598}/R^{CDS}$	3,322	0	1	298	2,281	2,591	2,850	3,439	0
$S_{EC-5598}/R^{-CDS}$	24,248	5,214	6,901	10,340	14,682	16,401	18,475	22,245	1,389

Table 4.13: The EC bacteria's DNA 9-nullomer set intersection ratio comparisons for statistics with length-7 subsequence partitioning

S/R^τ	\mathbb{A}_B^1	\mathbb{A}_B^2	\mathbb{A}_B^3	\mathbb{A}_B^4	\mathbb{A}_B^5	\mathbb{A}_B^6	\mathbb{A}_B^7	\mathbb{A}_U
S_{EC-536}/R^{ALL}	0.0	0.0	0.022	0.295	0.308	0.329	0.393	0.0
S_{EC-536}/R^{CDS}	0.0	0.0	0.039	0.330	0.364	0.399	0.482	0.0
S_{EC-536}/R^{-CDS}	0.041	0.067	0.126	0.211	0.241	0.277	0.342	0.009
$S_{EC-5598}/R^{ALL}$	0.0	0.0	0.019	0.269	0.300	0.318	0.376	0.0
$S_{EC-5598}/R^{CDS}$	0.0	0.0	0.042	0.323	0.354	0.389	0.472	0.0
$S_{EC-5598}/R^{-CDS}$	0.030	0.051	0.109	0.200	0.236	0.271	0.336	0.006

Table 4.14: The EC bacteria's DNA 10-nullomer set cardinality comparisons for statistics with length-7 subsequence partitioning

S/R^τ	N	\mathbb{A}_B^1	\mathbb{A}_B^2	\mathbb{A}_B^3	\mathbb{A}_B^4	\mathbb{A}_B^5	\mathbb{A}_B^6	\mathbb{A}_B^7	\mathbb{A}_U
S_{EC-536}/R^{ALL}	59,585	99	4,041	23,158	41,817	47,801	52,802	56,405	95
S_{EC-536}/R^{CDS}	83,054	382	8,123	36,266	58,691	68,063	74,765	79,818	288
S_{EC-536}/R^{-CDS}	491,039	362,906	387,142	406,369	421,972	429,537	439,834	456,539	324,804
$S_{EC-5598}/R^{ALL}$	57,934	71	3,416	21,557	39,443	45,370	50,413	54,033	62
$S_{EC-5598}/R^{CDS}$	83,510	341	7,462	35,465	57,289	66,791	73,528	79,285	221
$S_{EC-5598}/R^{-CDS}$	459,321	322,325	348,710	368,540	385,692	392,911	402,475	418,988	282,149

Table 4.15: The EC bacteria's DNA 10-nullomer set intersection ratio comparisons for statistics with length-7 subsequence partitioning

S/R^τ	\mathbb{A}_B^1	\mathbb{A}_B^2	\mathbb{A}_B^3	\mathbb{A}_B^4	\mathbb{A}_B^5	\mathbb{A}_B^6	\mathbb{A}_B^7	\mathbb{A}_U
S_{EC-536}/R^{ALL}	0.0	0.017	0.136	0.307	0.342	0.374	0.399	0.0
S_{EC-536}/R^{CDS}	0.0	0.03	0.173	0.327	0.370	0.405	0.436	0.0
S_{EC-536}/R^{-CDS}	0.379	0.423	0.462	0.498	0.512	0.530	0.559	0.310
$S_{EC-5598}/R^{ALL}$	0.0	0.015	0.133	0.305	0.343	0.378	0.404	0.0
$S_{EC-5598}/R^{CDS}$	0.0	0.028	0.175	0.327	0.371	0.408	0.444	0.0
$S_{EC-5598}/R^{-CDS}$	0.341	0.389	0.431	0.471	0.485	0.503	0.532	0.269

Table 4.16: The EC bacteria's DNA 10-nullomer ranking histogram chi-square comparisons for statistics with length-7 subsequence partitioning

S/R^T	Histogram	N	A_B^1	A_B^2	A_B^3	A_B^4	A_B^5	A_B^6	A_B^7	A_U
$SEC-536/R^{ALL}$	$H[{}^0Q_{10,1}^{R^{ALL}}]$	0.8733	0.9070	0.9323	0.9035	0.9079	0.9007	0.8892	0.9068	0.98
$SEC-536/R^{ALL}$	$H[{}^0Q_{10,2}^{R^{ALL}}]$	0.2080	0.9051	0.2861	0.2580	0.2364	0.2250	0.2124	0.2109	0.98
$SEC-536/R^{ALL}$	$H[{}^0Q_{10,3}^{R^{ALL}}]$	0.2044	0.8999	0.2861	0.2864	0.2488	0.2271	0.2125	0.2103	0.98
$SEC-536/R^{ALL}$	$H[{}^0Q_{10,4}^{R^{ALL}}]$	0.2553	0.8825	0.2862	0.2865	0.3250	0.2939	0.2718	0.2634	0.9789
$SEC-536/R^{ALL}$	$H[{}^0Q_{10,5}^{R^{ALL}}]$	0.2950	0.8372	0.2857	0.2870	0.3257	0.3461	0.3177	0.3064	0.9230
$SEC-536/R^{ALL}$	$H[{}^0Q_{10,6}^{R^{ALL}}]$	0.3308	0.7378	0.2851	0.2886	0.3284	0.3489	0.3666	0.3497	0.7827
$SEC-536/R^{ALL}$	$H[{}^0Q_{10,7}^{R^{ALL}}]$	0.3580	0.5089	0.2850	0.2939	0.3381	0.3594	0.3774	0.392	0.5353
$SEC-536/R^{CDS}$	$H[{}^0Q_{10,1}^{R^{CDS}}]$	0.7065	0.8652	0.7974	0.7259	0.7391	0.7354	0.7226	0.7664	0.98
$SEC-536/R^{CDS}$	$H[{}^0Q_{10,2}^{R^{CDS}}]$	0.3968	0.8685	0.5510	0.4710	0.4400	0.4201	0.4051	0.4003	0.98
$SEC-536/R^{CDS}$	$H[{}^0Q_{10,3}^{R^{CDS}}]$	0.5730	0.8755	0.5512	0.7790	0.6920	0.6400	0.6008	0.5889	0.98
$SEC-536/R^{CDS}$	$H[{}^0Q_{10,4}^{R^{CDS}}]$	0.6877	0.8844	0.5518	0.7793	0.8279	0.7715	0.7279	0.709	0.98
$SEC-536/R^{CDS}$	$H[{}^0Q_{10,5}^{R^{CDS}}]$	0.7595	0.8931	0.5532	0.7805	0.8286	0.8538	0.8076	0.7862	0.98
$SEC-536/R^{CDS}$	$H[{}^0Q_{10,6}^{R^{CDS}}]$	0.8100	0.8970	0.5591	0.7842	0.8314	0.8563	0.8653	0.8415	0.9748
$SEC-536/R^{CDS}$	$H[{}^0Q_{10,7}^{R^{CDS}}]$	0.8411	0.8789	0.5782	0.7960	0.8405	0.8636	0.8726	0.8799	0.9284
$SEC-536/R^{-CDS}$	$H[{}^0Q_{10,1}^{R^{-CDS}}]$	0.9799	0.9795	0.9797	0.9799	0.9799	0.9799	0.9799	0.9778	0.98
$SEC-536/R^{-CDS}$	$H[{}^0Q_{10,2}^{R^{-CDS}}]$	0.9705	0.9795	0.9725	0.9725	0.9718	0.9710	0.9704	0.9689	0.98
$SEC-536/R^{-CDS}$	$H[{}^0Q_{10,3}^{R^{-CDS}}]$	0.9676	0.9795	0.9725	0.9705	0.9697	0.9690	0.9684	0.9671	0.98
$SEC-536/R^{-CDS}$	$H[{}^0Q_{10,4}^{R^{-CDS}}]$	0.9668	0.9794	0.9725	0.9705	0.9695	0.9689	0.9683	0.9668	0.98
$SEC-536/R^{-CDS}$	$H[{}^0Q_{10,5}^{R^{-CDS}}]$	0.9653	0.9789	0.9724	0.9705	0.9695	0.9684	0.9676	0.9658	0.98
$SEC-536/R^{-CDS}$	$H[{}^0Q_{10,6}^{R^{-CDS}}]$	0.9632	0.9784	0.9722	0.9704	0.9694	0.9683	0.9675	0.9654	0.98
$SEC-536/R^{-CDS}$	$H[{}^0Q_{10,7}^{R^{-CDS}}]$	0.9606	0.9772	0.9715	0.9700	0.9690	0.9681	0.9674	0.9652	0.9799
$SEC-5598/R^{ALL}$	$H[{}^0Q_{10,1}^{R^{ALL}}]$	0.9745	0.9450	0.9686	0.9746	0.9748	0.9734	0.9721	0.9778	0.98
$SEC-5598/R^{ALL}$	$H[{}^0Q_{10,2}^{R^{ALL}}]$	0.2237	0.9441	0.3112	0.2788	0.2551	0.2417	0.2288	0.2275	0.98
$SEC-5598/R^{ALL}$	$H[{}^0Q_{10,3}^{R^{ALL}}]$	0.2219	0.9385	0.3114	0.3134	0.2729	0.2489	0.2322	0.2287	0.98
$SEC-5598/R^{ALL}$	$H[{}^0Q_{10,4}^{R^{ALL}}]$	0.2806	0.9187	0.3113	0.3136	0.3618	0.3274	0.3014	0.2911	0.98
$SEC-5598/R^{ALL}$	$H[{}^0Q_{10,5}^{R^{ALL}}]$	0.3241	0.8576	0.3116	0.3141	0.3625	0.3853	0.3528	0.3390	0.9756
$SEC-5598/R^{ALL}$	$H[{}^0Q_{10,6}^{R^{ALL}}]$	0.3664	0.6807	0.3123	0.3161	0.3655	0.3884	0.4095	0.3895	0.8126
$SEC-5598/R^{ALL}$	$H[{}^0Q_{10,7}^{R^{ALL}}]$	0.3968	0.4601	0.3135	0.3231	0.3762	0.3997	0.4214	0.4375	0.4844
$SEC-5598/R^{CDS}$	$H[{}^0Q_{10,1}^{R^{CDS}}]$	0.4600	0.4616	0.4456	0.4150	0.4465	0.4483	0.4495	0.4626	0.98
$SEC-5598/R^{CDS}$	$H[{}^0Q_{10,2}^{R^{CDS}}]$	0.2710	0.4615	0.3987	0.3365	0.3130	0.2955	0.2809	0.2770	0.98
$SEC-5598/R^{CDS}$	$H[{}^0Q_{10,3}^{R^{CDS}}]$	0.2995	0.4611	0.3990	0.4369	0.3792	0.3440	0.3186	0.3110	0.98
$SEC-5598/R^{CDS}$	$H[{}^0Q_{10,4}^{R^{CDS}}]$	0.3869	0.4614	0.3992	0.4371	0.5103	0.4575	0.4222	0.4058	0.9799
$SEC-5598/R^{CDS}$	$H[{}^0Q_{10,5}^{R^{CDS}}]$	0.4611	0.4665	0.3991	0.4379	0.5115	0.5598	0.5120	0.4889	0.9750
$SEC-5598/R^{CDS}$	$H[{}^0Q_{10,6}^{R^{CDS}}]$	0.5168	0.4762	0.3964	0.4415	0.5153	0.5636	0.5859	0.5555	0.8171
$SEC-5598/R^{CDS}$	$H[{}^0Q_{10,7}^{R^{CDS}}]$	0.5586	0.4754	0.3860	0.4542	0.5288	0.5763	0.5980	0.6154	0.5143
$SEC-5598/R^{-CDS}$	$H[{}^0Q_{10,1}^{R^{-CDS}}]$	0.9750	0.9722	0.9741	0.9756	0.9753	0.9749	0.9742	0.9632	0.98
$SEC-5598/R^{-CDS}$	$H[{}^0Q_{10,2}^{R^{-CDS}}]$	0.9469	0.9721	0.9539	0.9519	0.9498	0.9482	0.9473	0.9449	0.98
$SEC-5598/R^{-CDS}$	$H[{}^0Q_{10,3}^{R^{-CDS}}]$	0.9448	0.9717	0.9538	0.9522	0.9498	0.9486	0.9473	0.9450	0.98
$SEC-5598/R^{-CDS}$	$H[{}^0Q_{10,4}^{R^{-CDS}}]$	0.9426	0.9708	0.9538	0.9522	0.9495	0.9486	0.9471	0.9443	0.98
$SEC-5598/R^{-CDS}$	$H[{}^0Q_{10,5}^{R^{-CDS}}]$	0.9405	0.9686	0.9536	0.9521	0.9493	0.9478	0.9459	0.9429	0.98
$SEC-5598/R^{-CDS}$	$H[{}^0Q_{10,6}^{R^{-CDS}}]$	0.9375	0.9659	0.9531	0.9519	0.9490	0.9476	0.9464	0.9426	0.9799
$SEC-5598/R^{-CDS}$	$H[{}^0Q_{10,7}^{R^{-CDS}}]$	0.9342	0.9612	0.9516	0.9510	0.9482	0.9471	0.9460	0.9434	0.9795

Table 4.17: The analysis summary of the EC bacteria 5-FS distributions in Figures 4.6 and 4.7

S/R^τ	Standard Deviation	Skewness	Kurtosis
S_{EC-536}/R^{ALL}	0.007	0.335	5.167
S_{EC-536}/R^{CDS}	0.007	0.459	-0.867
S_{EC-536}/R^{-CDS}	0.035	4.171	17.201
$S_{EC-5598}/R^{ALL}$	0.007	0.341	-0.894
$S_{EC-5598}/R^{CDS}$	0.007	0.401	-0.866
$S_{EC-5598}/R^{-CDS}$	0.032	3.888	14.570

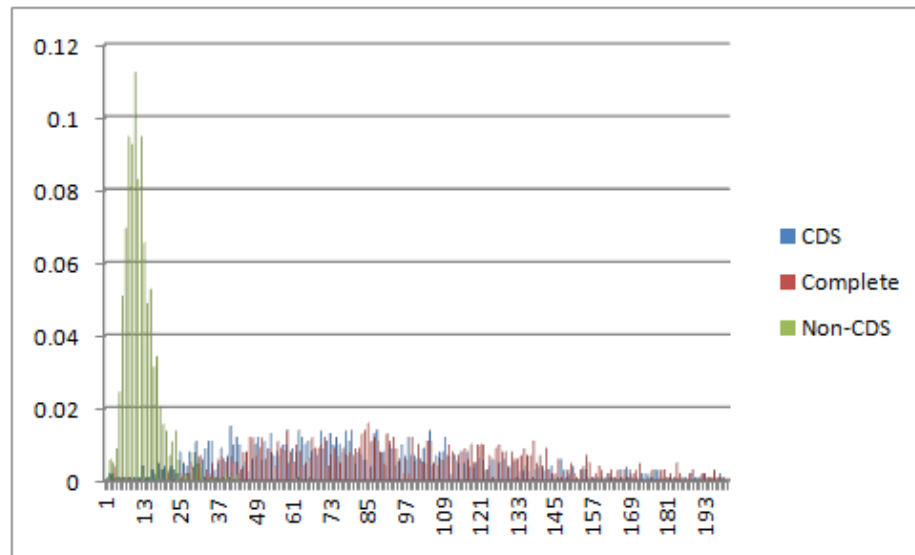


Figure 4.6: EC-536: The DNA $\Gamma_5^{S_{EC-536}}$ region comparison with a frequency spectral-range $[0, 10000]$ for the N data sets (only $[0, 200]$ is shown)

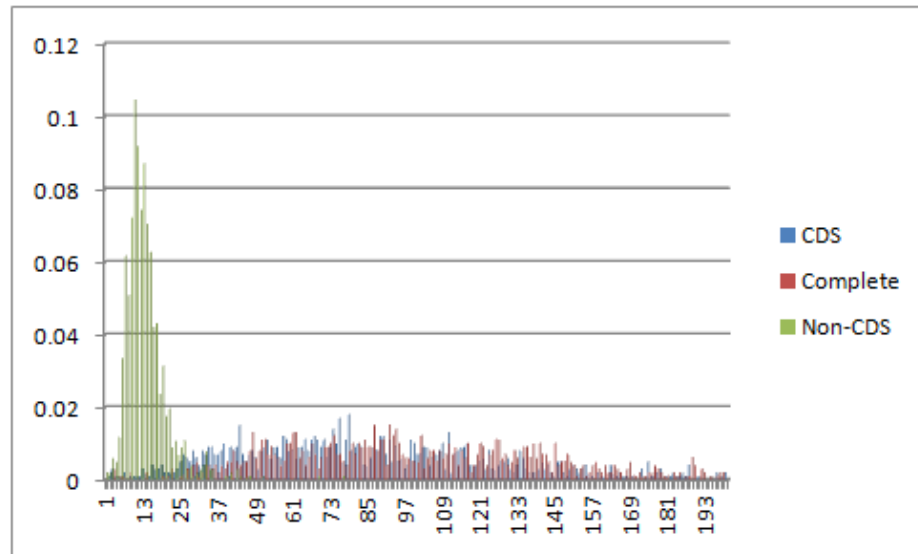


Figure 4.7: EC-55989: The DNA $\Gamma_5^{SEC-55989}$ region comparison with a frequency spectral-range $[0, 10000]$ for the \mathbb{N} data sets (only $[0, 200]$ is shown)

4.3.4 Virus Strain Results: *Human immunodeficiency virus*

This section reports the *DNA/RNA* nullomer results and the 3-FS results obtained from conducting this experiment on two distinct strains and three distinct regions of HIV.

Tables 4.18 and 4.19 display the experimental parameters. In Table 4.19, we see that the HIV-2 genome is the longest, and that in both strains, the coding region is longer than the non-coding region.

Table 4.20 displays the 5-nullomer set cardinality and intersection ratio statistics. For both strains, we see that the complete region 5-nullomer set cardinality is the smallest and that of the non-coding region is the greatest. Moreover, for both strains, for all regions, the \mathbb{A}_U 5-nullomer set cardinalities and intersection ratios are the smallest, where those for the complete and coding regions are zero. Furthermore, for both strains, for all regions, the \mathbb{A}_B 5-nullomer set cardinalities and intersection ratios monotonically increase as the partition length increases. Additionally, for both strains, for the non-coding regions, the \mathbb{N} 5-nullomer set cardinalities are greater than those of the \mathbb{A}_B and \mathbb{A}_U . Likewise, for the HIV-1 strain, for complete and coding regions, the 5-nullomer set cardinalities are greater than those of the \mathbb{A}_B^1 , and less than those of the \mathbb{A}_B^2 and \mathbb{A}_B^3 . Finally, for the HIV-2 strain, for complete and coding regions, the 5-nullomer set cardinalities are greater than those of the \mathbb{A}_B^1 and \mathbb{A}_B^2 , and less than those of the \mathbb{A}_B^3 , with the exception of the complete region, which is actually greater than the length-3 value.

Table 4.21 displays the 6-nullomer set cardinality and intersection ratio statistics. For both strains, we see that the complete region 6-nullomer set cardinality is the smallest and the non-coding region is the greatest. Moreover, for both strains, for all

regions, the \mathbb{A}_U 6-nullomer set cardinalities and intersection ratios are the smallest. Furthermore, for both strains, for all regions, the \mathbb{A}_B 6-nullomer set cardinalities and intersection ratios monotonically increase as the partition length increases. Additionally, for both strains, for the non-coding regions, the \mathbb{N} 6-nullomer set cardinalities are greater than those of the \mathbb{A}_B and \mathbb{A}_U . So for the complete and coding regions of both strains, the \mathbb{N} 6-nullomer set cardinalities are greater than those of the \mathbb{A}_B^1 and less than those of the \mathbb{A}_B^2 and \mathbb{A}_B^3 .

Table 4.22 displays the 7-nullomer set cardinality and intersection ratio statistics. For both strains, we see that the complete region 7-nullomer set cardinality is the smallest and the non-coding region is the greatest. Moreover, for both strains, for all regions, the \mathbb{A}_U 7-nullomer set cardinalities and intersection ratios are the smallest, with the exception of the HIV-1 non-coding region, which is equivalent to that of the \mathbb{A}_B^1 . Furthermore, for both strains, for all regions, the \mathbb{A}_B 7-nullomer set cardinalities and intersection ratios monotonically increase as the partition length increases. So for all three regions of both strains, we see that the \mathbb{N} 7-nullomer set cardinalities are greater than those of the \mathbb{A}_B and \mathbb{A}_U .

Table 4.23 displays the chi-squares for Rankseq's 7-nullomer probability histograms. For both strains, for all three regions, and for all histogram lengths, with the exception of the HIV-2 strain's $P(3)$ histogram for the non-coding region, the randomly-unbiased chi-squares are the greatest. Moreover, based on these results, it is possible to use the chi-square values for the \mathbb{N} and \mathbb{A}_B data sets, for both strains, for all histogram lengths, to delineate the coding region from the non-coding region: for the HIV-1 strain, the coding region chi-square range is $[0.1874, 0.2498]$ and the non-coding region chi-square range is $[0.6029, 0.8839]$, and likewise for the HIV-2 strain, the coding region chi-square range is $[0.1351, 0.1743]$ and the non-coding region chi-square

range is $[0.4795, 0.5174]$. Therefore, based on these chi-square ranges, it is possible to distinguish between the two strains because the HIV-2 ranges are smaller and do not overlap with the HIV-1 ranges. To summarize, the non-coding region 7-nullomer statistics of the \mathbb{N} and \mathbb{A}_B sequences are similar to those of the \mathbb{A}_U sequences: the non-coding regions are more random than the coding regions.

Figures 4.8 and 4.9 display the 3-FS results for the \mathbb{N} data sets. In Table 4.24, we see an analysis summary of these distributions. Interestingly, the kurtosis of all regions for both strains is negative, except for HIV-1's non-coding region. Moreover, all regions of both strains exhibit a positive skew. Furthermore, non-coding region of HIV-1 has the greatest skew, and the non-coding region of HIV-2 has the smallest skew. Similarly to the EC bacteria, the non-coding regions for both HIV strains are clearly distinct from the coding regions.

Table 4.18: The HIV's DNA/RNA k -FS analysis configuration

Variable	Value	Affected Program
ncbi_filter	NULL/CDS/Non-CDS	Cseq
sequence_type	DNA	Cseq
sequence_length	7	Cseq
subsequence_partition_length	3	Rankseq
num_histogram_bins	50	Histoseq
num_dataset_instances	30	Genseq
maximum_count	300	Freqseq
maximum_sequence_length	7	Freqseq
freqseq_num_histogram_bins	20	Freqseq
normalize	yes	Freqseq

The conclusions of this experiment are recapitulated in Section 5.1.

Table 4.19: The HIV’s DNA/RNA sequence data sets. Here, the superregion length $|R^\tau|$ is used as Genseq’s “generation_size”

S/R^τ	Region Type	$ S $
S_{HIV-1}/R^{ALL}	Complete	8,610
S_{HIV-1}/R^{CDS}	Coding	9,181
S_{HIV-1}/R^{-CDS}	Non-Coding	571
S_{HIV-2}/R^{ALL}	Complete	10,359
S_{HIV-2}/R^{CDS}	Coding	8,785
S_{HIV-2}/R^{-CDS}	Non-Coding	1,574

Table 4.20: The HIV’s DNA/RNA 5-nullomer set cardinality and intersection ratio statistical comparisons with length-3 subsequence partitioning

S/R^τ	N	\mathbb{A}_B^1	\mathbb{A}_B^2	\mathbb{A}_B^3	\mathbb{A}_U
S_{HIV-1}/R^{ALL}	8	0 (0.0)	28 (0.583)	29 (0.567)	0 (0.0)
S_{HIV-1}/R^{CDS}	32	0 (0.0)	44 (0.367)	48 (0.394)	0 (0.0)
S_{HIV-1}/R^{-CDS}	486	351 (0.356)	430 (0.525)	451 (0.569)	344 (0.339)
S_{HIV-2}/R^{ALL}	10	0 (0.0)	4 (0.0)	7 (0.127)	0 (0.0)
S_{HIV-2}/R^{CDS}	10	0 (0.0)	8 (0.02)	12 (0.16)	0 (0.0)
S_{HIV-2}/R^{-CDS}	212	52 (0.049)	129 (0.257)	166 (0.350)	54 (0.052)

Table 4.21: The HIV’s DNA/RNA 6-nullomer set cardinality and intersection ratio statistical comparisons

S/R^τ	N	\mathbb{A}_B^1	\mathbb{A}_B^2	\mathbb{A}_B^3	\mathbb{A}_U
S_{HIV-1}/R^{ALL}	624	138 (0.061)	660 (0.538)	676 (0.557)	53 (0.0128)
S_{HIV-1}/R^{CDS}	746	195 (0.092)	760 (0.607)	793 (0.632)	70 (0.0158)
S_{HIV-1}/R^{-CDS}	3,347	3,120 (0.765)	3,188 (0.798)	3,204 (0.807)	3,115 (0.761)
S_{HIV-2}/R^{ALL}	432	52 (0.022)	337 (0.268)	387 (0.356)	30 (0.009)
S_{HIV-2}/R^{CDS}	498	118 (0.045)	445 (0.349)	500 (0.425)	64 (0.016)
S_{HIV-2}/R^{-CDS}	2,513	1,919 (0.471)	2,118 (0.577)	2,197 (0.613)	1,928 (0.473)

Table 4.22: The HIV’s DNA/RNA 7-nullomer set cardinality and intersection ratio statistical comparisons

S/R^τ	N	\mathbb{A}_B^1	\mathbb{A}_B^2	\mathbb{A}_B^3	\mathbb{A}_U
S_{HIV-1}/R^{ALL}	7,408	6,001 (0.419)	7,121 (0.629)	7,294 (0.646)	5,378 (0.326)
S_{HIV-1}/R^{CDS}	7,782	6,500 (0.457)	7,537 (0.655)	7,735 (0.674)	5,762 (0.349)
S_{HIV-1}/R^{-CDS}	15,536	15,297 (0.934)	15,326 (0.9375)	15,333 (0.939)	15,297 (0.934)
S_{HIV-2}/R^{ALL}	6,702	4,929 (0.325)	6,018 (0.515)	6,256 (0.547)	4,655 (0.281)
S_{HIV-2}/R^{CDS}	7,206	6,004 (0.398)	6,877 (0.563)	7,080 (0.588)	5,646 (0.343)
S_{HIV-2}/R^{-CDS}	14,378	13,543 (0.827)	13,656 (0.842)	13,714 (0.849)	13,551 (0.827)

Table 4.23: Rankseq's HIV DNA/RNA 7-nullomer probability histogram chi-square comparisons with length-3 subsequence partitioning

S/R^τ	Histogram	\mathbb{N}	\mathbb{A}_B^1	\mathbb{A}_B^2	\mathbb{A}_B^3	\mathbb{A}_U
S_{HIV-1}/R^{ALL}	$H[{}^0Q_{7,1}^{R^{ALL}}]$	0.1837	0.1968	0.196	0.1922	0.9609
S_{HIV-1}/R^{ALL}	$H[{}^0Q_{7,2}^{R^{ALL}}]$	0.2199	0.1948	0.2334	0.2291	0.7963
S_{HIV-1}/R^{ALL}	$H[{}^0Q_{7,3}^{R^{ALL}}]$	0.2219	0.1896	0.2332	0.2341	0.4273
S_{HIV-1}/R^{CDS}	$H[{}^0Q_{7,1}^{R^{CDS}}]$	0.1874	0.1988	0.1968	0.1929	0.9585
S_{HIV-1}/R^{CDS}	$H[{}^0Q_{7,2}^{R^{CDS}}]$	0.2352	0.1932	0.2476	0.2443	0.7751
S_{HIV-1}/R^{CDS}	$H[{}^0Q_{7,3}^{R^{CDS}}]$	0.2368	0.1873	0.2471	0.2498	0.4121
S_{HIV-1}/R^{-CDS}	$H[{}^0Q_{7,1}^{R^{-CDS}}]$	0.8205	0.7799	0.8027	0.8839	0.9414
S_{HIV-1}/R^{-CDS}	$H[{}^0Q_{7,2}^{R^{-CDS}}]$	0.6307	0.7170	0.6385	0.6438	0.7965
S_{HIV-1}/R^{-CDS}	$H[{}^0Q_{7,3}^{R^{-CDS}}]$	0.6079	0.6423	0.6357	0.6198	0.6524
S_{HIV-2}/R^{ALL}	$H[{}^0Q_{7,1}^{R^{ALL}}]$	0.1360	0.1454	0.1430	0.1428	0.5778
S_{HIV-2}/R^{ALL}	$H[{}^0Q_{7,2}^{R^{ALL}}]$	0.1111	0.1451	0.1206	0.1169	0.4909
S_{HIV-2}/R^{ALL}	$H[{}^0Q_{7,3}^{R^{ALL}}]$	0.1167	0.1400	0.1220	0.1261	0.3345
S_{HIV-2}/R^{CDS}	$H[{}^0Q_{7,1}^{R^{CDS}}]$	0.1743	0.1705	0.1660	0.1640	0.7609
S_{HIV-2}/R^{CDS}	$H[{}^0Q_{7,2}^{R^{CDS}}]$	0.1351	0.1674	0.1419	0.1417	0.5264
S_{HIV-2}/R^{CDS}	$H[{}^0Q_{7,3}^{R^{CDS}}]$	0.1451	0.1599	0.1446	0.1545	0.3508
S_{HIV-2}/R^{-CDS}	$H[{}^0Q_{7,1}^{R^{-CDS}}]$	0.5174	0.4945	0.4978	0.4980	0.5535
S_{HIV-2}/R^{-CDS}	$H[{}^0Q_{7,2}^{R^{-CDS}}]$	0.4795	0.4966	0.4928	0.4865	0.5044
S_{HIV-2}/R^{-CDS}	$H[{}^0Q_{7,3}^{R^{-CDS}}]$	0.4894	0.4882	0.4982	0.5123	0.4944

Table 4.24: The analysis summary of the HIV 3-FS distributions in Figures 4.8 and 4.9

S/R^τ	Standard Deviation	Skewness	Kurtosis
S_{HIV-1}/R^{ALL}	0.052	0.557	-0.938
S_{HIV-16}/R^{CDS}	0.054	0.904	-0.141
S_{HIV-1}/R^{-CDS}	0.103	1.840	1.685
S_{HIV-2}/R^{ALL}	0.067	0.994	-0.222
S_{HIV-2}/R^{CDS}	0.052	0.520	-1.099
S_{HIV-2}/R^{-CDS}	0.059	0.894	-0.617

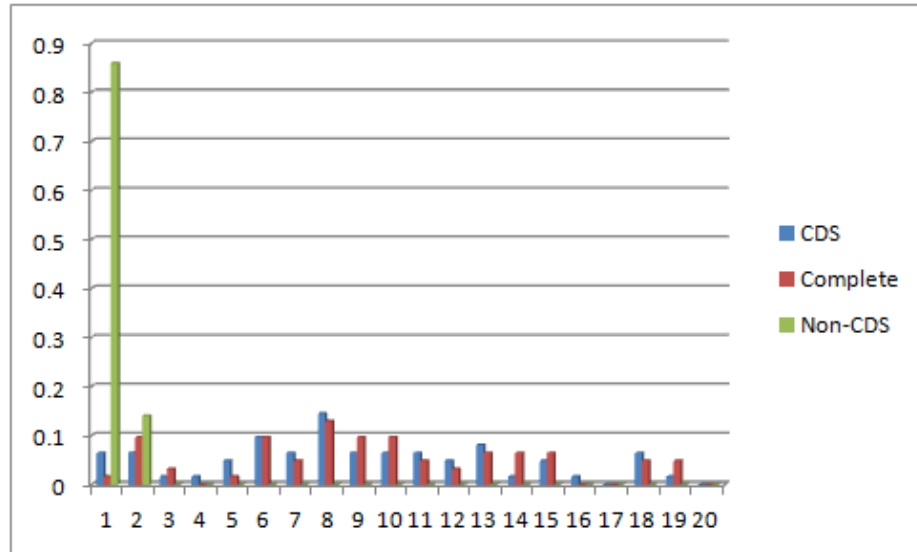


Figure 4.8: HIV-1: The DNA/RNA $\Gamma_3^{S_{HIV-1}}$ region comparison with a frequency spectral-range $[0, 300]$ for the \mathbb{N} data set (only $[0, 20]$ is shown)

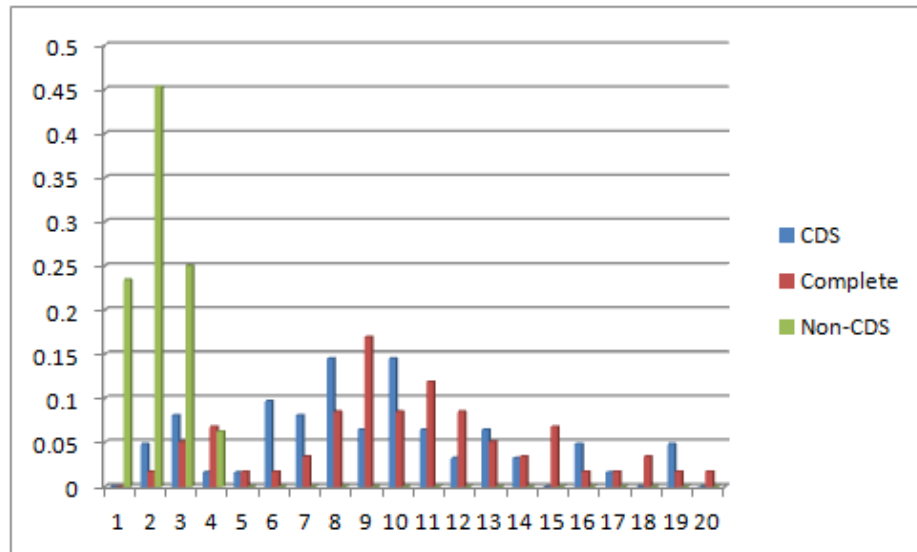


Figure 4.9: HIV-2: The DNA/RNA $\Gamma_3^{S_{HIV-2}}$ region comparison with a frequency spectral-range $[0, 300]$ for the \mathbb{N} data set (only $[0, 20]$ is shown)

4.4 Experiment 2: NCBI Genome Database Evolution and Time Series Analysis: Prime Prediction Assessment

4.4.1 Objective Summary

This experiment employs an ANN to investigate the prime phenomena by assessing the chronological predictability within the growing NCBI database for DNA. This supervised machine learning approach aims to capture the evolutionary behavior of the NCBI database as the prime set cardinality monotonically *decreases* over time. This investigation attempts to forecast the Boolean observed state for primes by extracting the corresponding sequence traits and compiling them into feature vectors. This experiment seeks answers to the following inquiries:

1. Is it feasible to forecast the Boolean observed prime states as the NCBI database evolves and grows using an ANN?
2. Can our software analysis suite make a legitimate scientific assessment of this phenomena?

4.4.2 Training, Testing, and Prediction Results: The Artificial Neural Network

The objective is to assess the predictability of DNA 16-primes as the NCBI database evolves over this 18-month period. In this case, we use Rankseq length-8 partitioning statistics to compile feature vector examples from the chronologically ordered DNA data sets from the contiguous NCBI database snapshots for training, testing, and prediction.

Data Sets

For each monthly NCBI snapshot, we use Tdataformat to create both a balanced and an unbalanced data set. The balanced series is equivalent to the unbalanced series except that in the balanced data sets, minority oversampling is used to compile an equal number of positive and negative examples in the data sets. Tables 4.25 and 4.26 display the chronologically ordered monthly NCBI database snapshot datasets for the DNA 16-primers with length-8 subsequence partitioning statistics used to train the ANN via supervised learning. Each training example of the 16-prime data sets contains 14-element feature vectors, which correspond to 14 Rankseq attributes, where the first 8 attributes are the prime probabilities for the partition length $1 \leq \rho \leq 8$ in the form

$$v_\rho = {}^0Q_{16,\rho}^{S_{A,B}}. \quad (4.34)$$

So additionally, for an arbitrary monthly NCBI database snapshot $S_{A,B}$, $\forall s \in {}^0B_{16}^{S_{A,B}}$, we have

$$v_9 = \frac{F(g, s) + F(c, s)}{F(a, s) + F(t, s) + F(c, s) + F(g, s)}, \quad (4.35)$$

$$v_{10} = \frac{F(a, s) + F(t, s)}{F(g, s) + F(c, s)}, \quad (4.36)$$

$$v_{11} = \frac{F(cp, s)}{F(c, s) \times F(g, s) \times |s|}, \quad (4.37)$$

$$v_{12} = \frac{F(a, s) + F(g, s)}{|s|}, \quad (4.38)$$

$$v_{13} = \frac{F(c, s) + F(t, s)}{|s|}, \quad (4.39)$$

$$v_{14} = \frac{F(a, s) + F(t, s)}{|s|}, \quad (4.40)$$

for the GC-content, GC-ratio, CpG suppression ratio, purine density, pyrimidine density, and AT-density, respectively, where ${}^0B_{16}^{S_{A,B}}$ is the prime set using the formal notation of Section 4.2.

We define S_A and S_B as the DNA sequence snapshots for months A and B , respectively. Moreover, we define ${}^0B_{16}^{S_A}$ and ${}^0B_{16}^{S_B}$ as the 16-prime sets for A and B , respectively. Furthermore, we define ${}^0B_{16}^{S_{A,B}}$ and ${}^1B_{16}^{S_{A,B}}$ as the negative and positive training example sets for the snapshot $S_{A,B}$, respectively, such that

$${}^0B_{16}^{S_{A,B}} = {}^0B_{16}^{S_A} \cap {}^0B_{16}^{S_B}, \quad (4.41)$$

$${}^1B_{16}^{S_{A,B}} = {}^0B_{16}^{S_B} - {}^0B_{16}^{S_A}. \quad (4.42)$$

Table 4.25: The size statistics for the *balanced* NCBI data set snapshots

Month Range	$S_{A,B}$	Size (MB)	# Total Examples
2010.01 to 2010.02	$S_{1,2}$	1,100	8,245,612
2010.02 to 2010.03	$S_{2,3}$	972	7,776,448
2010.03 to 2010.04	$S_{3,4}$	953	7,624,336
2010.04 to 2010.05	$S_{4,5}$	926	7,406,358
2010.05 to 2010.06	$S_{5,6}$	879	7,031,366
2010.06 to 2010.07	$S_{6,7}$	818	6,544,838
2010.07 to 2010.08	$S_{7,8}$	791	6,326,778
2010.08 to 2010.09	$S_{8,9}$	780	6,242,432
2010.09 to 2010.10	$S_{9,10}$	684	5,471,318
2010.10 to 2010.11	$S_{10,11}$	659	5,270,778
2010.11 to 2010.12	$S_{11,12}$	649	5,191,386
2010.12 to 2011.01	$S_{12,13}$	589	4,711,660
2011.01 to 2011.03	$S_{13,14}$	470	3,754,590
2011.03 to 2011.04	$S_{14,15}$	463	3,701,668
2011.04 to 2011.05	$S_{15,16}$	443	3,542,622
2011.05 to 2011.06	$S_{16,17}$	426	3,407,204
2011.06 to 2011.07	$S_{17,18}$	401	3,205,760

So we define φ_- as the ratio of *negative* training examples, which is identical to the ratio of **prime** \rightarrow **prime** transitions, and we define φ_+ as the ratio of *positive*

Table 4.26: The size statistics for the *unbalanced* NCBI data set snapshots

Month Range	$S_{A,B}$	Size (MB)	# Total Examples	$ {}^1B_{16}^S $	$ {}^0B_{16}^S $
2010.01 to 2010.02	$S_{1,2}$	576	4,605,784	482,978	4,122,806
2010.02 to 2010.03	$S_{2,3}$	516	4,123,878	235,654	3,888,224
2010.03 to 2010.04	$S_{3,4}$	478	3,890,482	78,314	3,812,168
2010.04 to 2010.05	$S_{4,5}$	477	3,812,284	109,105	3,703,179
2010.05 to 2010.06	$S_{5,6}$	464	3,706,729	191,046	3,515,683
2010.06 to 2010.07	$S_{6,7}$	440	3,515,937	243,518	3,272,419
2010.07 to 2010.08	$S_{7,8}$	410	3,274,347	110,958	3,163,389
2010.08 to 2010.09	$S_{8,9}$	396	3,163,429	42,213	3,121,216
2010.09 to 2010.10	$S_{9,10}$	391	3,122,114	386,455	2,735,659
2010.10 to 2010.11	$S_{10,11}$	344	2,751,170	115,781	2,635,389
2010.11 to 2010.12	$S_{11,12}$	330	2,636,007	40,314	2,595,693
2010.12 to 2011.01	$S_{12,13}$	325	2,595,701	239,871	2,355,830
2011.01 to 2011.03	$S_{13,14}$	295	2,358,580	481,285	1,877,295
2011.03 to 2011.04	$S_{14,15}$	236	1,884,839	34,005	1,850,834
2011.04 to 2011.05	$S_{15,16}$	232	1,854,416	83,105	1,771,311
2011.05 to 2011.06	$S_{16,17}$	222	1,776,063	72,461	1,703,602
2011.06 to 2011.07	$S_{17,18}$	219	1,747,427	144,547	1,602,880

training examples, which is identical to the ratio of **prime** \rightarrow **oligomer** transitions.

Therefore, we define

$$\mathbf{prime} \rightarrow \mathbf{prime} : \varphi_-^{S_{A,B}} = \frac{|{}^0B_{16}^{S_{A,B}}|}{|{}^0B_{16}^{S_{A,B}}| + |{}^1B_{16}^{S_{A,B}}|}, \quad (4.43)$$

$$\mathbf{prime} \rightarrow \mathbf{oligomer} : \varphi_+^{S_{A,B}} = \frac{|{}^1B_{16}^{S_{A,B}}|}{|{}^0B_{16}^{S_{A,B}}| + |{}^1B_{16}^{S_{A,B}}|}, \quad (4.44)$$

as the ratio of negative and positive training examples for the NCBI snapshot $S_{A,B}$, respectively, such that $\varphi_-^{S_{A,B}} + \varphi_+^{S_{A,B}} = 1$, where $|{}^0B_{16}^{S_{A,B}}| + |{}^1B_{16}^{S_{A,B}}|$ is the *total* number of examples. Next, we define α_- and α_+ as Predictseq’s prediction *default accuracies* for the negative and positive examples, respectively. Thus, in terms of specific snapshots, we define $\alpha_-^{S_{A,B}}$ and $\alpha_+^{S_{A,B}}$ as Predictseq’s negative and positive example default accuracies for the NCBI snapshot $S_{A,B}$: so ${}^0B_{16}^{S_{A,B}}$ is to $\alpha_-^{S_{A,B}}$ just as ${}^1B_{16}^{S_{A,B}}$ is to $\alpha_+^{S_{A,B}}$. Therefore, we use

$$\Lambda_- = \alpha_- \times \varphi_-, \quad (4.45)$$

$$\Lambda_+ = \alpha_+ \times \varphi_+, \quad (4.46)$$

$$\Lambda_{total} = \Lambda_- + \Lambda_+, \quad (4.47)$$

to calculate Predictseq’s accuracies (performance/fitness) for the negative, positive, and total examples in $S_{A,B}$, respectively. Predictseq’s total accuracy is compared to the random biased guessing Λ_{BRG} in the form

$$\Lambda_{BRG} = ((1 - \alpha_+) \times \varphi_-) + (\alpha_+ \times \varphi_+). \quad (4.48)$$

Now, because NCBI occasionally modifies its records, there do exist **oligomer** → **prime** transitions that slightly influence our data sets, so we define this “error bar” E as the number of **oligomer** → **prime** transitions. See Table 4.29 for these results.

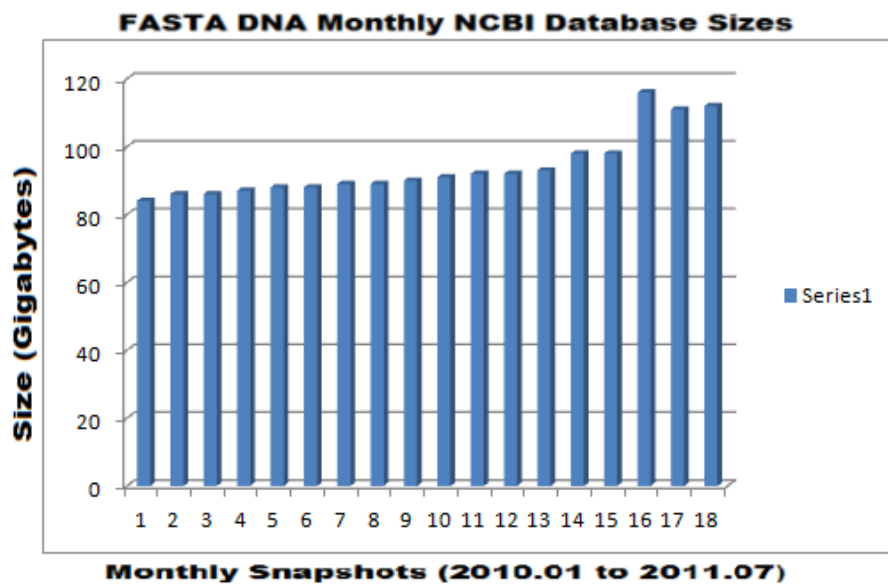


Figure 4.10: The FASTA DNA monthly NCBI database sizes ranging from January 2010 to July 2011

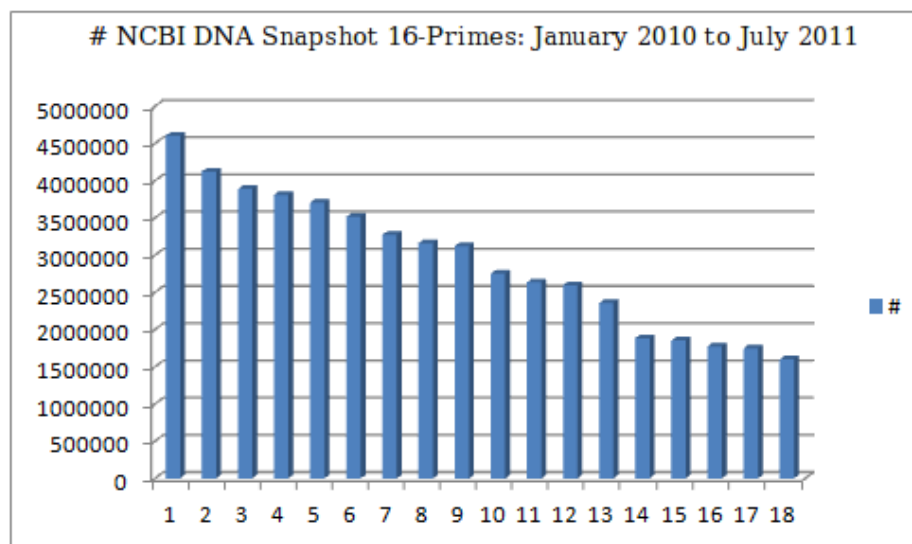


Figure 4.11: The DNA 16-prime set cardinalities for the NCBI database snapshots ranging from January 2010 to July 2011

Note: Although this experiment was systematically conducted over an 18-month period, the February 2011 NCBI snapshot was incomplete and thereby merged into the subsequent month—giving us a total of 17 data sets.

Results: ANN Training and Testing Accuracy Evaluations

In this section, we report the ANN configuration, training, and testing results of the NCBI data sets for (Boolean-valued) observed prime state prediction.

Table 4.27 displays the ANN architecture and training configuration for the *Quickprop* (Q), *Incremental Quickprop* (IQ), and *Resilient Backprop* (RB) algorithms. Table 4.28 displays the supervised learning training accuracies and fitness for the ANN on the (balanced) chronologically ordered monthly database snapshots—the most fit ANN state between the three training algorithms is bold highlighted and selected for the testing phase.

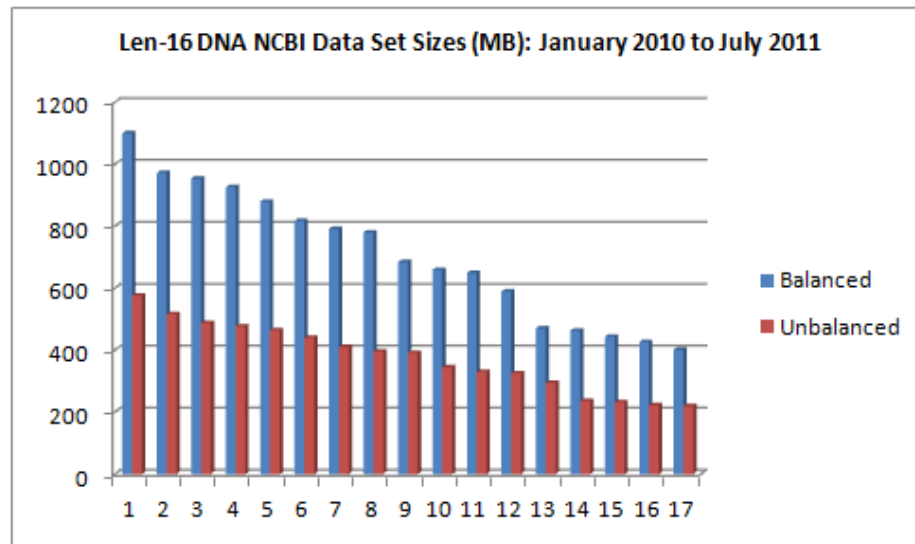


Figure 4.12: The DNA 16-prime set sizes (in megabytes) for the NCBI ANN training and testing data sets ranging from January 2010 to July 2011

The conclusions of this experiment are recapitulated in Section 5.1.

Table 4.27: The ANN training configuration for the observed prime state predictions on the monthly NCBI database snapshots

Parameter	Value
Learning Rate:	0.5
Learning Momentum:	0.5
Input (Layer) Size:	14
Hidden (Layer) Size:	4
Output (Layer) Size:	1
Activation Function:	Sigmoid
Epochs:	40,000
Target Accuracy:	90 %

Table 4.28: The ANN training accuracies for 16-prime state prediction on the *balanced* monthly DNA data sets ranging from January 2010 to July 2011

$S_{A,B}$	Q (%)	IQ (%)	RB (%)
$S_{1,2}$	75.0	74.8	75.2
$S_{2,3}$	75.0	74.8	75.1
$S_{3,4}$	75.0	74.8	75.0
$S_{4,5}$	75.0	74.8	75.4
$S_{5,6}$	75.0	74.8	75.5
$S_{6,7}$	74.9	74.8	74.9
$S_{7,8}$	75.0	74.8	75.1
$S_{8,9}$	75.0	74.8	75.1
$S_{9,10}$	75.0	74.7	75.7
$S_{10,11}$	75.1	74.7	75.2
$S_{11,12}$	75.0	74.7	75.1
$S_{12,13}$	75.4	74.7	75.5
$S_{13,14}$	74.9	74.6	75.3
$S_{14,15}$	75.2	74.6	75.3
$S_{15,16}$	75.0	74.6	75.3
$S_{16,17}$	75.0	74.7	75.1
$S_{17,18}$	75.1	74.7	75.1

Table 4.29: Predictseq’s ANN prediction accuracies for the 16-prime state *unbalanced* monthly DNA data sets ranging from February 2010 to July 2011. We see that Predictseq’s accuracy Λ_{total} outperformed the random biased guessing Λ_{BRG} in $\frac{14}{16}$ cases.

$S_{A,B}$	φ_- % ($ {}^0B_{16}^S $)	α_- %	Λ_- %	φ_+ % ($ {}^1B_{16}^S $)	α_+ %	Λ_{total} %	Λ_{BRG} %	E #
$S_{1,2}$	89.54 (4,122,806)	n/a	n/a	10.46 (482,978)	n/a	n/a	n/a	1,072
$S_{2,3}$	94.35 (3,888,224)	63.82	60.21	5.65 (235,654)	36.44	62.27	62.02	2,258
$S_{3,4}$	97.99 (3,812,168)	63.19	61.92	2.01 (78,314)	40.64	62.73	58.98	116
$S_{4,5}$	97.24 (3,703,179)	77.46	75.32	2.76 (109,105)	28.57	76.11	70.25	3,550
$S_{5,6}$	94.86 (3,515,683)	61.3	58.15	5.14 (191,046)	46.53	60.54	53.11	254
$S_{6,7}$	93.13 (3,272,419)	56.37	52.50	6.87 (243,518)	45.86	55.64	53.57	1,928
$S_{7,8}$	96.62 (3,163,389)	65.65	63.43	3.38 (110,958)	39.05	64.75	60.21	40
$S_{8,9}$	98.69 (3,121,216)	55	54.28	1.31 (42,213)	46.25	54.88	53.65	898
$S_{9,10}$	88.12 (2,735,659)	76.76	67.64	11.88 (386,455)	29.51	71.14	65.62	15,511
$S_{10,11}$	95.81 (2,635,389)	64.24	61.55	4.19 (115,781)	41.65	63.29	57.65	618
$S_{11,12}$	98.47 (2,595,693)	57.54	56.66	1.53 (40,314)	45.53	57.35	54.33	8
$S_{12,13}$	90.86 (2,355,830)	55.52	50.45	9.14 (239,871)	43.47	54.41	55.34	2,750
$S_{13,14}$	79.9 (1,877,295)	49.69	39.70	20.1 (481,285)	53.04	50.36	48.18	7,544
$S_{14,15}$	98.39 (1,850,834)	56.09	55.19	1.61 (34,005)	43.98	55.89	55.83	3,582
$S_{15,16}$	95.78 (1,771,311)	61.71	59.11	4.22 (83,105)	38.1	60.71	60.90	4,752
$S_{16,17}$	98.39 (1,703,602)	61.58	60.59	1.61 (72,461)	41.2	61.25	58.52	43,825
$S_{17,18}$	91.75 (1,602,880)	50.14	46.00	8.25 (144,547)	57.18	50.72	44.01	364

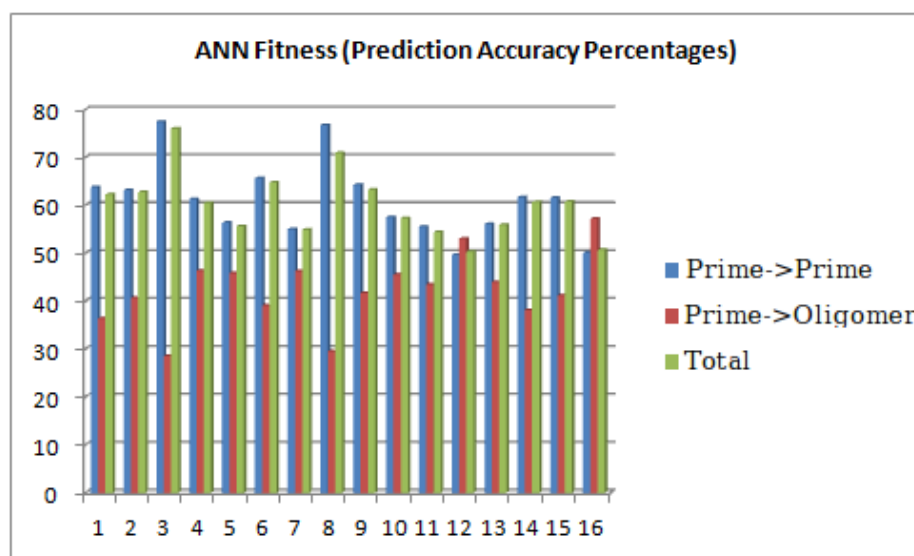


Figure 4.13: A depiction of the ANN 16-prime state prediction accuracies for the (unbalanced) monthly DNA data sets ranging from February 2010 to July 2011

CHAPTER 5

CONCLUSION

5.1 Results Discussion

In this section, we recapitulate the experimental results of Sections 4.3 and 4.4, respectively.

5.1.1 Experiment 1

Nullomers: Absent k -mer Statistics

In the ten model organisms, based on the AA nullomer probability, ranking, cardinality, and intersection/overlap results of Tables 4.3 and 4.4, and the chi-square results of Table 4.5, we see that the \mathbb{N} and \mathbb{A}_B data sets deviate substantially from the \mathbb{A}_U data sets—leading us to conclude that *the \mathbb{N} and \mathbb{A}_B AA sequences are non-random and therefore exhibit structural bias*—which supports our hypothesis.

In the EC bacteria, we considered the DNA/RNA nullomer probability, ranking, cardinality, and intersection/overlap results of Tables 4.10, 4.12, 4.14, 4.11, 4.13, and 4.15, and the chi-square results of Table 4.16. We conclude that the \mathbb{N} and \mathbb{A}_B sequences for the complete and coding regions deviate substantially from the \mathbb{A}_U data sets and are therefore non-random, which supports our hypothesis. Moreover,

we conclude that the non-coding regions of \mathbb{N} and \mathbb{A}_B exhibit statistics similar to \mathbb{A}_U and therefore appear random—contradicting our hypothesis.

In the HIV, we considered the DNA/RNA nullomer probability, ranking, cardinality, and intersection/overlap results of Tables 4.20, 4.21, 4.22, and 4.15, and the chi-square results of Table 4.23. Similarly to the EC bacteria, we conclude that the \mathbb{N} and \mathbb{A}_B sequences for the complete and coding regions of the HIV virus strains deviate substantially from the \mathbb{A}_U data sets and are therefore non-random, which supports our hypothesis. Furthermore, we conclude that the non-coding regions of \mathbb{N} and \mathbb{A}_B exhibit statistics similar to \mathbb{A}_U and therefore appear random, which contradicts our hypothesis.

In general, the \mathbb{A}_U sequences are strongly confined to just a small fraction of specific bins within the total histogram(s), whereas the \mathbb{N} and \mathbb{A}_B are more dispersed. The \mathbb{A}_U concentration arises because all characters in these data sets are generated by Genseq with an equal probability, whereas the characters of \mathbb{N} and \mathbb{A}_B are biased so the characters in these data sets are naturally-evolved (and generated via Genseq) with variable probabilities: \mathbb{N} and \mathbb{A}_B exhibit constraints while \mathbb{A}_U does not.

Oligomers and k -FS: Present k -mer Statistics

In the ten model organisms, we observe that the AA 3-FS results of Figures 4.1, 4.2, 4.3, 4.4, and 4.5 are uni-modal histogram distributions.

In the EC bacteria, we observe that the DNA 5-FS of Figures 4.6 and 4.7 are uni-modal histogram distributions for the complete, coding, and non-coding regions. The non-coding region distributions exhibit a *substantial* variation from the complete and coding regions. In particular, the non-coding distributions exhibit a positive skew and a smaller standard deviation, relative to the rest. From this, we conclude that

the non-coding regions for both strains are more random and thus exhibit less bias than the coding regions.

In the HIV, we observe that the DNA 3-FS of Figures 4.8 and 4.9 are uni-modal histogram distribution non-coding regions, yet the complete and coding region modalities are unclear, perhaps due to the relatively short genome lengths of the virus strains. The non-coding region distributions exhibit a *substantial* variation from the complete and coding regions (similarly to the EC bacteria). In particular, the non-coding distributions exhibit a positive skew and a smaller standard deviation, relative to the rest. From this, we conclude that the non-coding regions for both strains are more random and thus exhibit less bias than the coding regions, which is similar to the EC bacteria.

5.1.2 Experiment 2

Training

In the ANN *training* results of Table 4.28, we observed that in 17/17 training instances on the balanced (minority oversampled) monthly NCBI data sets for the prime states, the RB training algorithm matched or outperformed the Q and IQ algorithms in terms of training accuracy, and in 3 of these instances Q matched RB.

Moreover, we observed that the ANN training accuracies were quite consistent, with a range of 74.9% to 75.7%, an average of 75.23%, a median of 75.2%, and a standard deviation of 0.21%. In this experiment, the ANN architecture and training configuration of Table 4.27 slightly outperformed the rest for 40,000 epochs; we varied the training parameters and tried several distinct configurations, but found that changing these attributes imposed little or no impact on the final ANN fitness

for this particular problem domain.

Testing and Prediction

In the ANN *testing and prediction* results of Table 4.29 and Figure 4.13, we observed that the *prime-to-prime state* ANN prediction accuracies ranged from 49.69% to 77.46%, with an average of 61.0%, a median of 61.44%, and a standard deviation of 7.89%; the *prime-to-oligomer state* ANN prediction accuracies ranged from 28.57% to 57.18%, with an average of 42.3%, a median of 42.56%, and a standard deviation of 7.37%; therefore, the *total prime state* ANN prediction accuracies ranged from 50.37% to 76.06%, with an average of 60.08%, a median of 60.59%, and a standard deviation of 6.84%.

From the side-by-side comparison of columns Λ_{total} and Λ_{RBG} in Table 4.29, we conclude that Predictseq’s ANN performs better than random guessing: it is possible to train an ANN to predict, to some degree, the DNA 16-primers for subsequent months of the chronologically-ordered NCBI database, which contradicts our hypothesis. Here, it is evident that the ANN outperformed the biased random guessing in $\frac{14}{16}$ monthly snapshots.

5.2 Implication

In this section, we suggest post-experimental ramifications.

5.2.1 Experiment 1

As demonstrated, the statistical analysis utilities of this experimental software package employed to instrument this thesis are a bio-informatics “Swiss-Army Knife” for

organism DNA and AA sequence analysis. In this k -FS and nullomer experiment, we only considered the ten model organisms, the EC bacteria, and the HIV; however, these techniques can be applied to any organism, set of organisms, or subset of the NCBI database. The CSeq space and time enhancements for the GeneSIS cluster and the object-oriented filtering framework provide a powerful and flexible software platform for these sorts of investigations.

5.2.2 Experiment 2

Our assessment of prime prediction for length-16 DNA sequences revealed that it is possible to forecast, to some degree, the future prime states of the rapidly-evolving NCBI database—a potentially useful discovery—especially as additional FASTA and Genbank records are submitted to NCBI at accelerated rates. In general, the more knowledge acquired regarding the dynamics and evolution of DNA, AA, and biochemistry in the NCBI database, the closer we will be to understanding disease mechanisms. Prime prediction is a credible step in this direction.

5.3 Future Exploration

In this section, we propose future research trajectories along this mode of analysis.

5.3.1 Experiment 1

In the DNA portion of the k -FS and nullomer experiment, we only considered the complete, coding, and non-coding regions for the subject organisms. It would be interesting to consider additional regions such as the gene, promoter, tRNA, transposon, and etc. Similarly to the DNA regions, it would also be interesting to

explore properties of various AA regions. It is noteworthy that CSeq's Genbank screening system allows the user to logically define sophisticated filters, for both regular expression and region-specific filters. Future studies of this flavor should take advantage of these features and apply these filters to organisms throughout the phylogenetic tree of life.

A graphical user interface for Scriptgen would make the application and k -FS analysis configuration more user friendly. A user could easily manage configuration by creating a new file, opening a previous file, and/or saving an existing file to disk. Also, general usage could be improved by increasing user error verbosity and adding more complex exception handling.

Genseq's artificial sequences generator operates as a single Markov chain. It would be interesting to incorporate dual Markov chains into Genseq, where each symbol is a function of two synchronized random processes, rather than just a single process. Perhaps, the interdependent processes will provide a more "natural" and "rich" random sequence generator?

Clearly, genetic mutation mechanisms are responsible for the evolved k -FS and nullomer results. Thus, a rigorous mathematical framework and field theory for the dynamics and mechanisms of bio-molecular interactions must be developed to reconcile experimental and theoretical dissonance. To achieve this, physicists must first establish a unified field theory. Second, the probability framework of quantum mechanics must be extended from the sub-atomic and atomic realms to that of the molecular. This will provide a deep and precise explanation of the observed k -FS results and DNA double helix, and thereby equip biochemists with a rich methodology to make advanced calculations and predictions for genetic mutations and evolutionary trajectories. Third, an abstract function framework must be developed and employed

in biochemistry to mathematically associate the 2D DNA structure with 3D AA structure using the k -FS and nullomer probability as a basis. Fourth and finally, this proposed theory describing the results of [7, 26, 8] should then be connected with the results of [42, 43, 33, 15, 28] using the language of [29] and [2] to formally depict bio-molecular arrangement.

5.3.2 Experiment 2

Given the scope of this thesis, only several ANN architectures and training configurations were considered. We suggest that future prime prediction research should explore additional ANN parameters to determine if superior training, testing, and performance can be achieved. As the NCBI database growth accelerates, such alternatives may become increasingly important due to the sheer amount of rapid genome data increase.

In this experiment, we assessed DNA prime prediction. We suggest that future forecasting efforts should additionally consider AA prime prediction with the provided statistical analysis utilities.

A graphical user interface for Predictseq would make the application and prime assessment configuration more user friendly. A user could easily manage configuration by creating a new file, opening a previous file, and/or saving an existing file to disk. Also, general usage could be improved by increasing user error verbosity and adding more complex exception handling.

The Predictseq and Tdataformat applications are currently limited to the ANN, but contain skeleton code for a Naive Bayes Classifier and a Support Vector Machine. It may be beneficial to finish integrating these prime prediction alternatives, execute

them on the NCBI database snapshots, and compare the training, testing, and performance results to that of the ANN.

5.4 Recapitulation

In this thesis, we investigated the k -FS distributions and nullomer phenomena for a set of subject organism DNA and AA sequences. We considered statistics for the accelerated growth of the NCBI database over an 18-month span and deployed a statistical software analysis suite to attack these problems by assessing nullomer predictability.

In Chapter 2, we highlighted the influential literature of this thesis and discussed how these fundamental notions directed the k -mer investigation.

In Chapter 3, we introduced the statistical software application suite that was designed to instrument the k -mer-based sequence analysis. We summarized key data structures and algorithms, and explained the purpose of individual utilities by providing pseudo-code with the execution summary. We discussed how complete organism genome sequences are obtained from NCBI are processed, interpreted, and evaluated by the software to analyze the associated k -FS and nullomer sets. These genome statistics were systematically compared against artificially-generated genomes to determine the present degree of structural bias.

In Chapter 4, we defined a set of experiments to conduct with our software suite and report the results. First, we examined the k -FS pertaining to the AA sequences of ten individual model organisms and conducted a focused DNA comparative analysis on various strains of EC bacteria and HIV. The second experiment assessed the nullomer predictability by chronologically analyzing complete monthly DNA snapshots

of the NCBI database as a time series using an ANN.

Finally, we've discussed the results and implications of this thesis, and suggested future projections along this mode of biological exploration.

REFERENCES

- [1] C. Acquisti, G. Poste, D. Curtiss, and S. Kumar. Nullomers: really a matter of natural selection? *PloS one*, 2(10):e1022, 2007.
- [2] M.F. Barnsley. *Superfractals*. Cambridge Univ Pr, 2006.
- [3] VN Blinov and VL Golo. Acoustic spectroscopy of dna in the gigahertz range. *Physical Review E*, 83(2):21904, 2011.
- [4] D.J. Brooks, J.R. Fresco, A.M. Lesk, and M. Singh. Evolution of amino acid frequencies in proteins over deep time: inferred order of introduction of amino acids into the genetic code. *Molecular Biology and Evolution*, 19(10):1645–1655, 2002.
- [5] C. Burge, A.M. Campbell, and S. Karlin. Over and under-representation of short oligonucleotides in dna sequences. *Proceedings of the National Academy of Sciences*, 89(4):1358, 1992.
- [6] C. Bystroff, V. Thorsson, and D. Baker. Hmmstr: a hidden markov model for local sequence-structure correlations in proteins. *Journal of molecular biology*, 301(1):173–190, 2000.
- [7] Yaw-Hwang. Chen, Su-Long. Nyeo, and Chiung-Yuh. Yeh. Model for the distributions of k-mers in DNA sequences. *Physics Review E*, 72, 2005.
- [8] B. Chor, D. Horn, N. Goldman, Y. Levy, and T. Massingham. Genomic DNA k-mer spectra: models and modalities. *Genome biology*, 10(10):R108, 2009.
- [9] K.C. Chou. The biological functions of low-frequency vibrations (phonons). 4. resonance effects and allosteric transition. *Biophysical chemistry*, 20(1-2):61–71, 1984.
- [10] KC Chou. Biological functions of low-frequency vibrations (phonons). iii. helical structures and microenvironment. *Biophysical journal*, 45(5):881–889, 1984.
- [11] K.C. Chou. Low-frequency motions in protein molecules. beta-sheet and beta-barrel. *Biophysical journal*, 48(2):289–297, 1985.

- [12] K.C. Chou. The biological functions of low-frequency vibrations (phonons). vi. a possible dynamic mechanism of allosteric transition in antibody molecules. *Biopolymers*, 26(2):285–295, 1987.
- [13] K.C. Chou. Low-frequency collective motion in biomacromolecules and its biological functions. *Biophysical Chemistry*, 30(1):3–48, 1988.
- [14] K.C. Chou and Y.S. Kiang. The biological functions of low-frequency vibrations (phonons): 5. a phenomenological theory. *Biophysical chemistry*, 22(3):219–235, 1985.
- [15] L. Demetrius. Quantum statistics and allometric scaling of organisms. *Physica A: Statistical Mechanics and its Applications*, 322:477–490, 2003.
- [16] P. Deschavanne, A. Giron, J. Vilain, C. Dufraigne, and B. Fertil. Genomic signature is preserved in short dna fragments. In *Bio-Informatics and Biomedical Engineering, 2000. Proceedings. IEEE International Symposium on*, pages 161–167. IEEE, 2000.
- [17] P.J. Deschavanne, A. Giron, J. Vilain, G. Fagot, and B. Fertil. Genomic signature: characterization and classification of species assessed by chaos game representation of sequences. *Molecular Biology and Evolution*, 16(10):1391–1399, 1999.
- [18] C. Dutta and J. Das. Mathematical characterization of chaos game representation: New algorithms for nucleotide sequence analysis. *Journal of molecular biology*, 228(3):715–719, 1992.
- [19] N. Echols, P. Harrison, S. Balasubramanian, N.M. Luscombe, P. Bertone, Z. Zhang, and M. Gerstein. Comprehensive analysis of amino acid and nucleotide composition in eukaryotic genomes, comparing genes and pseudogenes. *Nucleic acids research*, 30(11):2515–2523, 2002.
- [20] Y. Fofanov, Y. Luo, C. Katili, J. Wang, Y. Belosludtsev, T. Powdrill, C. Belapurkar, V. Fofanov, T.B. Li, S. Chumakov, et al. How independent are the appearances of n-mers in different genomes? *Bioinformatics*, 20(15):2421–2428, 2004.
- [21] DR Forsdyke. Relative roles of primary sequence and (g+ c)% in determining the hierarchy of frequencies of complementary trinucleotide pairs in dnas of different species. *Journal of molecular evolution*, 41(5):573–581, 1995.
- [22] Y. GAVEL and G. HEIJNE. The distribution of charged amino acids in mitochondrial inner-membrane proteins suggests different modes of membrane

- integration for nuclearly and mitochondrially encoded proteins. *European Journal of Biochemistry*, 205(3):1207–1215, 1992.
- [23] A.J. Gentles and S. Karlin. Genome-scale compositional comparisons in eukaryotes. *Genome research*, 11(4):540–546, 2001.
- [24] M. Gerstein. A structural census of genomes: comparing bacterial, eukaryotic, and archaeal genomes in terms of protein structure1. *Journal of molecular biology*, 274(4):562–576, 1997.
- [25] G. Gordon. Extrinsic electromagnetic fields, low frequency (phonon) vibrations, and control of cell function: a non-linear resonance system. *Journal of Biomedical Science and Engineering*, 1(3):152–156, 2008.
- [26] G. Hampikian and T. Andersen. Absent sequences: nullomers and primes. *Biocomputing 2007*, page 355, 2006.
- [27] B. Haubold, N. Pierstorff, F. Möller, and T. Wiehe. Genome comparison without alignment using shortest unique substrings. *BMC bioinformatics*, 6(1):123, 2005.
- [28] Y. Huang and X.S. Yang. Horseshoes in chromosome’s attractors. *Chaos, Solitons & Fractals*, 32(5):1686–1691, 2007.
- [29] B.B. Mandelbrot. *The fractal geometry of nature*. Wh Freeman, 1983.
- [30] V. Neduva, R. Linding, I. Su-Angrand, A. Stark, F. De Masi, T.J. Gibson, J. Lewis, L. Serrano, and R.B. Russell. Systematic discovery of new recognition peptides mediating protein interaction networks. *PLoS biology*, 3(12):e405, 2005.
- [31] J.M. Otaki, S. Ienaka, T. Gotoh, and H. Yamamoto. Availability of short amino acid sequences in proteins. *Protein science*, 14(3):617–625, 2005.
- [32] P.C. Painter, L. Mosher, and C. Rhoads. Low-frequency modes in the raman spectrum of dna. *Biopolymers*, 20(1):243–247, 1981.
- [33] A. Provata and Y. Almirantis. Fractal cantor patterns in the sequence structure of dna. *FRACTALS-LONDON-*, 8(1):15–28, 2000.
- [34] J. Qi, B. Wang, and B.I. Hao. Whole proteome prokaryote phylogeny without sequence alignment: a k-string composition approach. *Journal of molecular evolution*, 58(1):1–11, 2004.
- [35] G. Reinert, S. Schbath, and M.S. Waterman. Probabilistic and statistical properties of words: an overview. *Journal of Computational Biology*, 7(1-2):1–46, 2000.

- [36] S. Robin and S. Schbath. Numerical comparison of several approximations of the word count distribution in random sequences. *Journal of Computational Biology*, 8(4):349–359, 2001.
- [37] P.M. Sharp and G. Matassi. Codon usage and genome evolution. *Current opinion in genetics & development*, 4(6):851–860, 1994.
- [38] C.C. Shih and S. Georghiou. Harmonic analysis of dna dynamics in a viscous medium. *Journal of biomolecular structure & dynamics*, 17(5):921, 2000.
- [39] J. Sved and A. Bird. The expected equilibrium of the cpg dinucleotide in vertebrate genomes under a mutation model. *Proceedings of the National Academy of Sciences*, 87(12):4692, 1990.
- [40] T. Tuller, B. Chor, and N. Nelson. Forbidden penta-peptides. *Protein Science*, 16(10):2251–2259, 2007.
- [41] I. Ulitsky, D. Burstein, T. Tuller, and B. Chor. The average common substring approach to phylogenomic reconstruction. *Journal of Computational Biology*, 13(2):336–350, 2006.
- [42] G.B. West, J.H. Brown, and B.J. Enquist. A general model for the origin of allometric scaling laws in biology. *Science*, 276(5309):122, 1997.
- [43] G.B. West, J.H. Brown, and B.J. Enquist. The fourth dimension of life: fractal geometry and allometric scaling of organisms. *Science*, 284(5420):1677, 1999.

APPENDIX A

USER MANUAL

A.1 Overview

This chapter contains the Linux command line usage for the *k*-mer and nullomer statistical software analysis suite.

A.2 CSeq

In this section, we provide the usage for *k*-mer processing and reprocessing, along with example FASTA and Genbank filter files.

A.2.1 Processor

Usage: ./process file.list maxseqLen [- < cmd0 >< arg0 >][- < cmd1 >< arg1 >]...[- < cmdN >< argN >]

Description: Calculates the *k*-FS for organism genome and protein sequences.

Command(s):

[-p]	Print oligomer statistics
[-pn]	Print nullomer statistics
[-pl]	Print long
[-h]	Output help/command menu
[-c < string >]	Alphabet symbols
[-o < outputFile >]	Output file
[-ssplitIDmaxSplits]	Split identification and maximum number of splits
[-readonly]	Database read-only
[-f < string >]	Filter file
[-rc]	Calculate reverse complements

A.2.2 Reprocessor

Usage: ./reprocess file.list seqLen [- < cmd0 > < arg0 >][- < cmd1 > < arg1 >]...[- < cmdN > < argN >]

Description: Calculates the (previously processed) *k*-FS for organism genome and protein sequences as a post-processing utility.

Command(s):

[-jp]	Just print.
[-p]	Print oligomer statistics
[-pn]	Print nullomer statistics
[-o < outputFile >]	Output file
[-ssplitIDmax.Splits]	Split identification and maximum number of splits
[-rc]	Calculate reverse complements
[-h]	Output help/command menu

A.2.3 FASTA Filtering

An example of a CSeq FASTA record filter file which requires the *human* regular expression to logically exist:

```
fasta_filter:
  exist=yes
  value=(.)*[Hh]omo [Ss]apien(.)*
```

An example of a CSeq FASTA record filtering file which requires the *chicken* regular expression to logically *not* exist *and* additionally the *cattle* regular expression to *not* exist:

```
fasta_filter:
  exist=no
  value=(.)*[Gg]allus [Gg]allus(.)*
AND
fasta_filter:
  exist=no
  value=(.)*[Bb]os [Tt]aurus(.)*
```

A.2.4 Genbank Filtering

An example of a CSeq Genbank record regular expression filter file which requires the *polar bear* to logically exist *OR* the *tiger* regular expression to logically not exist at the depth-1 meta-data component (using key/integer-valued parameters):

```
genbank_filter:
  input_mode=key
  filter_type=regex
  exist=yes
  value=(.)*[Pp]olar [Bb]ear(.)*
  depth1_attribute=6
  depth2_field=0
  depth3_subfield=0
OR
genbank_filter:
  input_mode=key
  filter_type=regex
  exist=no
  value=(.)*[Tt]iger(.)*
  depth1_attribute=6
  depth2_field=0
```

```
depth3_subfield=0
```

An example of a CSeq Genbank record regular expression filter file which requires the *cds* (coding region specifier) to logically exist at the depth-2 meta-data component (using string-valued parameters):

```
genbank_filter:
  input_mode=string
  filter_type=region
  exist=yes
  value=(.)*[Tt]iger(.)*
  depth1_attribute=features
  depth2_field=cds
  depth3_subfield=NULL
```

An example of a CSeq Genbank record region-specific filter file which screens for the non-*cds* region (using string-valued parameters):

```
genbank_filter:
  input_mode=string
  filter_type=region
  exist=no
  region=cds
```

An example of a CSeq Genbank record region-specific filter file which logically screens for the *cds* AND *promoter* regions (using string-valued parameters):

```
genbank_filter:
  input_mode=string
  filter_type=region
  exist=yes
  region=cds
```

AND

```
genbank_filter:
  input_mode=string
  filter_type=region
  exist=yes
  region=promoter
```

An example of a CSeq Genbank record region-specific filter file which logically screens for the *cds* OR *promoter* regions (using string-valued parameters):

```
genbank_filter:
  input_mode=string
  filter_type=region
  exist=yes
  region=cds
```

OR

```
genbank_filter:
  input_mode=string
  filter_type=region
  exist=yes
  region=promoter
```

A.3 Analysis Applications

In this section, we provide the usage for utilities designated for the post-processing stage of the k -mer and prime/nullomer analysis.

A.3.1 Rankseq

Usage: ./rankseq [- < cmd0 >< arg0 >][- < cmd1 >< arg1 >]...[- < cmdN >< argN >]

Description: Calculates the transitional probabilities associated with each sequence motif with respect to the underlying subsequence probabilities

Command(s):

<code>[-single < sequence >]</code>	Required: Single sequence or multiple sequences listed in a file of specified name
<code>[-multiple < filename >]</code>	Required: Name of file containing the list of CSeq frequency statistics filenames
<code>[-statfiles < filename >]</code>	Required: Specifies the alphabet as "DNA" or "protein"
<code>[-alphabet < dna protein >]</code>	Required: Maximum subsequence length to partition the sequence motifs by
<code>[-partition < integer >]</code>	Optional: Print help information
<code>[-h]</code>	

A.3.2 NcbiStat

Usage: ./ncbistat [- < cmd0 >< arg0 >][- < cmd1 >< arg1 >]

Description: Calculates the total sequence length of the supplied NCBI data set in symbols (DNA or protein characters)

Command(s):

<code>[-input < filename >]</code>	Required: Name of the file containing a list of NCBI files
<code>[-filter < filename >]</code>	Optional: Name of the filter file
<code>[-h]</code>	Optional: Print help information

A.3.3 Genseq

Usage: ./genseq [- < cmd0 >< arg0 >][- < cmd1 >< arg1 >]...[- < cmdN >< argN >]

Description: Generates an alphabet-specific sequence of particular size using either (1) CSeqStat frequency statistics or (2) randomly.

Command(s):

<code>[-randgen][--statgen]</code>	Required: Generation mode, specify random or statistical generation mode
<code>[-statistics < filename >]</code>	Required: Name of the file which contains the list binary statistics frequency files
<code>[-qlen < integer >]</code>	Required: Length of string to query for frequency statistics
<code>[-slen < integer >]</code>	Required: Maximum sequence processing length
<code>[-alphabet < dna protein >]</code>	Required: Specifies the alphabet as "DNA" or "protein"
<code>[-size < integer >]</code>	Required: Size (in symbols) of data set to generate
<code>[-seed < integer >]</code>	Optional: Set the pseudo-random seed value
<code>[-p]</code>	Optional: Causes program to print results to screen
<code>[-pn]</code>	Optional: Causes program to print nulls to screen
<code>[-o < filename >]</code>	Optional: Set the name of the output file. If not specified results will be written to the screen
<code>[-s < splitID >< maxSplits >]</code>	Optional: The number of splits, and splitID is the split that this instantiation of the program will gather stats on
<code>[-rc]</code>	Optional: Reprocess binary statistics files for reverse complements
<code>[-h]</code>	Optional: Print help information

A.3.4 Freqseq

Usage: `./freqseq [- < cmd0 >< arg0 >][- < cmd1 >< arg1 >]...[- < cmdN >< argN >]`

Description: Expresses the relative frequency of a specific sequence length as a function of the exact count, such that the $0 \leq \text{count} \leq \text{max}$ by generating the corresponding histogram.

Command(s):

<code>[-maxcount < integer >]</code>	Required: The maximum exact count
<code>[-slength < integer >]</code>	Required: The maximum sequence motif length
<code>[-statfiles < filename >]</code>	Required: Name of the file which contains the list binary frequency statistic files
<code>[-alphabet < dna protein >]</code>	Required: Specifies the alphabet as "DNA" or "protein"
<code>[-n < integer >]</code>	Optional: Number of histogram bins (Default: 10 bins)
<code>[-normalize]</code>	Optional: Normalize the histogram to display relative frequencies
<code>[-statistics]</code>	Optional: Calculate and output histogram bin distribution statistics
<code>[-title < string >]</code>	Optional: Name/title of the histogram(s) being generated, this single word value appears in the output header
<code>[-h]</code>	Optional: Print help information

A.3.5 Nullcountseq

Usage: ./nullcountseq [- < cmd0 > < arg0 >][- < cmd1 > < arg1 >]...[- < cmdN > < argN >]

Description: Calculates the average size and overlap ratio of nullomer sets identified in stat-generated and randomly-generated with respect to the real NCBI data set. The results are displayed in an n -by- m matrix comma-delimited format, such that n is the maximum length of the nullomer sequence set and m is the number of datasets being compared/contrasted

Command(s):

[-h]	Optional: Print help information
[-input < filename >]	Required: Name of file containing a list of file lists, such that each contains the path of the nullomer sets

A.3.6 Predictseq

Usage: ./predictseq [- < cmd0 > < arg0 >][- < cmd1 > < arg1 >]...[- < cmdN > < argN >]

Description: Supervised machine learning application used to assess nullomer predictability.

Command(s):

[-i < dataset >]	Required: Data set input file used to train, test, or make a prediction
[-train < ann svm nbc > < config_file > < target_accuracy > < epochs >]	Optional: Train system
[-test < ann svm nbc > < state_file >]	Optional: Test system
[-predict < ann svm nbc > < state_file >]	Optional Make a prediction
[-o < output_file >]	Required: Output directory
[-p < integer >]	Required: The (Rankseq) subsequence partition length
[-a < dna protein >]	Required: Alphabet (i.e. "DNA" or "protein")
[-h]	Optional: Print help information

Example Predictseq ANN configuration file:

```
learning_rate=0.1
learning_momentum=0.2
algorithm=FANN_TRAIN_QUICKPROP
input_size=AUTO
hidden_size=4
output_size=1
activation_function=FANN_SIGMOID
```

A.3.7 Tdataformat

Usage: ./tdataformat [- < cmd0 > < arg0 >][- < cmd1 > < arg1 >]...[- < cmdN > < argN >]

Description: Creates a Predictseq data set from (A) a Rankseq output file and (B) a set of nullomers.

Command(s):

[-i < rankseq_file > < nullomer_file >]	Required: Month A and month B input files
[-o < output_file >]	Required: Data set output file
[-t < ann svm nbc >]	Required: Learning algorithm format type
[-b]	Optional: Balance flag (over-sample the minority examples)
[-h]	Optional: Print help information

A.3.8 Tdatamerge

Usage: ./tdatamerge [- < cmd0 >< arg0 >][- < cmd1 >< arg1 >]

Description: Consolidates a list of Tdataformat datasets to a single file for use with Predictseq.

Command(s):

[-i < tdataformat_file_list >]	Required: File containing a list of Tdataformat filenames to merge.
[-o < filename >]	Required: Final data set output file.
[-h]	Optional: Print help information

A.3.9 34Seq

Usage: ./34seq [- < cmd0 >< arg0 >]

Description: Calculates the number sequences with contiguous nucleotide base pair triplets and quadruplets, given a list of sequences.

Command(s):

[-i < dna_sequence_file_list >]	Required: File containing a list of sequences to process.
[-h]	Optional: Print help information

A.3.10 Setstat

Usage: ./setstat [- < cmd0 >< arg0 >]

Description: Calculates the default accuracies and NCBI absent-sequence resubmission errors, given a filename list of nullomer/prime sets.

Command(s):

[-list < filename >]	Required: Filename list of nullomer/prime sets
[-h]	Optional: Print help information

A.4 Format and Display Applications

In this section, we provide the usage for utilities designated to the the post-ranking stage of the k -mer and prime/nullomer analysis.

A.4.1 Rangestat

Usage: ./rangestat [- < cmd0 >< arg0 >][- < cmd1 >< arg1 >]...[- < cmdN >< argN >]

Description: Determines the lower and upper bounds given a list of Rankseq output ranges.

Command(s):

[-range < filename >]	Required: Name of the file containing a list of Rankseq range output files
[-length < integer >]	Optional: Required only for oligomer-specific statistics; the maximum sequence length to query the frequency statistics
[-h]	Optional: Print help information

A.4.2 Histoseq

Usage: ./histoseq [- < cmd0 >< arg0 >][- < cmd1 >< arg1 >]...[- < cmdN >< argN >]

Description: Generates a histogram or set of histograms in *.csv format, based on the user-supplied Rankseq output file.

Command(s):

<code>[-rankseq < filename >]</code>	Required: Rankseq output file to generate the histogram from
<code>[-title < string >]</code>	Optional: Name/title of the histogram(s) being generated, this single word value appears in the output header
<code>[-range < filename >]</code>	Optional: File containing a list of Rankseq2 range files, used for global normalization of the data
<code>[-n < integer >]</code>	Optional: Number of histogram bins (Default: 10 bins)
<code>[-automerger]</code>	Optional: Automatically merges the histograms by normalizing the bin values
<code>[-normalize]</code>	Optional: Normalize the histogram to display relative frequencies
<code>[-statistics]</code>	Optional: Calculate and output histogram bin distribution statistics
<code>[-h]</code>	Optional: Print help/usage information

A.4.3 Histoavg

Usage: `./histoavg [- < cmd0 >< arg0 >][- < cmd1 >< arg1 >]...[- < cmdN >< argN >]`

Description: Averages a list of uniform-sized histograms and their bin values; consolidating them to a single histogram.

Command(s):

<code>[-input < filename >]</code>	Required: Name of file containing the list of uniform-sized histograms to be averaged/consolidated
<code>[-title < string >]</code>	Optional: Name/title of the histogram(s) being averaged, this single word value appears in the output header
<code>[-normalize]</code>	Optional: Normalize the histogram to display relative frequencies
<code>[-h]</code>	Optional: Print help information

A.4.4 Scriptgen

Usage: `./scriptgen [- < cmd0 >< arg0 >][- < cmd1 >< arg1 >]...[- < cmdN >< argN >]`

Description: Generates the scripts for the random analysis experiment based on the parameters in the configuration file.

Command(s):

<code>[-config < filename >]</code>	Required: Configuration file
<code>[-h]</code>	Optional: Print help information

Example Scriptgen configuration file:

```

experiment_title=2011-04-17_protein_Apis_mellifera_complete
executable_base_directory=/home/nschmidt/Development/cseq/src/
output_base_directory=/genfs-scratch/nschmidt/entropy_analysis/protein/
# [CSEQ]
ncbi_file_list=/genfs-scratch/nschmidt/entropy_analysis/protein/cfg/2011-04-17_protein_Apis_mellifera.input
ncbi_filter=NULL
sequence_type=PROTEIN
sequence_length=5
# [RANKSEQ]
subsequence_partition_length=3
# [HISTOSEQ]

```

```
num_histogram_bins=50
# [GENSEQ]
generation_size=4729600
num_dataset_instances=30
# [FREQSEQ]
freqseq_maximum_count=5000
freqseq_maximum_sequence_length=5
freqseq_num_histogram_bins=50
freqseq_normalize=yes
```

APPENDIX B

SOURCE CODE SNIPPETS

B.1 Overview

In this brief chapter we highlight source code snippets that are fundamental to instrumenting the prime probability ranking and prediction.

B.2 Analysis Applications

Figure B.1: Rankseq's sequence probability ranking algorithm

```

extern long double rankseq2_calculate_transitional_probabilities(
    RANKSEQ_CONFIG* config, RANKSEQ2_ELEMENT* element,
    const unsigned short max_plen, boost::shared_ptr<Base_Seq_DB>& stats)
{
    long double prob = 0.0, p_temp = 0.0;
    unsigned int start = 0, end = max_plen, length = strlen(element->sequence);
    string motif(element->sequence), temp = "", chars(stats->util.getBase());

    /** If short sequence, evaluate immediately */
    if(length < max_plen) { return (long double)(stats->getProbability(motif)); }

    /** Initialize probability */
    else { prob = 1.0; }
    temp = string(motif).substr(start, end - start);

    /** Acquire initial probability */
    prob *= (long double)stats->getProbability(temp);
    ++start;
    ++end;

    /** Evaluate each character concatenated to the sequence */
    while(end <= length)
    {
        temp = string(motif).substr(start, end - start);

        /** Ignore edge case */
        if(!temp.length() || (temp[0] == ' ')) { break; }

        /** Sum probabilities */
        p_temp = 0.0;
        for(int x = 0; x < (int)chars.length(); x++)
        {
            /** Evaluate by concatenating each character in alphabet */
            temp.replace(max_plen - 1, 1, 1, chars[x]);
            p_temp += (long double)stats->getProbability(temp);
        }

        /** Compute normalized probability of original string */
        temp = string(motif).substr(start, end - start);
        p_temp = (long double)stats->getProbability(temp) / p_temp;

        /** If legal probability, add to existing probability */
        if((p_temp) && (fpclassify(p_temp) == FP_NORMAL)) { prob *= (long double)p_temp; }

        ++start;
        ++end;
    }

    return prob;
}

```

APPENDIX C

DETAILED EXPERIMENTATION PROCEDURES

C.1 Overview

This chapter reports the detailed preparation and procedure the two k -mer experiments.

C.2 Experiment 1

C.2.1 Preparation

First, we select the model organisms of interest and prepare the corresponding configuration files. The Scriptgen utility (described in Section 3.4.4) is used to instrument this experiment on the GeneSIS cluster and requires that a configuration file for each subject organism is created by the user; each Scriptgen configuration file contains the following parameters to generate the appropriate cluster execution scripts:

1. **Experiment Title:** Name to associate with this particular k -mer analysis experiment (i.e. “20110417_protein_Apis_mellifera”). All files pertaining to the experiment (including the GeneSIS cluster command execution scripts and results) are stored in a sub-directory (of the output base directory) with this label.
2. **Executable Base Directory:** The absolute pathname of the base directory containing the compiled executables (i.e. “/home/nschmidt/Development/”).
3. **Output Base Directory:** The absolute pathname of the base directory to export the experimentrelated files to (i.e. “/home/nschmidt/kmer_analysis/protein/”).
4. **NCBI File List:** A file containing the list of NCBI input files to process (i.e. “/home/nschmidt/kmer_analysis/protein/2011-0417_Apis_mellifera.input”) with CSeq. In this case since we are interested in specific organisms, the most efficient method is to create a list file which contains only the Genbank files corresponding to the subject organism (yet recall that it is also possible to filter for organism-specific entries).
5. **NCBI Filter:** A file containing NCBI-specific filtering parameters (i.e. “NULL” for no filtering or “/home/nschmidt/kmer_analysis/protein/coding-regions” for filtering).
6. **Sequence Type:** The alphabet being processed (i.e. “PROTEIN” or “DNA”). NCBI input files that do not match this description are automatically discarded by CSeq and related software.
7. **Sequence Length:** The maximum sequence length that CSeq and related software will process (i.e. “6” or “14”).
8. **Sub-sequence Partitioning Length:** The maximum partitioning length that Rankseq will process and Genseq will use to generate artificial genome sequences with (i.e. “5” or “13”).
9. **Number of (Histoseq) Histogram Bins:** The number of histogram bins used by Histoseq and Histoavg (i.e. “50” or “200”).

10. **Generation Size:** The length of the artificial genome sequence to generate with Genseq (i.e. “4729600”). This value must match the length of the real organism genome sequence to be comparable, and must be manually identified using the NcbiStat utility (see Section 3.3.2) before executing the experiment.
11. **Number of Data Set Instances:** The number of artificial data set instances that Genseq will generate (i.e. “30”). This value must be set to acquire a proper distribution of data sets to perform a legitimate sequence analysis.
12. **Freqseq Maximum Count:** The upper limit for the Freqseq k -mer histogram results (i.e. “5000” or “20000”); the utility calculates the frequencies from 1 up to this value and maps the distribution to a histogram of specified bin size.
13. **Freqseq Maximum Sequence Length:** The maximum sequence length (i.e. “5” or “13”). This value must be less than the minimum nullomer length and have a corresponding count file, thus it must not exceed the sub-sequence partitioning length.
14. **Number of (Freqseq) Histogram Bins:** The number of histogram bins used by Freqseq (i.e. “50”).
15. **Freqseq Normalize:** The Freqseq histogram normalization flag (i.e. “yes” or “no”).

For an example of this particular file and Scriptgen usage see Section A.4.4.

C.2.2 Procedure

Recall that the GeneSIS cluster command scripts required to execute this experiment are automatically generated by the Scriptgen utility; however the parameters and options necessary to conduct this particular experiment manually are listed by the user.

Step 1: Process Organism-Specific NCBI Data

Supply the parameters discussed in this section to the CSeq executable “./process”. First, determine the subset of the NCBI database associated with the organism and create a file consisting of a list of genome input files. If filtering is required, define the filters by creating the appropriate filter file and specify it using the “-f” option. Determine the alphabet type associated with the organism (DNA or AA) using the “-a” option and select the nullomer print option “-pn”. Subsequently, choose a maximum target sequence processing length; let this value be n . Next define the preferred output directory using the “-o” option, and redirect the nullomer output accordingly.

Step 2: Reprocess Organism-Specific NCBI Data

Supply the parameters discussed in this section to the CSeq executable “./reprocess”. Given the maximum sequence processing length n , the “./reprocess” must be executed for all sub-subsequence processing lengths ranging from 1 to $n - 1$. Subsequently we create a file consisting the file path to the CSeq frequency output file and supply that as an argument. Next, we select the nullomer print option “-pn” and define the preferred output directory using the “-o” option, and redirect the nullomer output accordingly.

Step 3: Generate and Process Statistically-Biased Artificial Genome Data

Supply the parameters discussed in this section to the Genseq executable “./genseq”. Create a file containing a list of file paths corresponding to the CSeq frequency output using the “-statistics” option and choose the related “-statgen” option. Given the maximum sequence processing length n , the “./genseq” must be executed for all sub-subsequence processing lengths ranging from 1 to $n - 1$ using the “-slen” option. For each of those, the “./genseq” must be also executed for all sub-subsequence processing lengths ranging from 1 to $n - 1$ using the “-qlen” option. Determine the alphabet type associated with the organism using the “-a” option and additionally select the nullomer print option “-pn”. Specify the size of the data set to generate using the “-size” option. Next define the preferred output directory using the “-o” option, and redirect the nullomer output accordingly.

Step 4: Reprocess Statistically-Biased Artificial Genome Data

Supply the parameters discussed in this section to the CSeq executable `./reprocess`. Given the maximum sequence processing length n , the `./reprocess` must be executed for all sub-subsequence processing lengths ranging from 1 to $n - 1$ and for each of those because we previously generated data sets based on specific frequency statistics lengths. Subsequently, we create a file consisting of the file path to the CSeq frequency output file and supply that as an argument. Next we select the nullomer print option `-pn` and define the preferred output directory using the `-o` option, and redirect the nullomer output accordingly.

Generate and Process Random (Non-Biased) Artificial Genome Data

Supply the parameters discussed in this section to the Genseq executable `./genseq`. Given the maximum sequence processing length n , the `./genseq` must be executed for all sub-subsequence processing lengths ranging from 1 to $n - 1$ using the `-slen` option. Next include the `-randgen` option and determine the alphabet type associated with the organism (DNA or AA) using the `-a protein` option. Subsequently, supply the reverse complement using the `-rc` option and then select the nullomer print option `-pn`. Specify the size of the data set to generate using the `-size` option. Next define the preferred output directory using the `-o` option, and redirect the nullomer output accordingly.

Step 5: Reprocess Random (Non-Biased) Artificial Genome Data

Supply the parameters discussed in this section to the CSeq executable `./reprocess`. Given the maximum sequence processing length n , the `./reprocess` must be executed for all sub-subsequence processing lengths ranging from 1 to $n - 1$. If we are analyzing DNA sequences we must also reprocess for the reverse complement using the `-rc` option and reprocess the range up to n instead of just $n - 1$. Subsequently we create a file consisting of the file path to the CSeq frequency output file and supply that as an argument. Next we select the nullomer print option `-pn` and define the preferred output directory using the `-o` option, and redirect the nullomer output accordingly.

Step 6: Rank the Observed Nullomer Sequences

Supply the parameters discussed in this section to the Rankseq executable `./rankseq`. First, for each data set be sure that a file containing a list of frequency counts and the length- n nullomers have been created using the `-statfiles` and `-multiple` options, respectively. Next, supply the alphabet type associated with the organism (DNA or protein) using the `-a protein` option and the maximum subsequence partitioning length using the `-p` option. Finally, redirect the ranked nullomer output and range boundaries to standard output and standard error, respectively.

Step 7: Determine the Global Rank Range

Supply the parameters discussed in this section to the Rankseq executable `./rangestat`. First, for each data set create a file containing a list of Rankseq range boundary files; assign this file as input using the `-range` option. Finally, redirect the global bounds output accordingly.

Step 8: Construct Comparable Histograms from Nullomer Rankings

Supply the parameters discussed in this section to the Histoseq executable `./histoseq`. First, for each data set specify the Rankseq and Rangestat output files corresponding to the `-rankseq` and `-range`, respectively. Next, choose a title and specify it using the `-title` option along with the preferred number of bins via the `-n` option. We recommend using the additional histogram configuration options `-automerger`, `-normalize`, and `-statistics` flags. Finally, redirect the histogram output accordingly.

Step 9: Average the Artificial Genome Histograms for the Nullomers

Supply the parameters discussed in this section to the Histoavg executable `./histoavg`. First, for each data set create a file containing a list of normalized HistoSeq histogram output files and specify it using the `“-input”` option. Next, choose a title and specify it using the `“-title”` option along with the `“-normalize”` flag. Finally, redirect the consolidated/averaged histogram output accordingly.

Step 10: Identify the Nullomer Set Cardinalities and Intersections

Supply the parameters discussed in this section to the Nullcountseq executable `./nullcountseq`. First, for each data set create a file containing a list of nullomer set files and specify it using the `“-input”` option. Next, redirect the consolidated/averaged histogram output accordingly.

Step 11: Calculate the k -mer Frequency Spectras

Supply the parameters discussed in this section to the Freqseq executable `./freqseq`. First, for each data set supply the file containing a list of k -mer frequency statistics files using the `“-statfiles”` option, along with the maximum sequence length n using the `“-slength”` option. Next, choose a maximum count and specify it with the `“-maxcount”` option as well as the alphabet via the `“-alphabet”` option. Subsequently, choose the number of bins and the title using the respective `“-n”` and `“-title”` options and specify the `“-normalize”` and `“-statistics”` flags. Finally, redirect the output accordingly.

Step 12: Average the Artificial Genome Histograms for the Oligomers

Supply the parameters discussed in this section to the Histoavg executable `./histoavg`. First, for each data set create a file containing a list of normalized Freqseq histogram output files and specify it using the `“-input”` option. Next, choose a title and specify it using the `“-title”` option along with the `“-normalize”` flag. Finally, redirect the consolidated/averaged histogram output accordingly.

C.3 Experiment 2

C.3.1 Preparation

First, we select the most recent 18 months of NCBI DNA genome snapshots on GeneSIS and create the necessary input and output files/directories. This experiment does not require a script generator utility and therefore all the command files are created manually by the user.

Subsequently, Predictseq must be configured prior to the training process— for ANN mode, this is achieved by creating an ANN configuration file to reflect the user’s preference. The ANN configuration file must contain the following parameters:

1. **Learning Rate:** The rate at which to adjust the neuron interconnections during training (i.e. `“0.1”` or `“0.7”`).
2. **Learning Momentum:** The learning rate adjustment (i.e. `“0.1”` or `“0.7”`).
3. **(Training) Algorithm:** The supervised machine learning algorithm used to train the network (i.e. `“FANN_TRAIN_QUICKPROP”`).
4. **Input (Layer) Size:** The number of input layer neurons in the network. We recommend the value `“AUTO”`, which automatically detects the required number of inputs for the particular task (Rankseq sub-sequence partition length, alphabet type, etc.).
5. **Hidden (Layer) Size:** The number of hidden layer neurons in the network (i.e. `“4”`).
6. **Output (Layer) Size:** The number of output layer neurons in the network (i.e. `“1”`).
7. **Activation Function:** The neuron activation function (i.e. `“FANN_SIGMOID”`).

For an example of this particular file and Predictseq usage see Section A.4.4.

C.3.2 Procedure

Here we identify the process of assessing prime predictability. In this case, we consider the complete DNA NCBI snapshots A, B, C, and D where each corresponds to a chronologically-ordered monthly interval; for simplicity of description Predictseq is trained on the A-B data set, tested on the B-C data set, and used to predict the length n primes for the C-D data set. For this example, let $n = 16$ and the sub-sequence partitioning length $p = 14$ (Note: no primes must exist for length p , otherwise the statistics files will contain blank entries and Rankseq will complain).

Step 1: Process Month A NCBI Database Snapshot

First, CSeq executable “./process” is used to process the month A length-16 statistics. Thus, we execute:

- “./process month_A.ncbi_files 16 -c actg -o output_directory/monthA/s14 -s 1 4 > /dev/null”,
- “./process month_A.ncbi_files 16 -c actg -o output_directory/monthA/s24 -s 2 4 > /dev/null”,
- “./process month_A.ncbi_files 16 -c actg -o output_directory/monthA/s34 -s 3 4 > /dev/null”, and
- “./process month_A.ncbi_files 16 -c actg -o output_directory/monthA/s44 -s 4 4 > /dev/null”.

In this case the “-s” option is used because we are assuming that the computer node does not have enough random access memory to store the all possible length 16 sequences at once. Next we create a file called “month_A.original_counts” containing the following (tabless) four lines:

```
output_directory/monthA/s14-16-1of1.bin
output_directory/monthA/s24-16-2of1.bin
output_directory/monthA/s34-16-3of1.bin
output_directory/monthA/s44-16-4of1.bin
```

Step 2: Reprocess Month A NCBI Database Snapshot

Next, since we are investigating DNA, we need to use the CSeq executable “./reprocess” to consolidate the month A length-16 primes into a single file. Thus, we execute:

- *./reprocess month_A.original_counts 16 -pn -rc -c atcg -o output_directory/monthA/ > output_directory/monthA/nullomers_len16-rc.txt.*

In this case the “-rc” option is used because we wish to acquire the reverse complemented nullomers for the next step.

Subsequently, we re-use the CSeq executable “./reprocess” to calculate the month A statistics for lengths ranging from 1 to $n - 1$. Thus, we execute:

- “./reprocess month_A.original_counts 1 -pn -c atcg -o output_directory/monthA/ > output_directory/monthA/nullomers_len1.txt”,
- “./reprocess month_A.original_counts 2 -pn -c atcg -o output_directory/monthA/ > output_directory/monthA/nullomers_len2.txt”,
- ...,
- “./reprocess month_A.original_counts 14 -pn -c atcg -o output_directory/monthA/ > output_directory/monthA/nullomers_len14.txt”,
and
- “./reprocess month_A.original_counts 15 -pn -c atcg -o output_directory/monthA/ > output_directory/monthA/nullomers_len15.txt”.

Note that for lengths 1 to $n - 1$ we *do not* calculate the reverse complements, because the Rankseq utility requires the original statistics files to acquire proper counts for all considered sub-sequence combinations.

Next we create a file named “month_A.counts” containing the following (tab-less) sixteen lines:

```
output_directory/monthA/nullomers_len1_rc.txt
output_directory/monthA/nullomers_len2_rc.txt
...
output_directory/monthA/nullomers_len15_rc.txt
output_directory/monthA/nullomers_len16_rc.txt
```

Step 3: Rank the Observed Nullomer Sequences for Month A

Next, we rank the primes using the Rankseq executable “./rankseq” using the command:

- “./rankseq -multiple output_directory/monthA/nullomers_len16_rc.txt -statfiles month_A.counts -p 14 -a protein > output_directory/monthA/rankings...”

At this point we have completed all processing and post-processing required for the month A snapshot.

Step 4: Process Month B NCBI Database Snapshot

Step 1 is performed for month B and the original frequency counts are stored to the file “month_B.original.counts”.

Step 5: Create Training Data Set for Months A and B

Next, we create the training data set for months A and B using the Tdataformat executable “./tdataformat” with the command:

- “./tdataformat -i output_directory/monthA/rankings_len16_rc.csv output_directory/monthB/nullomers_len16_rc.txt -o output_directory/AB.dataset -t ann”.

If we wish to use minority over-sampling to balance the data set, we append the “-b” flag to the above command.

Step 6: Train Predictseq

Next, to train Predictseq on “AB.dataset” we use the “./predictseq” executable with the command:

- “./predictseq -i output_directory/AB.dataset -train ann ann.cfg 90 40000 -o output_directory/AB.trained_ann -p 14 -a DNA”

where “40000” denotes the number of generations, “90” denotes the target accuracy, and “ann.cfg” denotes Predictseq’s ANN configuration file.

Step 7: Reprocess Month B NCBI Database Snapshot

Step 2 is performed for month B. The length 16 reverse complement nullomers are exported to the file “output_directory/monthB/nullomers_len16_rc.txt” and the frequency files for month B are stored in the file “month_B.counts”.

Step 8: Rank the Observed Nullomer Sequences for Month B

Step 3 is performed for month B and the nullomer rankings are stored to the file “output_directory/monthB/rankings_len16_rc.csv”.

Step 9: Process Month C NCBI Database Snapshot

Step 1 is performed for month C and the original frequency counts are stored to the file “month_C.original.counts”.

Step 10: Create Testing Data Set for Months B and C

Next, we create the testing data set for months B and C using the Tdataformat executable “./tdataformat” with the command:

- “./tdataformat -i output_directory/monthB/rankings_len16_rc.csv output_directory/monthC/nullomers_len16_rc.txt -o output_directory/BC.dataset -t ann”.

If we wish to use minority over-sampling to balance the data set, we append the “-b” flag to the above command.

Step 11: Test Predictseq

Next, to test Predictseq on “BC.dataset” we use the “./predictseq” executable with the command:

- “./predictseq -i output_directory/BC.dataset -test ann output_directory/AB.trained_ann -o output_directory/BC.tested_ann -p 14 -a DNA”.

where “ann.cfg” denotes Predictseq’s AB trained ANN state file.

Step 12: Reprocess Month C NCBI Database Snapshot

Step 2 is performed for month C. The length 16 reverse complement nullomers are exported to the file “output_directory/monthC/nullomers_len16_rc.txt” and the frequency files for month C are stored in the file “month_C.counts”.

Step 13: Rank the Observed Nullomer Sequences for Month C

Step 3 is performed for month C and the nullomer rankings are stored to the file “output_directory/monthC/rankings_len16_rc.csv”.

Step 14: Process Month D NCBI Database Snapshot

Step 1 is performed for month D and the original frequency counts are stored to the file “month_D.original_counts”.

Step 15: Create Prediction Data Set for Months C and D

Next, we create the prediction data set for months C and D using the Tdataformat executable “./tdataformat” with the command:

- “./tdataformat -i output_directory/monthC/rankings_len16_rc.csv output_directory/monthD/nullomers_len16_rc.txt -o output_directory/CD.dataset -t ann”.

If we wish to use minority over-sampling to balance the data set, we append the “-b” flag to the above command.

Step 16: Make a Prediction

Next, to predict using Predictseq on the “CD.dataset” we use the “./predictseq” executable with the command:

- “./predictseq -i output_directory/CD.dataset -predict ann output_directory/AB.trained_ann -o output_directory/CD.predictions -p 14 -a DNA”.

where “ann.cfg” denotes Predictseq’s AB trained ANN state file.

APPENDIX D

GRAPHICAL RESULTS

D.1 Overview

In this brief chapter we provide supplementary histogram results related to the experiments of Chapter 4.

D.2 AA k -FS Results: *Apis mellifera* Example

For visual convenience, only the first 10 bins of the 50 bin histograms are displayed because, in all observed cases, the 40 remaining bin values monotonically decrease close to zero.

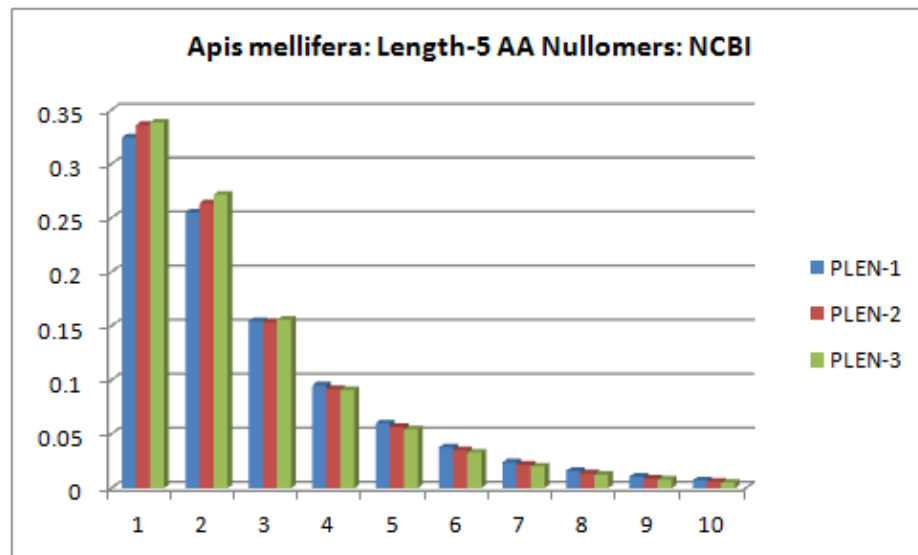


Figure D.1: The honey bee's length-5 AA nullomer ranking histogram for the *NCBI* data set

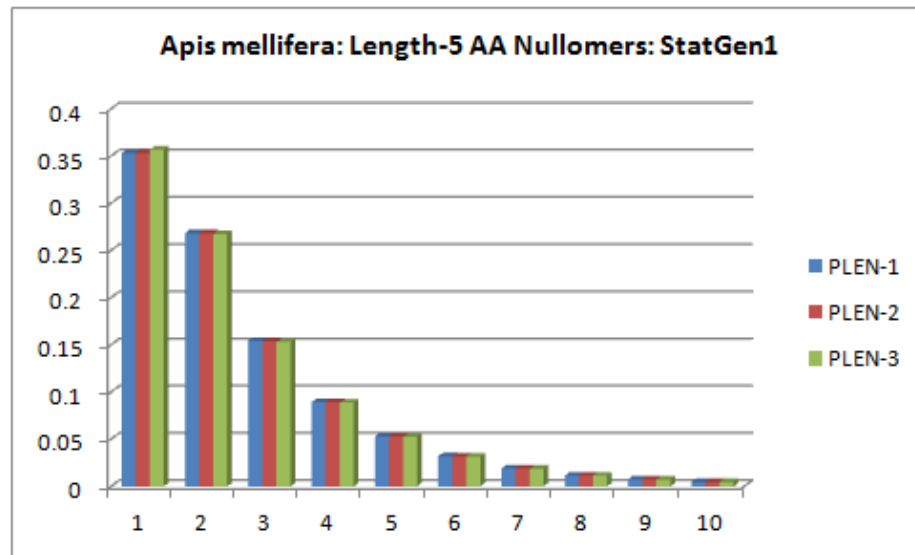


Figure D.2: The honey bee's length-5 AA nullomer ranking histogram for the *length-1 statistically generated* data set

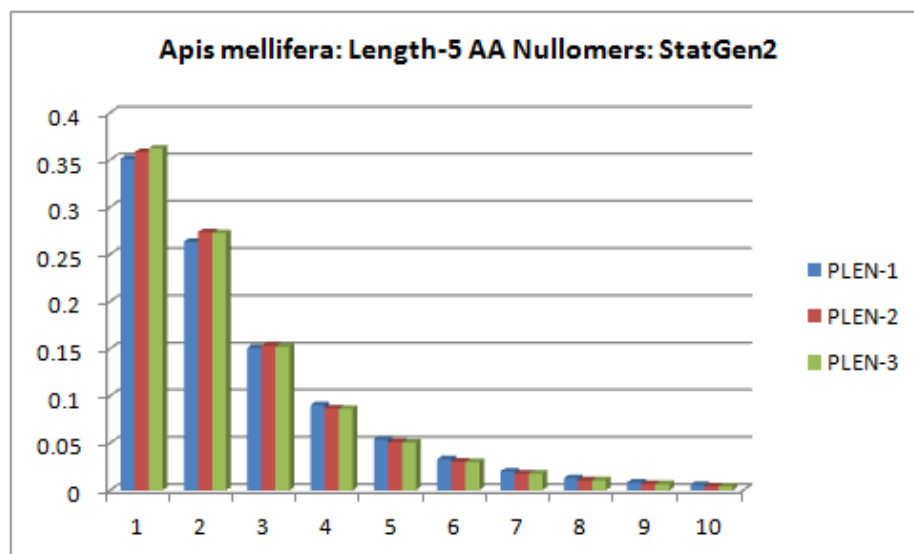


Figure D.3: The honey bee's length-5 AA nullomer ranking histogram for the *length-2* statistically generated data set

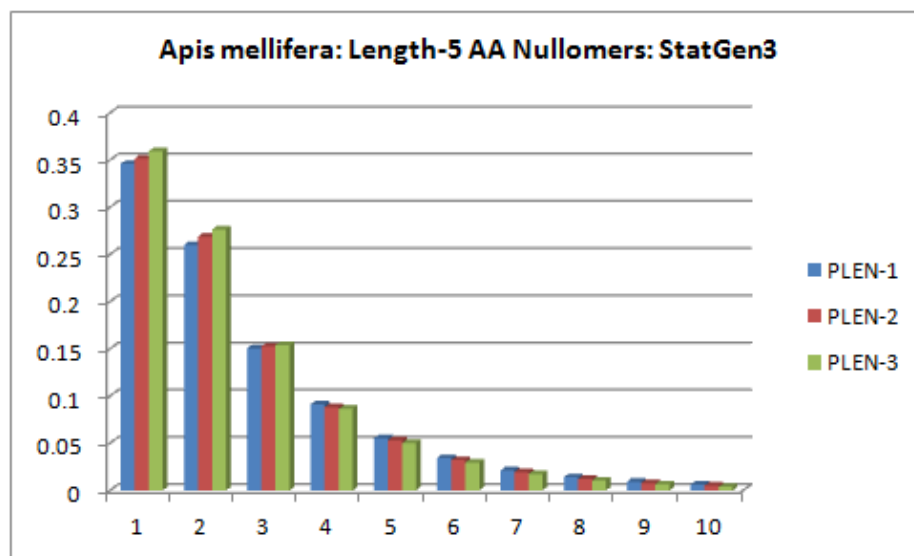


Figure D.4: The honey bee's length-5 AA nullomer ranking histogram for the *length-3* statistically generated data set

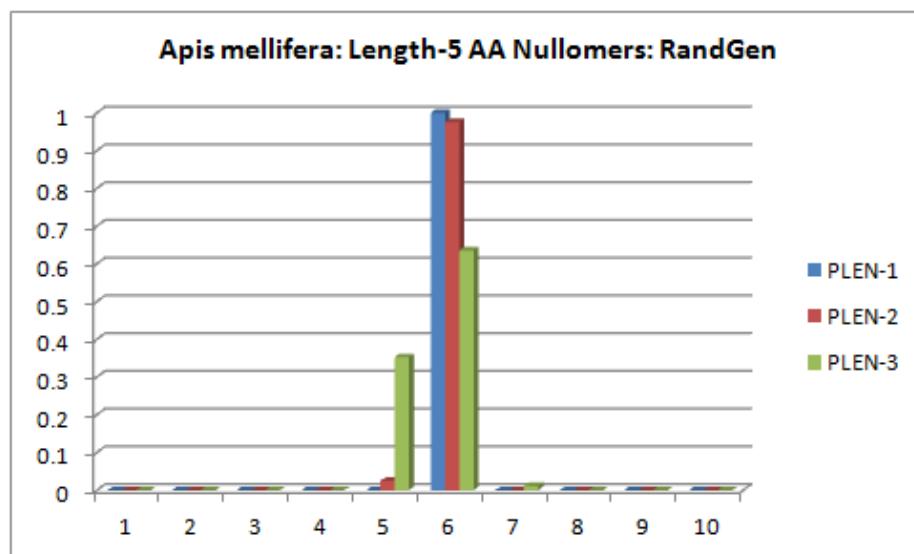


Figure D.5: The honey bee's length-5 AA nullomer ranking histogram for the *randomly generated* data set